(NASA-CR-120623) SOLAR ENERGY CONCENTRATOR SYSTEM FOR CRYSTAL GROWTH AND ZONE REFINING IN SPACE Final Report (Lockheed Missiles and Space Co.) 104 p HC $5.25 CSCL 10A

N75-18719

Unclas

G3/44 12370

LMSC-HREC TR D390666

Lockheed

Missiles & Space Company, Inc.

HUNTSVILLE RESEARCH & ENGINEERING CENTER

Cummings Research Park
4800 Bradford Drive,
Huntsville, Alabama

SOLAR ENERGY CONCENTRATOR SYSTEM FOR CRYSTAL GROWTH AND ZONE REFINING IN SPACE

FINAL REPORT

February 1975

Contract NAS8-30268

Prepared for National Aeronautics and Space Administration
Marshall Space Flight Center, Alabama 35812

by

J.H. McDermit

APPROVED: John W. Benefield
John W. Benefield, Supervisor
Fluid Mechanics Section

George D. Perry
for J.S. Farrior
Resident Director

FOREWORD

This report represents the results of work performed by the Lockheed-Huntsville Research & Engineering Center for the NASA-Marshall Space Flight Center under Contract NAS8-30268.

The NASA contract monitor for this study was Mr. R.C. Ruff.

ACKNOWLEDGMENTS

The author is grateful to Mr. S. J. Robertson for his assistance during the initial phases of this effort and to Mr. R.C. Ruff for the many helpful discussions during the course of this effort.

ABSTRACT

A study on the technological feasibility of using solar concentrators for crystal growth and zone refining in space has been performed. Previous studies of space-deployed solar concentrators were reviewed for their applicability to materials processing and a new state-of-the-art concentrator-receiver radiation analysis was developed. The radiation analysis is in the form of a general purpose computer program.

It was concluded from this effort that the technology for fabricating, orbiting and deploying large solar concentrators has been developed. It was also concluded that the technological feasibility of space processing materials in the focal region of a solar concentrator depends primarily on two factors: (1) the ability of a solar concentrator to provide sufficient thermal energy for the process and (2) the ability of a solar concentrator to provide a thermal environment that is conducive to the processes of interest. The analysis indicate that solar concentrators can satisfactorily provide both of these factors.

The radiation analysis and associated computer code can determine the heating distribution on any target with any orientation in the focal region of a solar concentrator. The computer code can treat such problems as target placement errors, concentrator surface imperfections, etc. This computer code also has the capability of designing solar concentrators that give prescribed heating distributions. Faceted (Fresnel) as well as continuous surface concentrators can be treated. This analysis was used to show the sensitivity of the heating distribution on targets to such factors as target geometry, target location, concentrator surface errors, etc. It has also been used to illustrate that solar concentrators can be designed to give prescribed heating distributions. From these results it can be concluded that solar concentrators can provide the thermal environment for space processing.

An analysis has also been developed for determining the relation between molten zone sizes and concentrator sizes. This analysis has been applied to three typical process materials of current interest, silicon, germanium and tungsten.

The results of this study indicate that solar concentrators are attractive for space processing, not only from the viewpoint of providing the required thermal environment but also from the viewpoint of system specific power and system flexibility. The results also indicate that a solar concentrator with practical dimensions can provide the required thermal energy, i.e., a concentrator with a diameter of 10 meters (or possibly less) can process bars of silicon and germanium up to 10 inches in diameter.

It is concluded that with additional analytical and experimental study, a solar concentrator system to provide thermal environments for all space processing applications can be developed.

CONTENTS

Section		Page
	FOREWORD	ii
	ACKNOWLEDGMENTS	ii
	ABSTRACT	iii
	NOMENCLATURE	ix
1	INTRODUCTION	1
2	BACKGROUND INFORMATION	6
	2.1 Crystal Growth	6
	2.2 Continuous Zone Refining	7
	2.3 Molten Zone Shape	8
	2.4 Controlling the Thermal Environment	8
	2.5 Concentrator Contamination	9
	2.6 Pointing the Solar Concentrator	9
	2.7 Target Placement	10
	2.8 Previous Solar Concentrator Development Studies	10
3	RADIATION ANALYSIS	12
	3.1 Ray Trace	13
	3.2 Energy Balance and Imaging the Solar Source	15
	3.3 The Solar Source	20
	3.4 Application of the Analysis to Solar Concentrators	28
	3.5 Target Placement Errors	37
	3.6 Optical Errors	42
	3.7 Reflector Design	42
	3.8 Parameter Definintions and Non-Dimensionalizing the Equations	45

CONTENTS (Continued)

Section		Page
4	PROCESS HEAT BALANCE	47
5	RESULTS	53
	5.1 Thermal Image on Targets Normal and Parallel to the Optical Axis	55
	5.2 The Influence of Placement Errors on the Thermal Image	58
	5.3 Optical Errors	64
	5.4 A Comparison of Fresnel and Paraboloid Concentrators	64
	5.5 Design of a Solar Concentrator to Give a Prescribed Concentration Distribution	72
	5.6 Estimation of Concentrator Sizes for Obtaining Molten Zones	77
	5.7 Specific Power Comparisons	79
6	CONCLUSIONS AND RECOMMENDATIONS	83
	REFERENCES	85
Appendix		
A	Solar Concentrator Analysis Program	A-1

LIST OF TABLES

Table		
1	Crystal Growing	3
2	Purification	3
3	Materials Properties	78
4	Specific Power Comparisons	82

LIST OF ILLUSTRATIONS

Figure		Page
1	Geometric Optics	14
2	Point Source Irradiating a Receiving Surface Through a Curved Reflecting Element	17
3	Overlaying Images Produced by Point Sources	19
4	Image Produced by Pinhole Reflector	21
5	Overlaying Images Produced by Pinhole Reflectors	22
6	Imaging the Solar Source	24
7	Intensity Variation in Solar Source Image	25
8	Axisymmetric Solar Concentrator-Receiver Configuration	29
9	Energy Balance	32
10	Solar Image on an Arbitrary Receiver	34
11	Irradiation on a Non-Planar Receiver	35
12	Target Placement Errors	39
13	Rotation of Surface Normal Vector	40
14	Statistical Perturbation of Reflector Surface	43
15	Reflector Surface Design	44
16	Configuration for Heat Balance	48
17	Solar Disc Model	53
18	Concentration on a Right Circular Cylinder Located on the Optical Axis of a Paraboloid with an Aperture Ratio of 4	56
19	Concentration on a Flat Receiver Normal to the Optical Axis of a Paraboloid of Aperture Ratio 4	57
20	Concentration Efficiency for a Paraboloid with Aperture Ratio = 4 Irradiating a Cylinder	59
21	Concentration on a Cylindrical Target Rotated 2 Minutes	60
22	Concentration on a Cylindrical Target Rotated 4 Minutes	61
23	Concentration on a Cylindrical Target Rotated 6 Minutes	62

LIST OF ILLUSTRATIONS (Continued)

Figure		Page
24	Concentration on a Cylindrical Target Rotated 8 Minutes	63
25	Concentration on a Cylindrical Target Translated 0.002 Units from the Optical Axis	65
26	Concentration on a Cylindrical Target Translated 0.004 Units from the Optical Axis	66
27	Concentration on a Cylindrical Target Translated 0.006 Units from the Optical Axis	67
28	Concentration on a Cylindrical Target Translated 0.009 Units from the Optical Axis	68
29	Concentration Distribution on a Cylindrical Target Translated 0.008 Units and Rotated 8 Minutes	69
30	Influence of Optical Errors on Concentration Distribution	70
31	Area Utilization for Fresnel Concentrators	71
32	A Comparison of Concentration Distribution of Paraboloid and Fresnel Concentrators	73
33	Fresnel Concentrator	74
34	Solar Concentrator Geometry to Give Prescribed Concentration Distribution	75
35	Thermal Image on a Cylinder from a Custom Concentrator	76
36	Power Requirements for Cylindric Molten Zones	80
37	Process Bar Diameter versus Concentrator Aperture	81

NOMENCLATURE

Symbol	Definition
A	area
a	aperture ratio ($a = D/f$)
B	inner diameter of the solar concentrator
C	concentration ratio
C_p	specific heat
D	aperture of the solar concentrator
d	bar diameter
E	irradiation
$\vec{e}$	unit vector
F	radiation geometry factor
f	focal length
G	solar disc brightness function
g	equal angle ray trace equation
h	coplanarity ray trace equation
I	radiant intensity
$\vec{i}$	unit vector in x-direction
$\vec{j}$	unit vector in y-direction
K	solar constant
k	thermal conductivity
$\vec{k}$	unit vector in z-direction
L	length of a molten zone or solid bar
M	radiant emittance
m	parameter in solar disc brightness function
$\vec{N}$	surface normal vector
P	perimeter of a receiver
p	point of interest
Q	radiant energy
q	heat source term
$\vec{R}$	position vector

NOMENCLATURE (Continued)

R	radius of the process material
r	receiver radial coordinate
S	implicit surface function
s	radial coordinate for an axisymmetric concentrator
T	temperature
$\vec{V}$	ray vector
V	molten zone velocity
x	spatial coordinate
y	spatial coordinate
z	spatial coordinate along the optical axis

Greek

α	absorptivity
β	angle of incidence
γ	reflectivity
Δ	displacement of the receiver from the optical axis
δ	defined by Eq. (58)
ϵ	emissivity
η	concentration efficiency
θ	angular coordinate for the receiver
λ	wave length
μ	angle between the optical axis and a surface normal
ν	distance from the center of the solar disc image
ξ	angle corresponding to a radial location in the solar disc
π	3.1415.....
ρ	density
σ	Stefan-Boltzmann constant or one standard deviation
τ	defined by Eq. (56)
ϕ	denotes function, e.g., function of $\beta = \phi(\beta)$
ψ	angular coordinate for the concentrator
ω	angle of rotation of the receiver

NOMENCLATURE (Continued)

Σ	summation
Φ	radiant flux
Ω	solid angle

Subscripts

1	normally associated with the concentrator
2	normally associated with the receiver
0	initial or center value or source
a	ambient
s	surface
p	point of interest
n	normal direction
f	freezing point

Section 1
INTRODUCTION

Space processing offers the potential for producing some unique products because it provides an environment of microgravity, high vacuum and the availability of the continuous supply of non-contaminating solar energy. The lack of gravity yields opportunities for reduced, more controllable natural convection in the liquid state, containerless processing, absence of sedimentation, and capillary-controlled fluid shaping and fluid motion. Reduced natural convection and containerless suspension for molten materials are highly advantageous in nucleation and solidification, which should lead to technologically advanced and economically viable materials made from metal alloys, eutectics, composites, solutions and pure components. The natural, high vacuum of space offers a contaminant-free atmosphere in which to melt, shape, mold and solidify process materials. The combination of the two preceding factors with the availability of non-atmospherically attenuated solar energy provides the unique opportunity for containerless melt zone processing of ultra-high melting point materials. Concentration of solar energy offers a source of high heat flux uncontaminated by combustion products, electric and magnetic fields, and in unending supply. In particular, the crystal growth and zone refining of high melting point materials appears very promising in space with a solar concentrator configuration.

One of the major problems of any extraterrestrial project is a sufficient supply of energy. For large scale operations such as the space processing of materials on a production basis the cost of energy in the form of batteries, fuel cells, etc., will be prohibitive. At this point in time the most attractive candidate processes for space processing involves the melting of rather large quantities of high melting point, high thermal conductivity, high specific heat materials. This will, of course, require a great deal of thermal energy. It has been proposed to conduct the processes in the focal region of a solar concentrator.

There is economic and technical justification for pursuing the preparation of single compound crystals (ceramic oxides and compound semiconductors) with maximum perfection, purity, and size to achieve high performance electronic components and devices. Other crystals that appear attractive at this time are garnet crystals for magnetic bubble memories and crystals that have electro-optic applications [1]. A primary advantage of zero-g for crystal growth is that crystals much larger than those grown on earth can be grown from a melt zone in space. The size of the earth-grown crystal depend primarily on the surface tension of the material. In zero-g crystals 4 to 8 inches in diameter and perhaps larger may be feasible. High purity tungsten for x-ray targets is also an attractive product for zero-g manufacturing [2]. Tungsten can be zone refined using the float zone technique without crucible contamination.

In addition to growing crystals and zone refining, some other possible applications of zero-g are production of biologicals, separation of materials, obtaining accurate values of physical properties, etc. Justification of space processing, candidate processes, etc., has been well studied [1-3]. Many of the processes, experiments, etc., mentioned in these studies require thermal energy. This of course is the function of a solar concentrator.

The advantages and disadvantages of crystal growth and zone refining in space with a solar concentrator are outlined in Tables 1 and 2. Many of the points in this table have been mentioned in the text. The table is self explanatory.

The objectives of this study as originally outlined were:

- Determine the feasibility of using a system of mirrors to concentrate solar energy for direct processing of materials.
- Define solar concentrator materials compatible with the space environment.
- Develop a design for a crystal growth and zone refining assembly.
- Specify materials that are most suitable to, and benefitted by solar processing in space.

Table 1
CRYSTAL GROWING

Process	Zero Gravity		High Vacuum		Solar Energy	
	Advantages	Disadvantages	Advantages	Disadvantages	Advantages	Disadvantages
1. Zone melting	• Larger molten zones • More controllable convective currents • Reduced strain in soft, newly formed crystal		• Reduced contamination • Reduced surface cooling and, hence, higher temperature capability • No pumping required for vacuum	• Outgas contamination • Mechanical equipment design for vacuum	• Limitless supply • High temperature capability • Uncontaminated	• Large collector required • Difficult optical design for proper focusing
2. Czochralski	• Container not required and, hence, reduced contamination • More controllable convective currents • Reduced strain in soft newly formed crystal	• Difficult design for securing melt	(Same as above)	(Same as above)	(Same as above)	(Same as above) (Optical design probably less difficult than for zone melting)

Table 2
PURIFICATION

Process	Zero Gravity		High Vacuum		Solar Energy	
	Advantages	Disadvantages	Advantages	Disadvantages	Advantages	Disadvantages
1. Zone melting	• Larger molten zones	• Reduced convection reduces refining effect.	• Reduced contamination	• Outgas contamination • Mechanical equipment design for vacuum	• Limitless supply • High temperature capability • Uncontaminated	• Large collector required

ORIGINAL PAGE IS OF POOR QUALITY

Upon reviewing the literature related to solar concentrators it was found that the design of large solar concentrators for space applications had received a great deal of attention during the early 1960s. The purpose of these concentrators was to power closed thermodynamic cycles for electrical power generation. However, the technology developed for these concentrators is directly applicable to the present study. The technology developed included every aspect of the problem from materials selection and fabrication to launching and deployment. Also upon reviewing the literature related to space processing it was found that a great deal of current effort is devoted to specifying materials that are most suitable to, and benefitted by processing in space [1-3]. Thus, some of the original objectives had already received much broader treatment than could be given to them in this limited study. Therefore the primary effort of this study was devoted to determining the feasibility of using a system of mirrors to concentrate solar energy for direct processing of materials and to developing a design for a crystal growth and zone refining assembly.

To determine the feasibility of conducting zone refining and crystal growth in the focal region of a solar concentrator the relationship between the processes and the concentrator must be understood. The purpose of the solar concentrator if of course to provide the thermal energy for the processes. Upon examining the processes of interest it was found that the success of the processes depends to a large degree on their thermal environment, e.g., to grow a high quality crystal, a near planar solid-liquid interface is mandatory. Thus the feasibility of using the solar concentrator for processing depends to a great extent on: (1) Can the solar concentrator supply sufficient thermal energy for the process?; and (2) Can the solar concentrator create a specific thermal environment for the process? These are the questions primarily considered in this report.

In the following section background information on various aspects of solar concentrators and the processes of interest is given. The topics covered are shown on the following page.

- Crystal growth
- Continuous Zone Refining
- Molten Zone Shape
- Controlling the Thermal Environment
- Concentrator Contamination
- Pointing the Solar Concentrator
- Target Placement, and
- Previous Solar Concentrator Studies.

Following the background material, a radiation analysis is presented for determining the irradiative distribution on targets placed in the focal region of solar concentrators. This analysis can consider any type of axisymmetric concentrator and any target configuration. Also system imperfections such as target placement errors, optical errors, etc., are considered.

Following the radiation analysis, a simplified heat transfer analysis is performed for a molten zone. This analysis allows estimates to be made of concentrator size versus process size.

By using the analyses developed in this study parametric data are generated to show the influence of various parameters on the thermal environment produced by solar concentrators.

Section 2
BACKGROUND INFORMATION

2.1 CRYSTAL GROWTH

In growing crystals from a melt, crystal perfection is often a function of the shape of the growing interface. The shape of this interface is controlled by the heat flow pattern in the system. The heat of fusion of the solidifying material is liberated at the solid-liquid interface and transported away from the interface by conduction, convection and radiation. The relative importance of each of these transport mechanisms depends on the conditions, physical properties and geometry of the system. For example, for growth above about 800 to 1000°C, radiation from the growth interface becomes more important. This importance increases if the crystal has any degree of transparency in the spectral range in the vicinity of the peak of the blackbody radiation curve for the growth temperature [4].

The growth interface shape is dictated by the heat flow pattern which is controlled by the overall thermal environment of the process. Although a particular heat transport mechanism is not significant at the interface, this mechanism may play a very active role in determining the growth interface shape.

The problem of the interaction of heat and mass flow with crystal structural imperfections is quite complex and in a relatively embryonic state of development [4]. The relation of crystal growth to the thermal environment for the melt growth technique is particularly well stated by Chu [5].

> "When a crystal is grown from a melt, the solidification process must be controlled to avoid random nucleation. Usually, a single crystal seed is used, and the solidification is allowed to take place on the surface of the seed by adjusting the thermal

> geometry. Under proper conditions, the growth continues the cry tallographic orientation of the seed to form a single crystal. The thermal conditions at the growing liquid-solid interface are the most important factors governing the crystal growth process and are influenced by many factors. In practice, the liquid is heated at a temperature above the melting point by conduction and radiation from a thermal source. The heat of fusion is generated at the interface at a rate directly proportional to the rate of solidification. Heat is lost from the interface by conduction through the grown crystal and by conduction and radiation from the crystal to thermal sinks provided by the container walls and any gaseous atmosphere. If there is a net accumulation of heat to the interface, the crystal will melt. If there is a net loss of heat at the interface, the crystal will grow at a rate determined by the rate of dissipation of heat of fusion. Thermal gradients in the liquid and solid determine the rate at which heat arrives at and leaves the interface, thus determining the rate of crystal growth. The control of temperature and temperature gradients are therefore of utmost importance in melt-growth techniques."

Although solar concentrators have not been used to grow crystals, other types of thermal imaging furnaces have been used for this application [6-8]. Many of the findings in these studies are applicable to the present study. For example some of the topics mentioned are thermal environment control, operating procedures, atmosphere control for the process, and some comments concerning the advantages and disadvantages of using imaging furnaces.

2.2 CONTINUOUS ZONE REFINING

Basically continuous zone refining is conducted by moving a molten zone along the length of a bar of material to bring about impurity segregation. The technique depends on differences in composition of the liquid and solid in equilibrium. By repeatedly sweeping the molten zone from one end of the bar to the other, the impurity concentration decreases at one end of the bar and increases at the other end. After a sufficient number of passes most of the impurities are swept from one end leaving a high purity material [e.g., see Ref.9].

2.3 MOLTEN ZONE SHAPE

An important aspect of float zone processing is the shape of the molten zone and the shape of the meniscus connecting the molten zone to the solid material. The molten zone shape and meniscus shape is dependent on the molten material surface tension (which is a strong function of temperature) and the geometry of the process, i.e., geometry of the feed stock and the processed material. The molten zone geometry also couples the process to the solar concentrator in that the geometry influences the irradiative distribution received, which in turn influences the solid-liquid interface, Marangoni convection,* etc. Although this study does not deal with the problem of molten zone shape and meniscus shape the problem has received attention [10-14].

2.4 CONTROLLING THE THERMAL ENVIRONMENT

As mentioned previously, crystal perfection and shape depend on its growth thermal environment, i.e., the crystal shape is dictated by the meniscus shape which depends on the surface temperature, and crystal quality is a strong function of the solid-liquid interface shape which is dictated by the total thermal environment. Thus an essential part of the solar concentrator system will be a control system which monitors the process temperature and controls the heat flux distribution. Various sensing and control techniques have been considered by previous investigators [15-21].

Obtaining a prescribed irradiative distribution on a target in the focal region of a solar concentrator can be achieved by positioning the target and/or adjusting the concentrator surface. Another alternative is the use of a secondary optical element to change the irradiative distribution. For example, one could use a "flux redistributor" such as that described by Glaser, et al., [17] if uniform irradiation is desired. One could, of course, design similar secondary elements to achieve other irradiative distributions.

The amount of radiant flux available to irradiate the receiving surface can be controlled by use of a cylindrical shutter [16] or a venetian blind arrangement [15].

*Convection induced by surface tension gradients.

Techniques are available for measuring the heat fluxes of solar furnaces [22] and the temperature of targets in the focal region [21, 23]. These measuring techniques can be coupled to controls for achieving the desired thermal environment.

2.5 CONCENTRATOR CONTAMINATION

There are many materials available for concentrator reflective surfaces [24-27]. However it seems that none would be immune to degradation due to protons and ultraviolet radiation [27, 28]. A protective coating would be essential for long term surface optical quality. The reflective surface can also be degraded by contamination due to process material outgassing. This can be prevented by shielding the reflector by enclosing the process area with glass, or if this contamination is very slow, it could be removed periodically using RF-excited oxygen plasma [10]. Analytical models are available for computing the adsorption and desorption of materials under specified conditions [29, 31].

It has also been suggested that a gas jet could be used to deflect outgassed molecules to reduce contamination if the process is to be conducted in the vacuum of space [32].

2.6 POINTING THE SOLAR CONCENTRATOR

It has been stated that a pointing accuracy of about 1 minute of arc is needed for a high quality solar concentrator [32]. Several devices have been developed for pointing solar furnaces [33-35] and appendages to space vehicles in general [36]. The pointing accuracy requirements for a solar concentrator are much more lenient than those for telescopes. Thus it seems that there will be no problem in achieving the required accuracy. However, the accuracy is such that it may be necessary to dynamically isolate the solar concentrator system from any manned laboratory.

2.7 TARGET PLACEMENT

The spatial location of the process or target in the focal region of the solar concentrator is of extreme importance. The rays being reflected onto the target are converging on the target from all portions of a solid angle that will probably exceed 4π steradians. The "focal region" of the concentrator is a relatively small volume. Thus any rotation or translation of the target from the desired position can cause great variations in the heating distribution and the magnitude of the heating.

2.8 PREVIOUS SOLAR CONCENTRATOR DEVELOPMENT STUDIES

Several efforts have been directed toward the development of solar concentrators for space applications [24, 37-44]. These efforts have been concerned with many aspects of the problem. They have covered fabrication techniques, reflective coatings, reflective surface degradation, deployment, surface accuracy requirements, etc.

Methods of fabricating and testing concentrators of practically any size seem to be well developed. A variety of deployable designs have been conceived, e.g., petal configurations, Fresnel type reflectors, umbrella configurations, and inflatable types [39, 41, 45]. Most of the compact designs for deployment have optical accuracies sufficient for obtaining concentrations that that would be suitable for many applications. However, the one piece non-folding type concentrator has the advantage that its performance can be well characterized before it is launched.

Electroformed nickel concentrators appear to be the most efficient one-piece concentrators. However, stretch-formed aluminum has a higher specific power based on weight. For a given power requirement an aluminum concentrator would have a greater diameter [41].

Rather comprehensive studies of solar concentrators for orbiting were conducted in Refs. [43] and [44]. In Ref. [43] the Air Force's EROS Program (Experimental Reflector Orbital Shot) is described in which a 4.5 foot diameter reflector of the Fresnel type was successfully orbited. The effort by Stewart [44] was concerned with paraboloid concentrators up to 30 feet in diameter. This is a rather comprehensive study that covers many aspects of solar concentrators that are of interest in this study. Although a complete review of this work cannot be given here some points of particular interest will be listed.

- The concentrator has a specific weight of 0.87 pounds per square foot of projected area.
- The reflective coating is chemically deposited silver with a reflectivity of at least 0.91.
- Blade grinding or plastic overlay master fabrication techniques are best for obtaining highly accurate, highly reflective concentrators.
- Calculated space environment degradation of the reflective surface will be less than 1% in the reflectance in 10,000 hours.
- The concentrator developed was ground tested and has good launch and orbit capability.

Section 3
RADIATION ANALYSIS

Analyses for determining the irradiation on receivers placed in the focal region of solar concentrators have been performed by many investigators [46-57]. If the attributes of all of these analyses were combined one would no doubt have an analysis of sufficient generality to treat any solar concentrator-receiver combination with consideration given to the various details such as limb darkening effects, optical errors, positioning errors, etc. Some of these analyses treat only flat receiving surfaces located in the focal plane of a paraboloid. Some do not consider variation in the solar disc radiance (limb darkening), most consider only paraboloid concentrators, etc. Thus, even though all aspects of the problem have been treated, it seemed that a general unified analysis did not exist. Thus an analysis was developed that is very general and considers as many aspects of the problems as possible and is applicable to any solar concentrator problem including the geometries that are of interest to crystal growth and zone refining. A computer code has been developed for this analysis.

The analysis consist primarily of developing ray trace expressions and energy balance relations that take into consideration the characteristics of the source. The radiation analysis is the heart of the computer code for solar concentrator analysis and design. A general treatment will be made of the radiation analysis. The analysis will then be modified as needed to treat the problem at hand.

The radiation from the solar source that is important to the thermal image in a solar concentrator is in a relatively narrow bandwidth (0.3μ to 3μ). Thus in the analysis that follows, the spectral properties of the radiation will not be considered.

3.1 RAY TRACE

Consider the reflecting surface described by the implicit function S , and the receiving surface S_2 as shown in Fig.1 . The law of reflection requires that $\beta_1 = \beta_1'$ and that $\vec{V}_1$, $\vec{V}_2$ and $\vec{N}_1$ are coplanar. These conditions can be stated mathematically as follows:

$$\left[\frac{\vec{V}_1}{|\vec{V}_1|} + \frac{\vec{V}_2}{|\vec{V}_2|}\right] \cdot \vec{N}_1 = 0 \tag{1}$$

$$\left[\vec{V}_1 \times \vec{V}_2\right] \cdot \vec{N}_1 = 0 \tag{2}$$

If the ray vector $\vec{V}_1$ originates at a point '0' then position vectors for the ray vector extremities can be written as follows:

$$\vec{R}_o = \vec{i}\, x_o + \vec{j}\, y_o + \vec{k}\, z_o \tag{3}$$

$$\vec{R}_1 = \vec{i}\, x_1 + \vec{j}\, y_1 + \vec{k}\, z_1 \tag{4}$$

$$\vec{R}_2 = \vec{i}\, x_2 + \vec{j}\, y_2 + \vec{k}\, z_2 \tag{5}$$

With the above the ray vectors can be expressed as:

$$\vec{V}_1 = \vec{R}_1 - \vec{R}_o \tag{6}$$

$$\vec{V}_2 = \vec{R}_2 - \vec{R}_1 \tag{7}$$

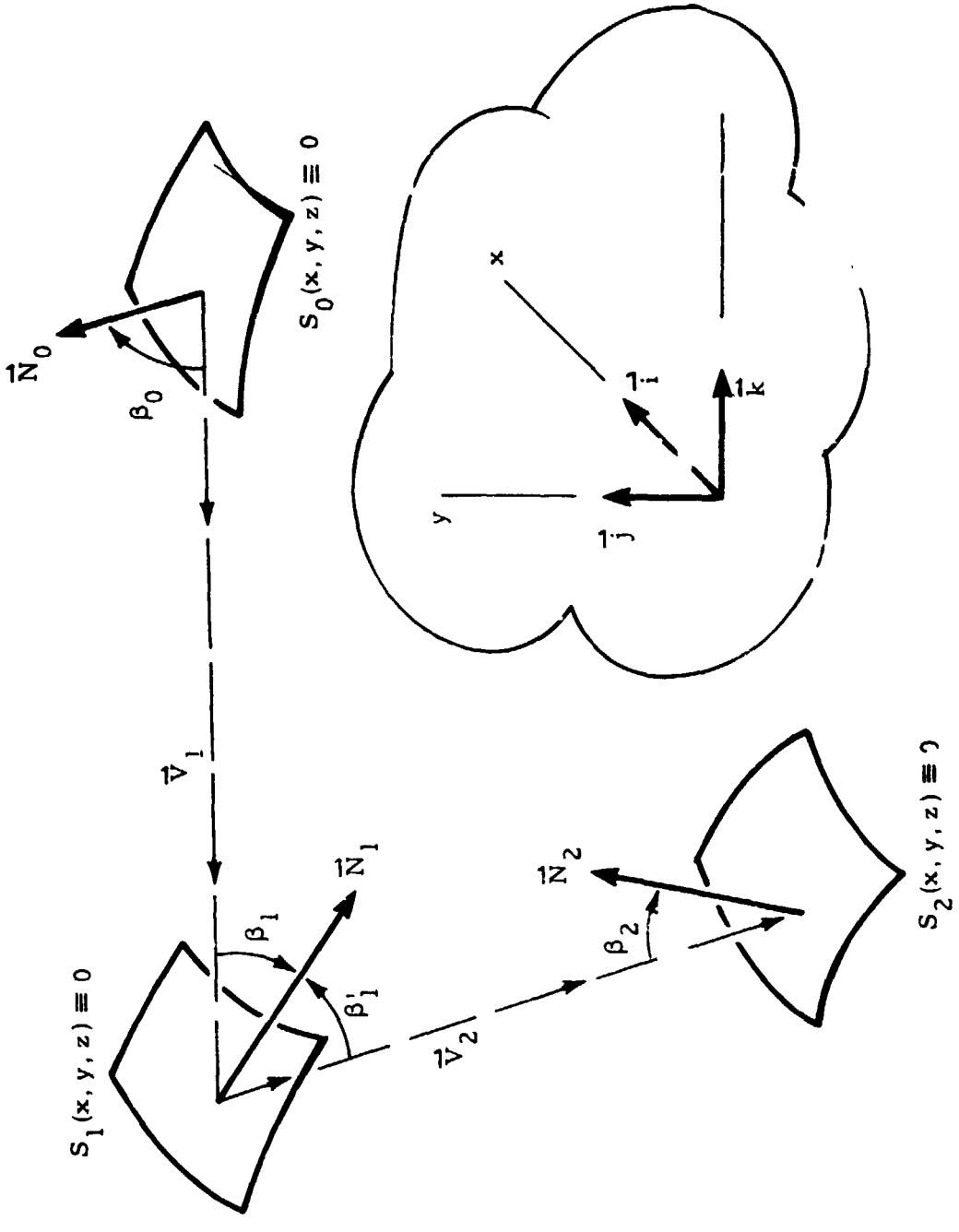

Fig. 1 - Geometric Optics

This of course gives the ray vectors in terms of the coordinates of the source, reflecting surface, and receiving surface. By making use of the fact that the gradient of a scalar function describing a surface is a vector normal to the surface, the ray trace equations can be expressed in terms of ray coordinates and partial derivatives of the reflecting surface, i.e., $\vec{N}_1$ or its negative image (depending on the function S_1) is given by

$$\vec{N}_1 = \vec{\nabla} S_1 \tag{8}$$

where

$$\vec{\nabla} = \vec{i}\,\frac{\partial}{\partial x} + \vec{j}\,\frac{\partial}{\partial y} + \vec{k}\,\frac{\partial}{\partial z} \tag{9}$$

With the relations above it can be seen that the ray trace equations (1) and (2) are partial differential equations in terms of the source, reflector, and receiver coordinates and the reflector surface derivatives. Equations (1) and (2) can be expressed in functional form as follows:

$$g(\vec{R}_o, \vec{R}_1, \vec{R}_2, \vec{\nabla} S_1) \equiv 0 \tag{10}$$

$$h(\vec{R}_o, \vec{R}_1, \vec{R}_2, \vec{\nabla} S_1) \equiv 0 \tag{11}$$

The above describes the path of a ray through any reflecting optical system. The application of these equations to the problem of interest will be made later.

3.2 ENERGY BALANCE AND IMAGING THE SOLAR SOURCE

Consider the arrangement in Fig. 1 where S_o is the radiation source, S_1 is the reflecting element and S_2 is the receiving surface. There are two ways to view the imaging of the source S_o onto the receiver S_2 through the reflecting element S_1. Let us explore these.

First, consider an emitting patch on the source that is sufficiently small relative to the characteristic dimensions of the system to be considered as a point source (see Fig. 2). The image of the reflector that is produced on the receiving surface depends on the geometry of the reflector (including curvature, etc.) and the geometry of the receiving surface on which the image is formed, and of course the relative spatial location of the source, reflector, and receiver

If this patch has area dA_o and radiant emittance M then the radiant flux from this area will be

$$\Phi_o = M\,dA_o \tag{12}$$

Consider an element of the reflecting surface dA_1 located relative to the source as given by $\vec{N}_o$, $\vec{V}_1$, and $\vec{N}_1$. The radiant intensity of the source can be expressed as a function of β_o, i.e.

$$I(\beta_o) = I_n\,\phi(\beta_o) \tag{13}$$

where I_n is the intensity in the direction of $\vec{N}_o$. For a prescribed $\phi(\beta_o)$, I_n can be determined from the total radiant flux by integrating over the half space seen by dA_o, i.e.

$$\Phi_o = \int_{4\pi} I(\beta_o)\,d\Omega \tag{14}$$

or

$$I_n = \frac{\Phi_o}{\int \phi(\beta_o)\,d\Omega} \tag{15}$$

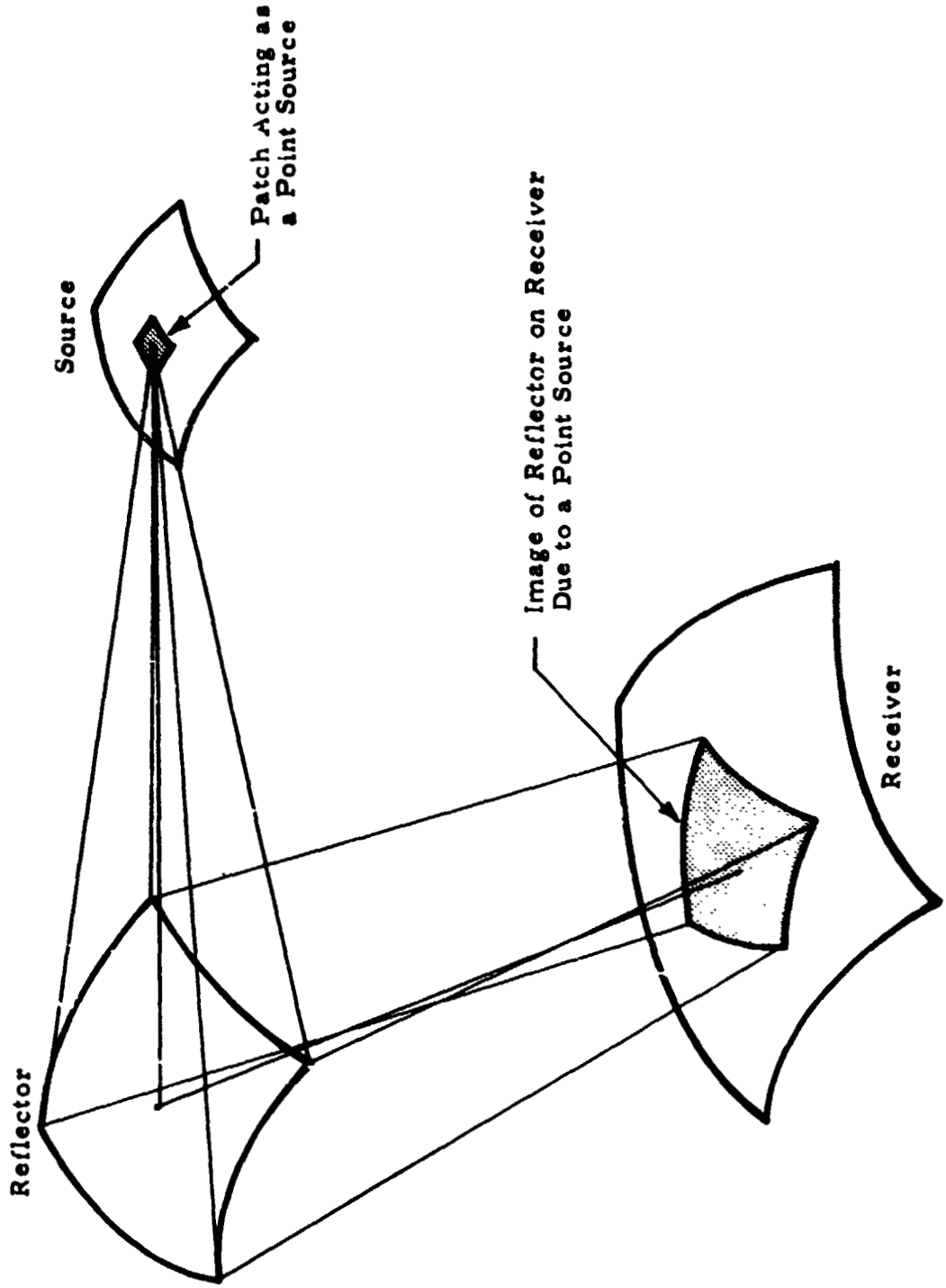

Fig. 2 - Point Source Irradiating a Receiving Surface Through a Curved Reflecting Element

Thus the radiant flux intercepted by dA_1 will be

$$d\Phi_1 = I_n \phi(\beta_o)\, d\Omega_1 \tag{16}$$

where the solid angle $d\Omega_1$ is given by

$$d\Omega_1 = \frac{dA_1 \cos\beta_1}{\vec{V}_1 \cdot \vec{V}_1} \tag{17}$$

or with (12), (15) and (17), (16) can be written

$$d\Phi_1 = \frac{M\, dA_o}{\int_{4\pi} \phi(\beta_o)\, d\Omega} \; \frac{\phi(\beta_o) \cos\beta_1\, dA_1}{\vec{V}_1 \cdot \vec{V}_1} \tag{18}$$

Thus if the source is characterized,(18) can be used to compute the radiant flux on dA_1 due to the emitting element dA_o.

The radiant flux available to irradiate dA_2 is $d\Phi_1$ after being attenuated by dA_1. If dA_1 has reflectivity γ_1, which can be dependent on β_1, then

$$d\Phi_2 = \gamma_1(\beta_1)\, d\Phi_1 \tag{19}$$

The irradiation on the receiving surface can be determined by differentiating the ray-trace equations (10) and (11) and coupling them to (19). If the source is extended then the irradiation at a point on the receiver is determined by integrating over the source through the reflecting surface. One may view this as the overlaying of reflector images produced by point sources as shown in Fig. 3.

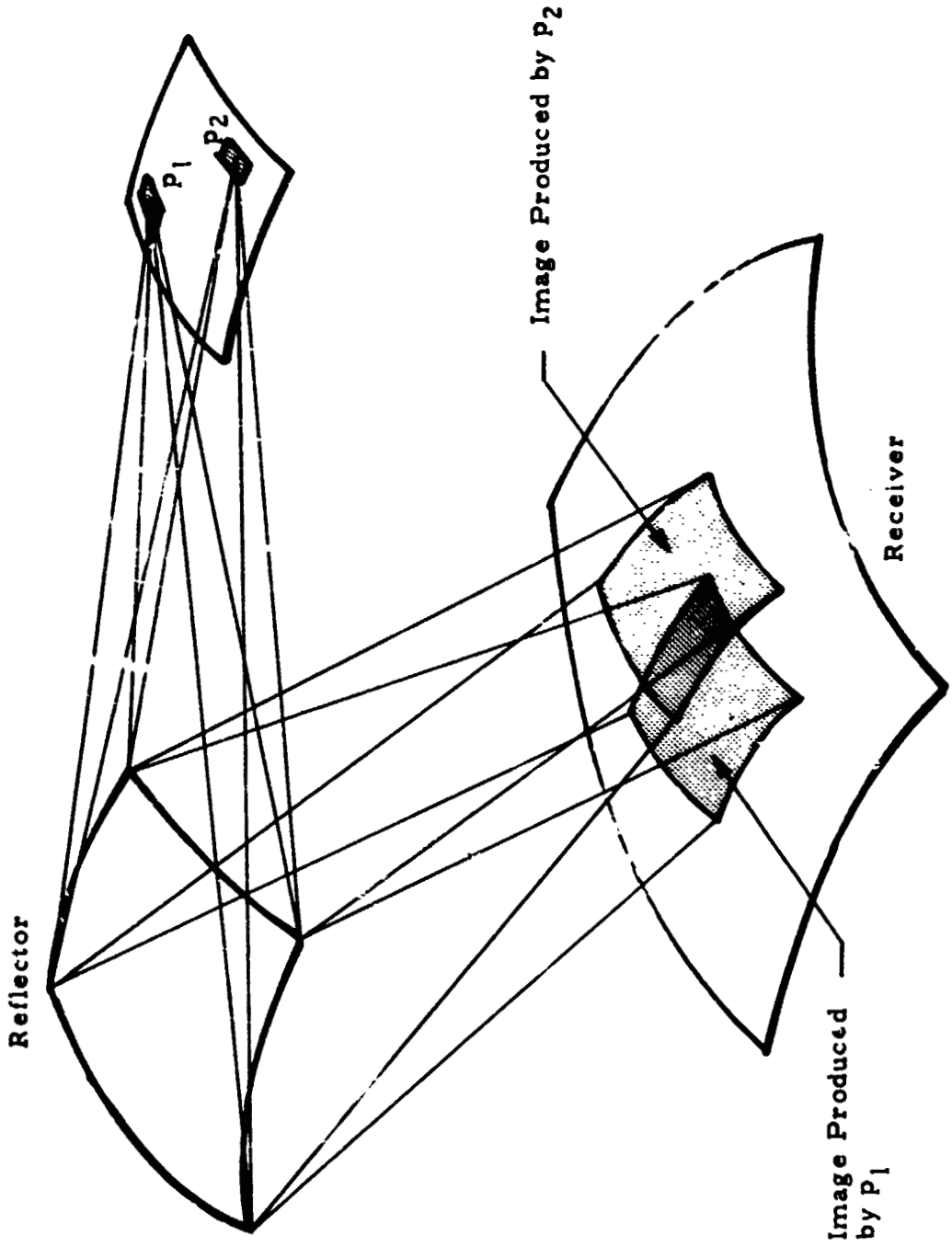

Fig. 3 - Overlaying Images Produced by Point Sources

Let us now consider an extended source being imaged onto a receiving surface. We will assume that the reflecting element is sufficiently small relative to the system characterizing dimensions that it will act as a 'pinhole,' i.e., the image formed on the receiving surface will be determined by the source shape and the receiving surface rather than by the shape of the reflecting surface. This situation is depicted in Fig. 4. The image geometry for each 'pinhole' is determined from ray trace equations and the geometry of the receiving surface. However, the irradiation within the image is dependent on the source characteristics as well as geometric considerations. Thus the irradiation at a point on the receiving surface is determined by integrating over the reflector while considering the source characteristics. One may view this as the overlaying of images produced by the source geometry as shown in Fig. 5.

The foregoing can be summarized as follows: the radiant flux incident on dA_1 can be computed from (18) by integrating over the source S_o, and that available to irradiate the receiver can be obtained by integrating (19). For the case of a point source the ray trace equations must be differentiated holding the source coordinate constant. This gives the mapping of the reflector onto the receiver. By coupling this to energy considerations an expression for the irradiation can be derived. However, for the situation of a pinhole reflector the reflector coordinates are held and the ray trace equations are differentiated. This gives the mapping of the source onto the receiver. By coupling this to the characteristics of the source an expression for the irradiation can be derived.

Thus there are basically two approaches that can be used to compute the thermal image of a radiation source such as the sun. Due to the characteristics of the source and its size relative to its distance from the reflecting surface, the second approach is more desirable for this application.

3.3 THE SOLAR SOURCE

Considerable effort has been devoted to characterizing the solar source in terms of its irradiance outside earth's atmosphere (solar constant), spectral

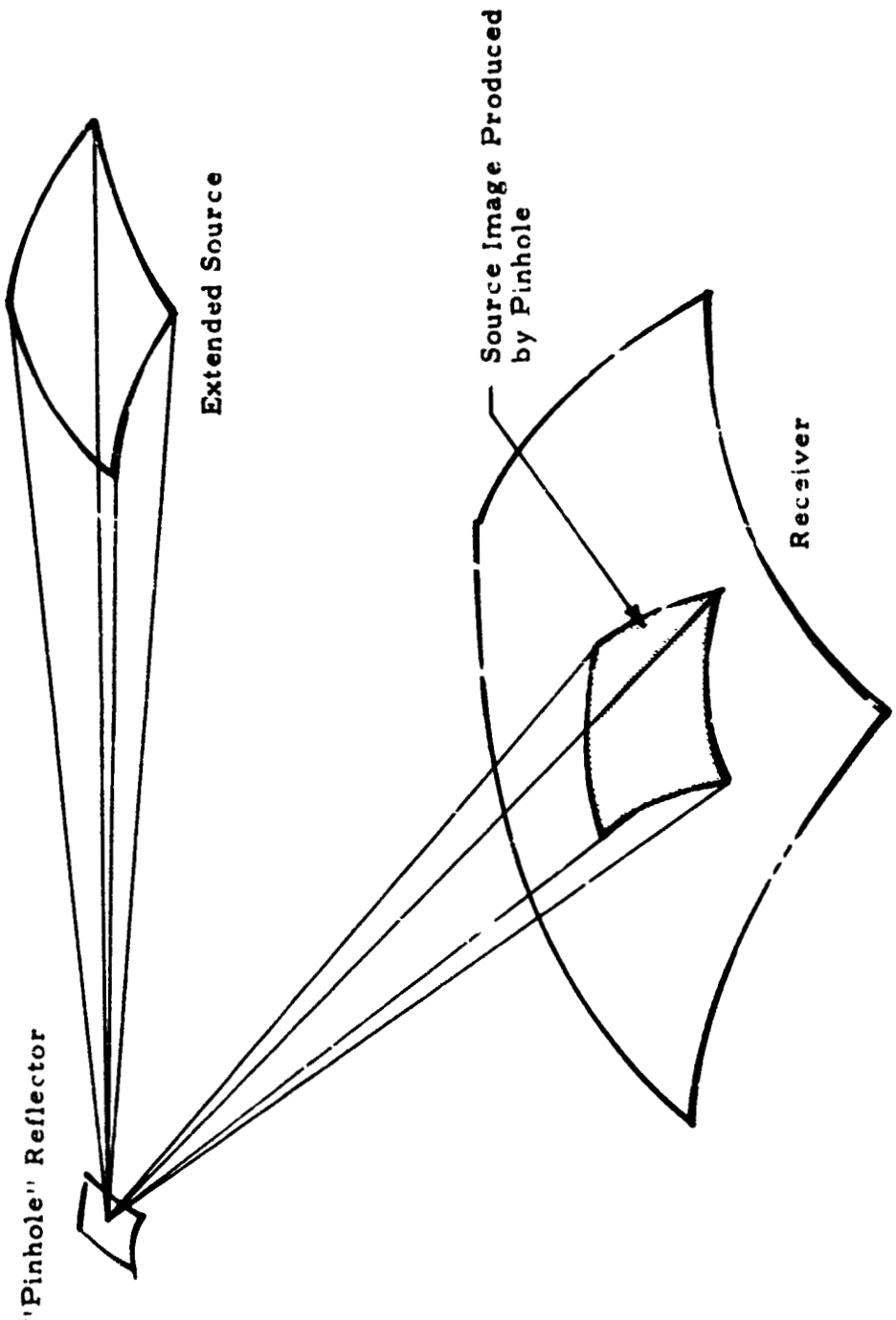

Fig. 4 - Image Produced by Pinhole Reflector

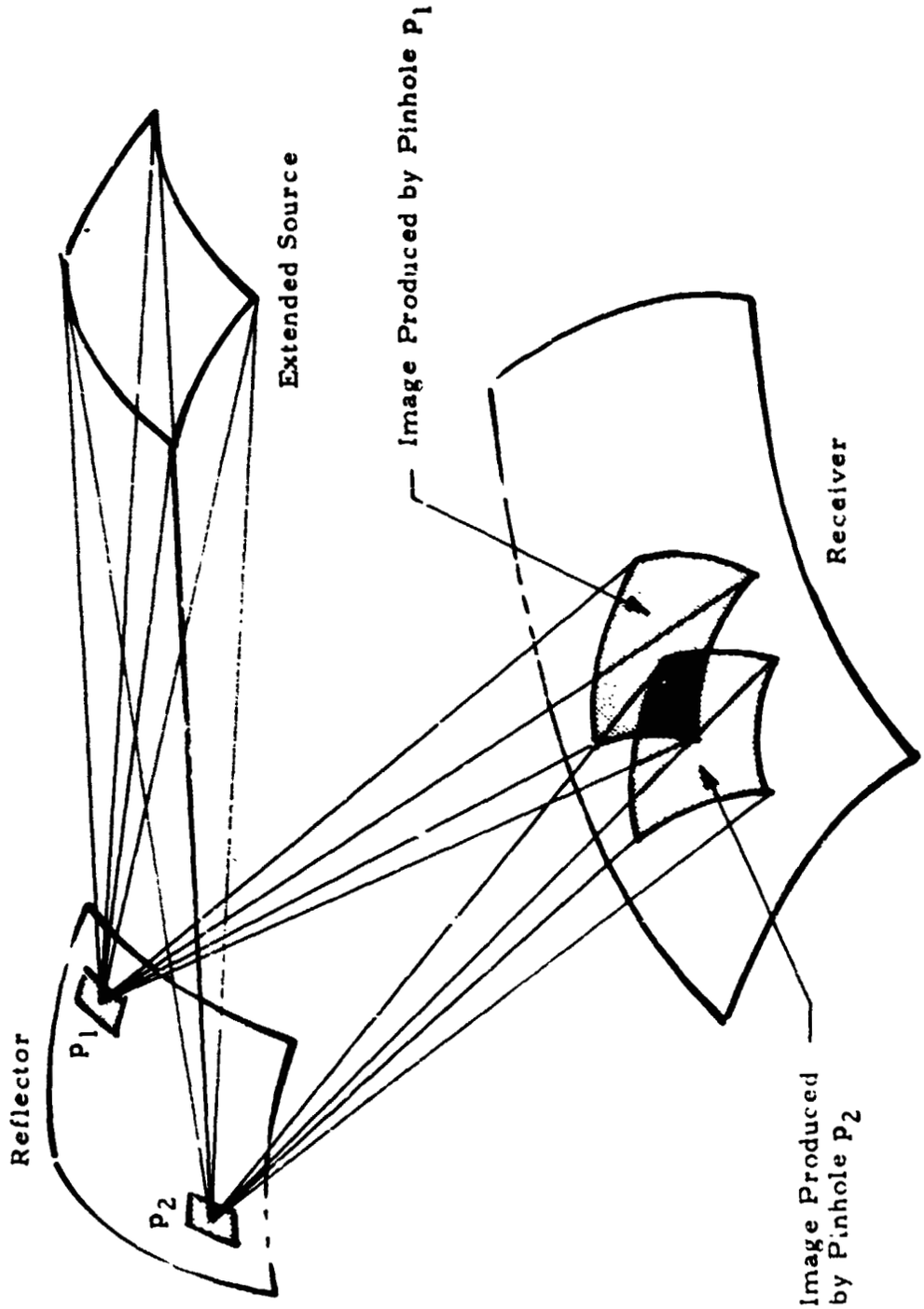

Fig. 5 - Overlaying Images Produced by Pinhole Reflectors

properties, and variation in radiance across the source [50, 58-61]. The most generally accepted value of the solar constant is 1.94 calories per square centimeter per minute. The thermal radiation from the solar source is primarily in the wavelength range of 0.3 to 3.0 microns. This is a relatively small wavelength variation. As a result the spectral properties of the radiation can normally be averaged for the purpose of computing a thermal image. However, the brightness or radiance as a function of position on the solar disc is very important in determining the irradiation distribution on targets in the focal region of solar concentrators [50]. There are several models of the solar disc available [50, 58]. The solar disc is normally assumed to subtend an angle of 32 minutes when viewed in the neighborhoold of earth. However, there are slight seasonal variations in the solar disc size due to the change in earth-sun distance. This variation is from 32.59 minutes in January to 31.52 minutes in July [57]. The effective temperature of the solar source as seen from our planet is somewhat controversial, however an often quoted number is 5800°K.

To describe the solar source let us consider a very small reflecting element imaging the solar disc onto a plane normal to the reflected ray vector as shown in Fig. 6. The radiance of the sun decreases from its center to the outer edge and thus the irradiation in the solar disc image varies in the same manner. Expressions for the intensity within the sun image integrated over all wavelengths have been given by Kamada [50] and Angstorm and Angstrom [58].

The variation in intensity can be expressed as a function of the angle between the ray vector of interest and the image centerline ray vector. Letting any ray vector to the sun image be $\vec{V}_\xi$ the intensity distribution across the sun image will decrease radially as shown in Fig. 7. The intensity within the sun image is expressed in terms of the image center intensity and the angle ξ. Intensity is defined in Eq. (20) shown on the following page.

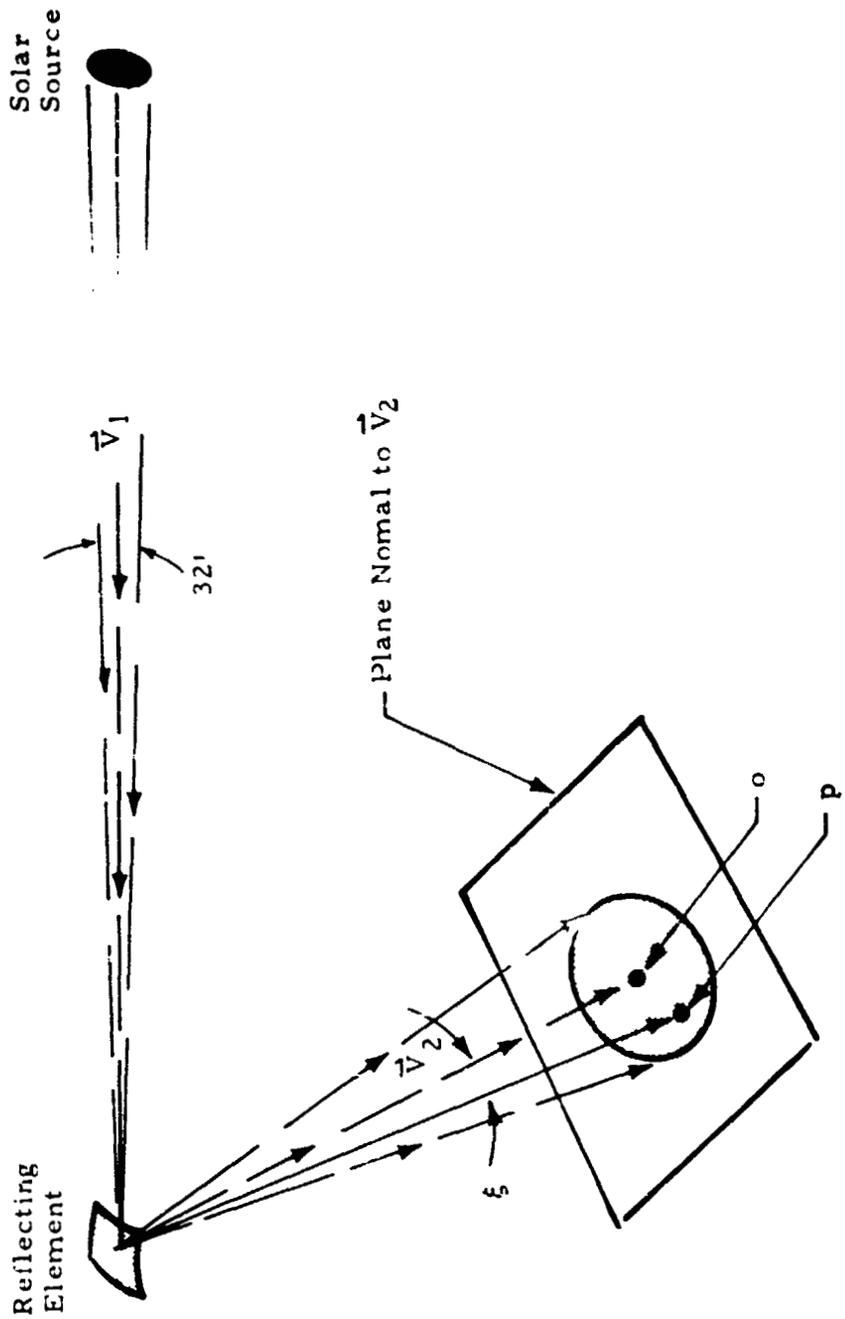

Fig. 6 - Imaging the Solar Source

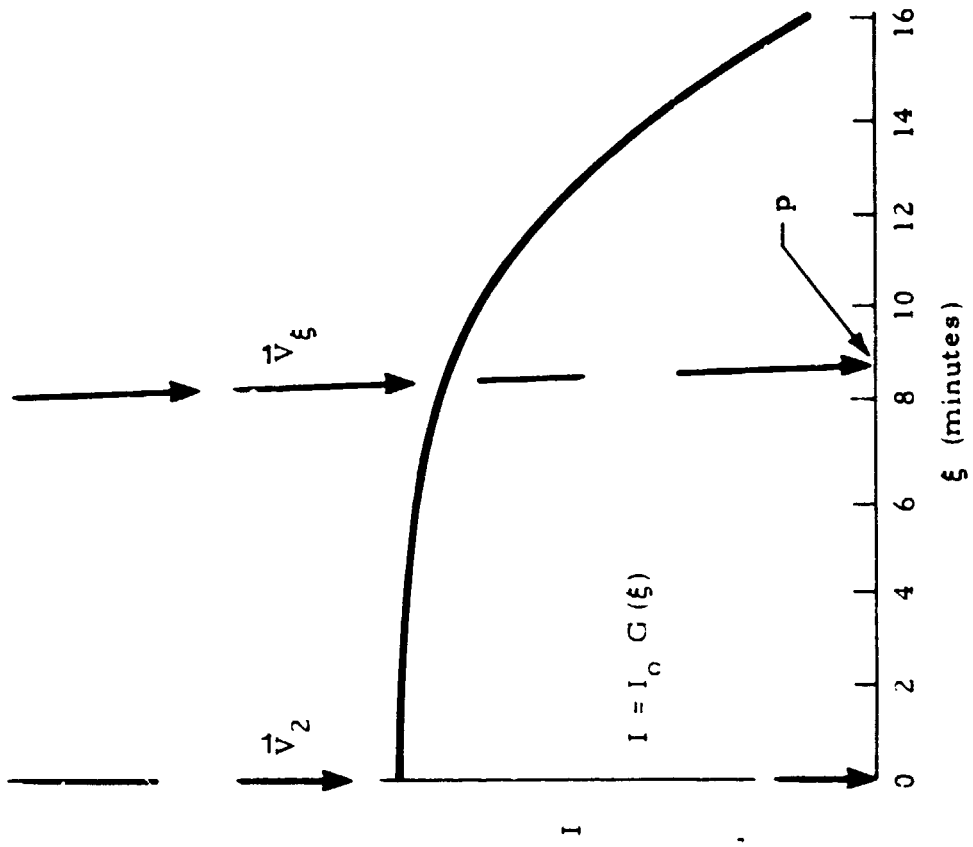

Fig. 7 - Intensity Variation in Solar Source Image

$$I = \frac{d\Phi}{d\Omega} \tag{20}$$

For an element of the image dA_2 located at the termination point of $\vec{V}_\xi$ (assuming ξ is small)

$$d\Omega = dA_2/(\vec{V}_\xi \cdot \vec{V}_\xi) \tag{21}$$

Irradiation is defined by

$$E = \frac{d\Phi}{dA} \tag{22}$$

Thus with the above the irradiation on the surface is related to the intensity by

$$E(\xi) = I(\xi)/(\vec{V}_\xi \cdot \vec{V}_\xi) \tag{23}$$

or

$$E(\xi) = E_o G(\xi)$$

The irradiation on the plane being considered must satisfy the energy balance

$$d\Phi_2 = \int E\, dA \tag{24}$$

The distance from the center ray to any point on the image can be expressed

$$\nu = \left|\vec{V}_2\right| \xi \tag{25}$$

Now

$$dA = 2\pi \ \nu \, d\nu \tag{26}$$

$$= \frac{2\pi \xi \, d\xi}{\vec{V}_2 \cdot \vec{V}_2}$$

Thus

$$d\Phi_2 = \frac{2\pi E_o}{\vec{V}_2 \cdot \vec{V}_2} \int_o^{\xi_o} G(\xi) \xi d\xi \tag{27}$$

From which

$$E_o = \frac{d\Phi_2}{2\pi \vec{V}_2 \cdot \vec{V}_2 \int_o^{\xi_o} G(\xi) \xi \, d\xi} \tag{28}$$

Thus with a prescribed intensity distribution and a prescribed reflecting element which gives the reflected radiant flux $d\Phi_2$ one can compute the irradiation at any point in the solar image produced by the reflecting element with the use of (23) and (28), i.e.,

$$E(\xi) = \frac{d\Phi_2 G(\xi)}{2\pi \vec{V}_2 \cdot \vec{V}_2 \int_o^{\xi_o} G(\xi) \xi \, d\xi} \tag{29}$$

The above gives the irradiation distribution on a plane normal to the reflected ray vector. This will be extended to non-planar receivers in another section. Equation (29) characterizes the solar source imaged by a small reflecting element.

The effects of limb darkening are important in high concentrations are achieved. In situations where the radiation is spread out over several sun image diameters, the limb darkening effects are obliterated.

3.4 APPLICATION OF THE ANALYSIS TO SOLAR CONCENTRATORS

The analysis developed in the previous sections will be applied to determine the heat flux on targets in the focal region of solar concentrators. The analysis developed is rather general and is applicable to any solar concentrator situation. However, for the particular situation under consideration the general analysis is not needed. An abbreviated form can be used without any loss of generality. The concentrator and receiver configurations of interest are axisymmetric. However, non-axisymmetric conditions will exist in the system due to pointing errors, optical imperfections, and target placement errors. However, for the particular situation at hand, a general analysis is best accomplished by using an axisymmetric analysis that is modified to consider the non-axisymmetric conditions.

For the axisymmetric configuration in Fig. 8, the coplanarity condition given by Eq. (2) will automatically be satisfied since all rays are meridional. Let the coordinate system be oriented such that the unit vector $\vec{k}$ is pointing toward the solar source. This of course implies

$$\vec{V}_1 = -\vec{k} \tag{30}$$

if s and r are taken as the concentrator and receiver axisymmetric coordinates, respectively, and $\vec{e}$ as a unit vector in the plane of symmetry (see Fig. 8) then the position vectors of the ray extremities given by (4) and (5) become

$$\vec{R}_1 = \vec{e}\, s + \vec{k}\, z_1 \tag{31}$$

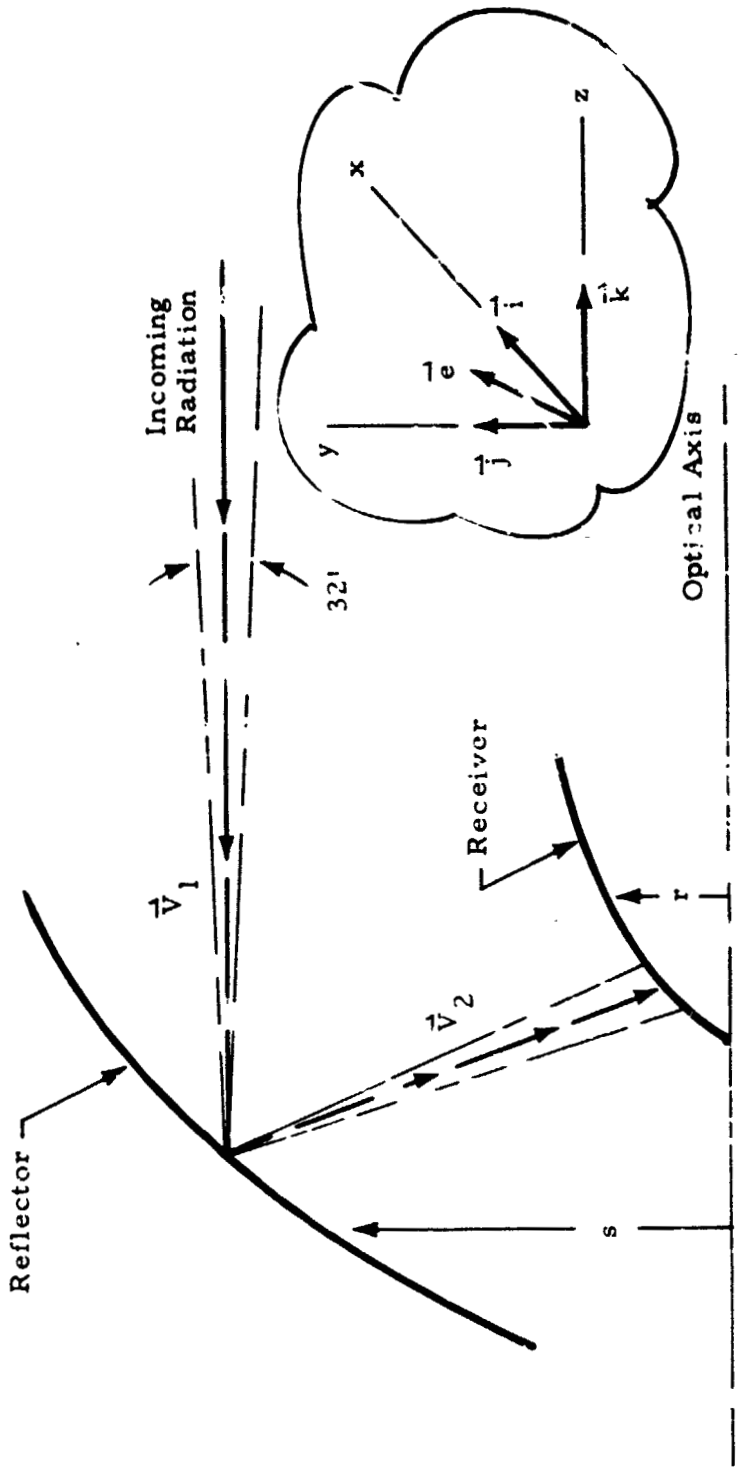

Fig. 8 - Axisymmetric Solar Concentrator-Receiver Configuration

$$\vec{R}_2 = \vec{e}\,r + \vec{k}\,z_2 \tag{32}$$

and the reflected ray vector (.) becomes

$$\vec{V}_2 = \vec{e}(r - s) + \vec{k}(z_2 - z_1) \tag{33}$$

For the axisymmetric situation

$$s = s(z_1) \tag{34}$$

or the implicit surface function is

$$S_1(s, z_1) = s - s(z_1) = 0 \tag{35}$$

and

$$\vec{N}_1 = \vec{\nabla} S_1 = \vec{e} - \vec{k}\,s' \tag{36}$$

Thus with (36), (33), and (30), the ray trace equation (1) becomes

$$\left[-\vec{k} + \frac{\vec{e}(r - s) + \vec{k}(z_2 - z_1)}{\sqrt{(r - s)^2 + (z_2 - z_1)^2}}\right] \cdot (\vec{e} - \vec{k}\,s') = 0 \tag{37}$$

or upon performing the dot product

$$s'\left[\left|\vec{V}_2\right| - (z_2 - z_1)\right] + (r - s) = 0 \tag{38}$$

where

$$\left|\vec{V}_2\right| = \sqrt{(r-s)^2 + (z_2 - z_1)^2} \tag{39}$$

Equation (38) gives the ray path for source centerline rays. Other rays from the source are described by the above and the source geometry.

Let us relate the axisymmetric coordinate s to the coordinates y and z. Defining

$$\psi = \cos^{-1}(\vec{e}\cdot\vec{j}) \tag{40}$$

$$y_1 = s\cos\psi \tag{41}$$

$$x_1 = s\sin\psi \tag{42}$$

Consider a differential element of the reflecting surface as shown in Fig. 9 the area of this element can be expressed

$$dA_1 = s\left[(ds)^2 + (dz_1)^2\right]^{1/2} d\psi \tag{43}$$

or

$$dA_1 = s\left[(s')^2 + 1\right]^{1/2} d\psi\, dz_1$$

If the irradiation on a plane normal to $\vec{V}_1$ is given by the solar constant K then the radiant flux intercepted by dA_1 will be

$$d\Phi_1 = K\, dA_1 \cos\beta_1 \tag{44}$$

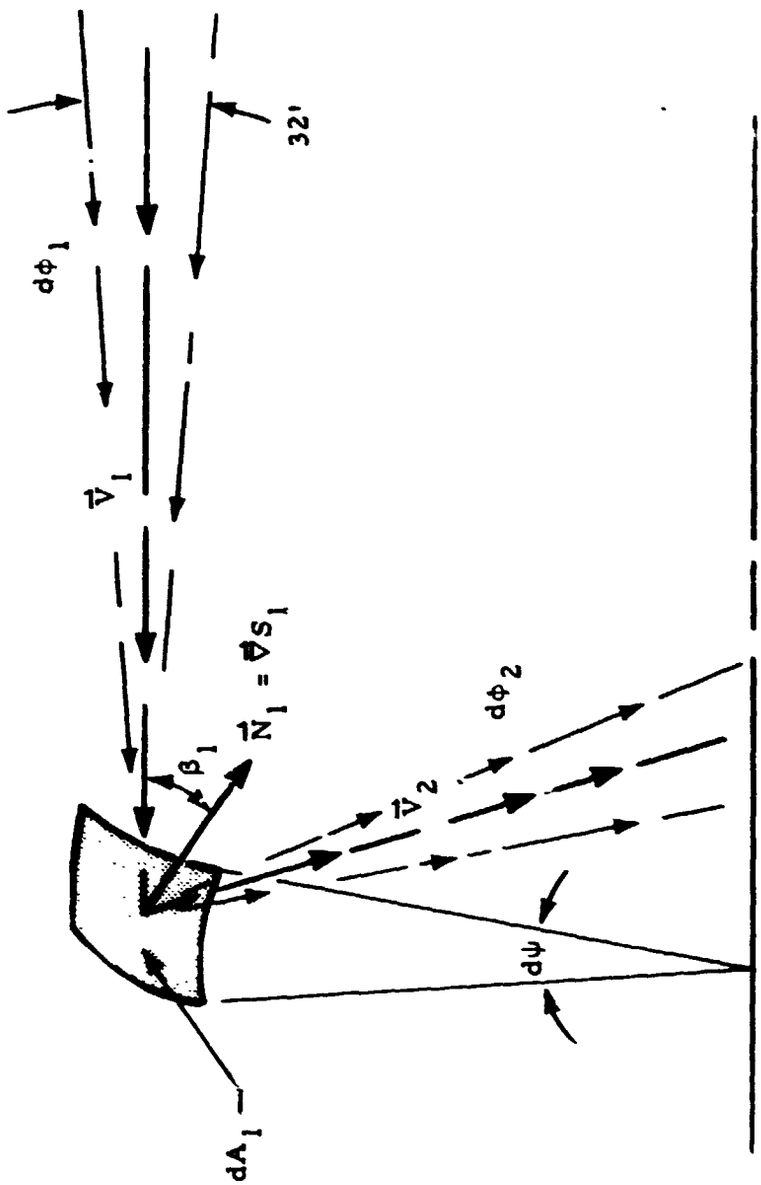

Fig. 9 - Energy Balance

where β_1 can be defined by

$$\beta_1 = \cos^{-1}\left(\frac{\vec{V}_1 \cdot \vec{N}_1}{\left|\vec{V}_1\right| \left|\vec{N}_1\right|}\right) \tag{45}$$

By combining (43), (44), and (45)

$$d\Phi_1 = K s s' \, d\psi \, dz_1 \tag{46}$$

If the reflecting element has reflectivity γ_1 which can be a function of β_1, the radiant flux reflected onto the receiver will be

$$d\Phi_2 = \psi_1 (\beta_1) K s s' d\psi \, dz_1 \tag{47}$$

It was shown previously how the irradiation on a receiving surface normal to the reflected ray could be computed if the incident radiant flux $d\Phi_2$ and the source description $G(\xi)$ were known. Let us now consider a general receiving surface onto which the solar source is being imaged as shown in Fig. 10. We wish to compute the irradiation at an arbitrary point p. Looking at a plane containing 0 and p as shown in Fig. 11, the irradiation on a plane normal to $\vec{V}_2$ and passing through p can be computed. If the coordinates of p are (x_p, y_p, z_p), $\vec{V}_\xi$ can be written as

$$\vec{V}_\xi = \vec{R}_p - \vec{R}_1 \tag{48}$$

where

$$\vec{R}_p = \vec{i}\, x_p + \vec{j}\, y_p + \vec{k}\, z_p \tag{49}$$

$$R_1 = \vec{i}\, s \sin\psi + \vec{j}\, s \cos\psi + \vec{k}\, z \tag{50}$$

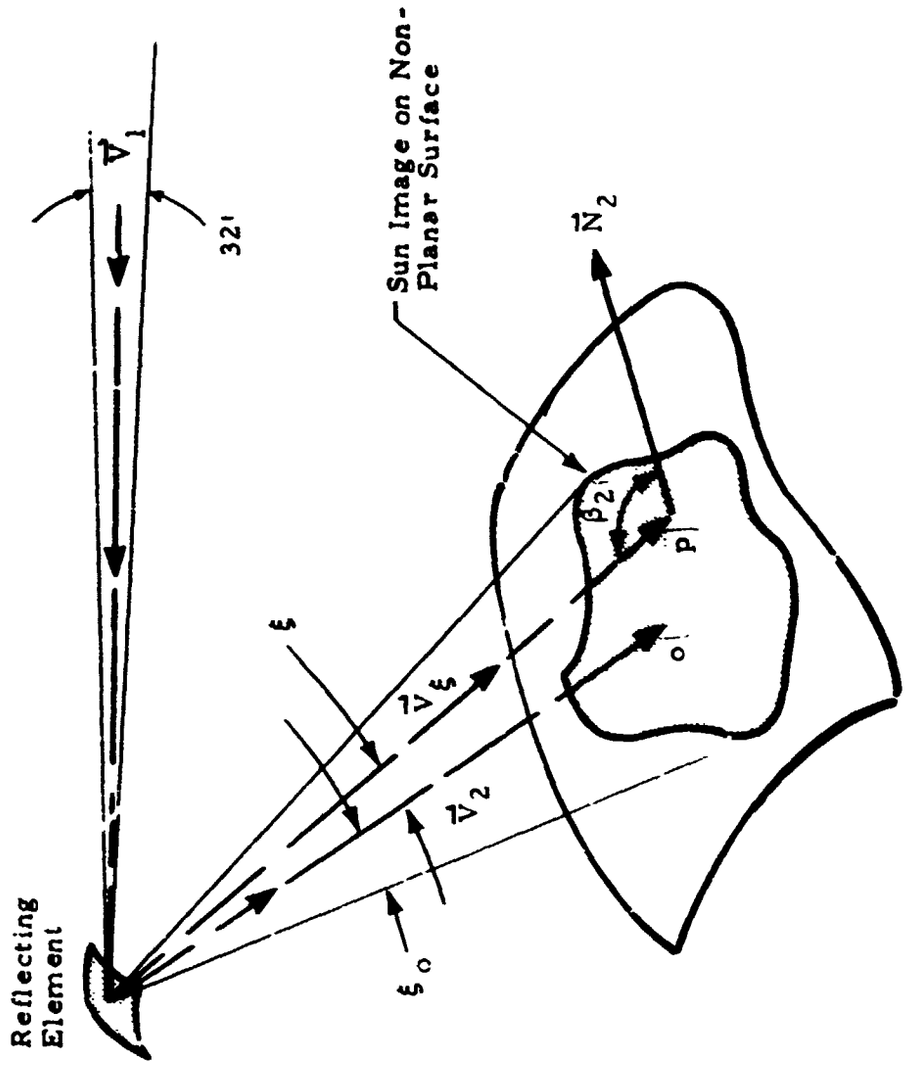

Fig. 10 - Solar Image on an Arbitrary Receiver

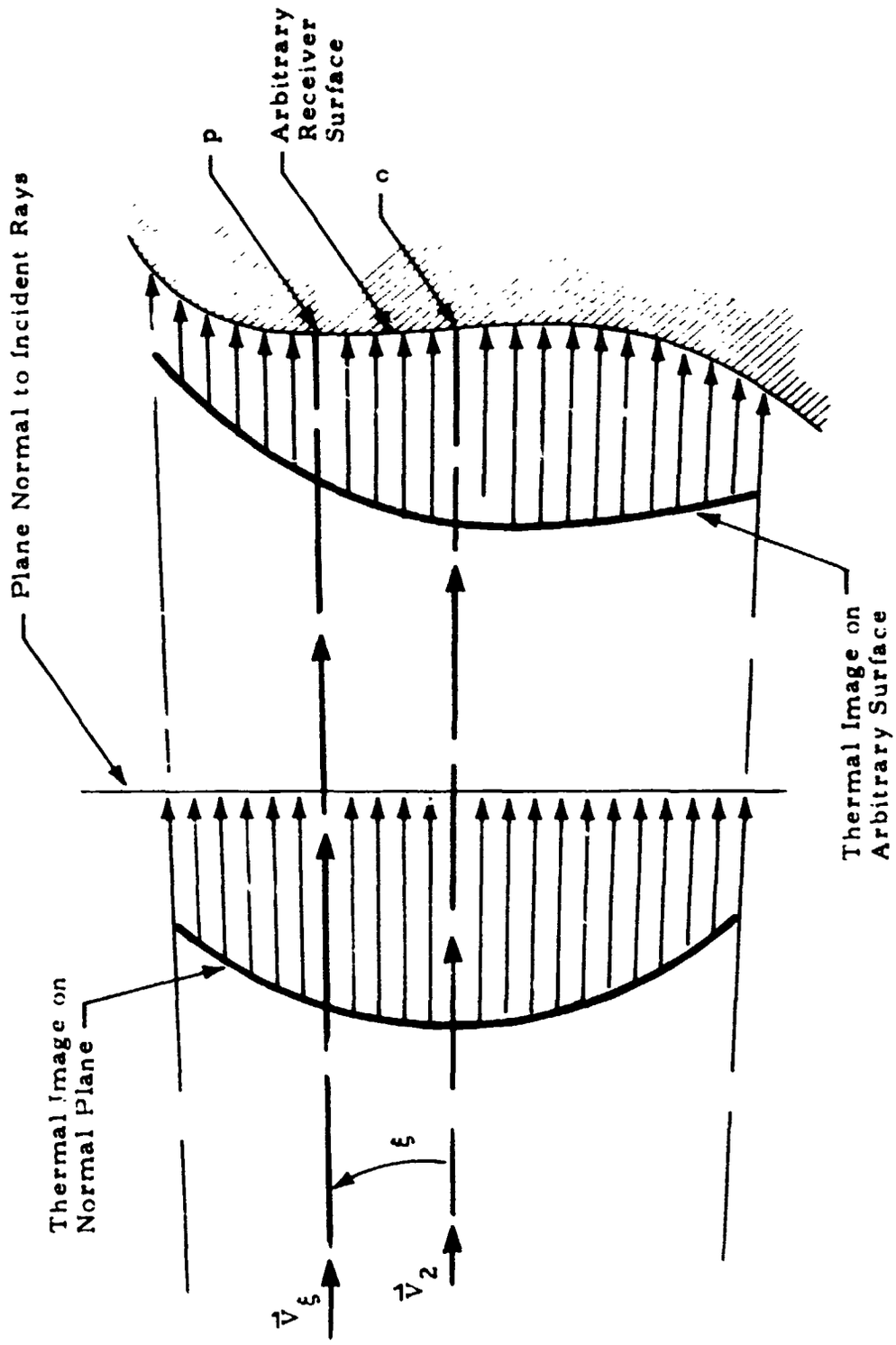

Fig. 11 - Irradiation on a Non-Planar Receiver

With the above ξ can be computed from

$$\xi = \sin^{-1} \frac{\left|\vec{V}_2 \times \vec{V}_\xi\right|}{\left|\vec{V}_2\right|\left|\vec{V}_\xi\right|} \tag{51}$$

The angle β_o between the incident ray R_ξ and the surface being irradiated can be computed from

$$\beta_o = \cos^{-1}\left(\frac{\vec{V}_2 \cdot \vec{N}_2}{\left|\vec{V}_2\right|\left|\vec{N}_2\right|}\right) \tag{52}$$

where

$$\vec{N}_2 = \vec{\nabla} S_2 (x_p, y_p, z_p) \tag{53}$$

The irradiation at p is given by

$$E_p = E(\xi) \cos\beta_2 \tag{54}$$

With (29) and (47) the above becomes

$$E_p = \frac{\gamma_1 (\beta_1) K s s' G(\xi) (\cos \beta_2) d\psi \, dz_1}{2\pi \, \vec{V}_\xi \cdot \vec{V}_\xi \int_o^{\xi_o} G(\xi) \xi \, d\xi} \tag{55}$$

The above gives the irradiation on an arbitrary receiving point with any orientation. This of course is for a differential element of the reflecting surface. To determine the total irradiation at a point the above must be integrated over

ψ and z_1, or in other words over the concentrator surface S_1. Let

$$\tau = \frac{\gamma_1(\beta_1)\, K\, s\, s'\, G(\xi) \cos\beta_2}{2\pi\, \vec{V}_\xi \cdot \vec{V}_\xi \int_0^{\xi_o} G(\xi)\, \xi\, d\xi} \tag{56}$$

Then

$$E_{tot} = \sum E_p = \iint_{\psi\, z_1} \delta(\xi, \beta_2)\, \tau\, d\psi\, dz_1 \tag{57}$$

where $\delta(\xi, \beta_2)$ is defined as follows

$$\delta(\xi, \beta_2) = \begin{cases} 1 & \begin{cases} \xi \le \xi_o \\ \beta_2 \le \pi/2 \end{cases} \\ 0 & \begin{cases} \xi > \xi_o \\ \beta_2 > \pi/2 \end{cases} \end{cases} \tag{58}$$

ξ and β_2 are dependent on ψ and z_1. The purpose of $\delta(\xi, \beta_2)$ is to take care of two points that must be considered in the integration process. These are: (1) if the receiver point lies outside the image formed by the reflecting element there is no contribution to the irradiation and (2) if the receiver point cannot 'see' the reflecting element there is no contribution to the irradiation.

3.5 TARGET PLACEMENT ERRORS

The irradiative distribution on a receiving surface placed in the focal region of a solar concentrator can be changed significantly by small changes in the spatial location and orientation of the receiving surface. If the receiver

is initially in the axisymmetric location any placement errors or intentional movements of the receiver can be described by a rotation in one plane and a translation along the axis normal to this plane as shown in Fig. 12. The new coordinates and orientation of the receiver can be expressed in terms of the original coordinates and surface normal vectors as follows.

The surface normal vector is expressed

$$\vec{N}_2 = \vec{i}\,\frac{\partial S_2}{\partial x} + \vec{j}\,\frac{\partial S_2}{\partial y} + \vec{k}\,\frac{\partial S_2}{\partial z} \tag{59}$$

where $S_2(x, y, z)$ is the implicit function describing the receiving surface. The component of N_2 in the x direction will not be changed. Thus let us consider only the components in the y-z plane being rotated as shown in Fig. 13. We can express the components in the y-z plane as

$$\vec{n} = \vec{j}\,\frac{\partial S_2}{\partial y} + \vec{k}\,\frac{\partial S_2}{\partial z} \tag{60}$$

Let us express $\vec{n}$ after rotation as

$$\vec{n}' = \vec{j}\left(\frac{\partial S_2}{\partial y}\right)' + \vec{k}\left(\frac{\partial S_2}{\partial z}\right)' \tag{61}$$

Now $|\vec{n}'| = |\vec{n}|$ and we can express the angles in Fig. 13 as follows

$$\cos\mu = \frac{\partial S_2}{\partial z} \,/\, |\vec{n}| \tag{62}$$

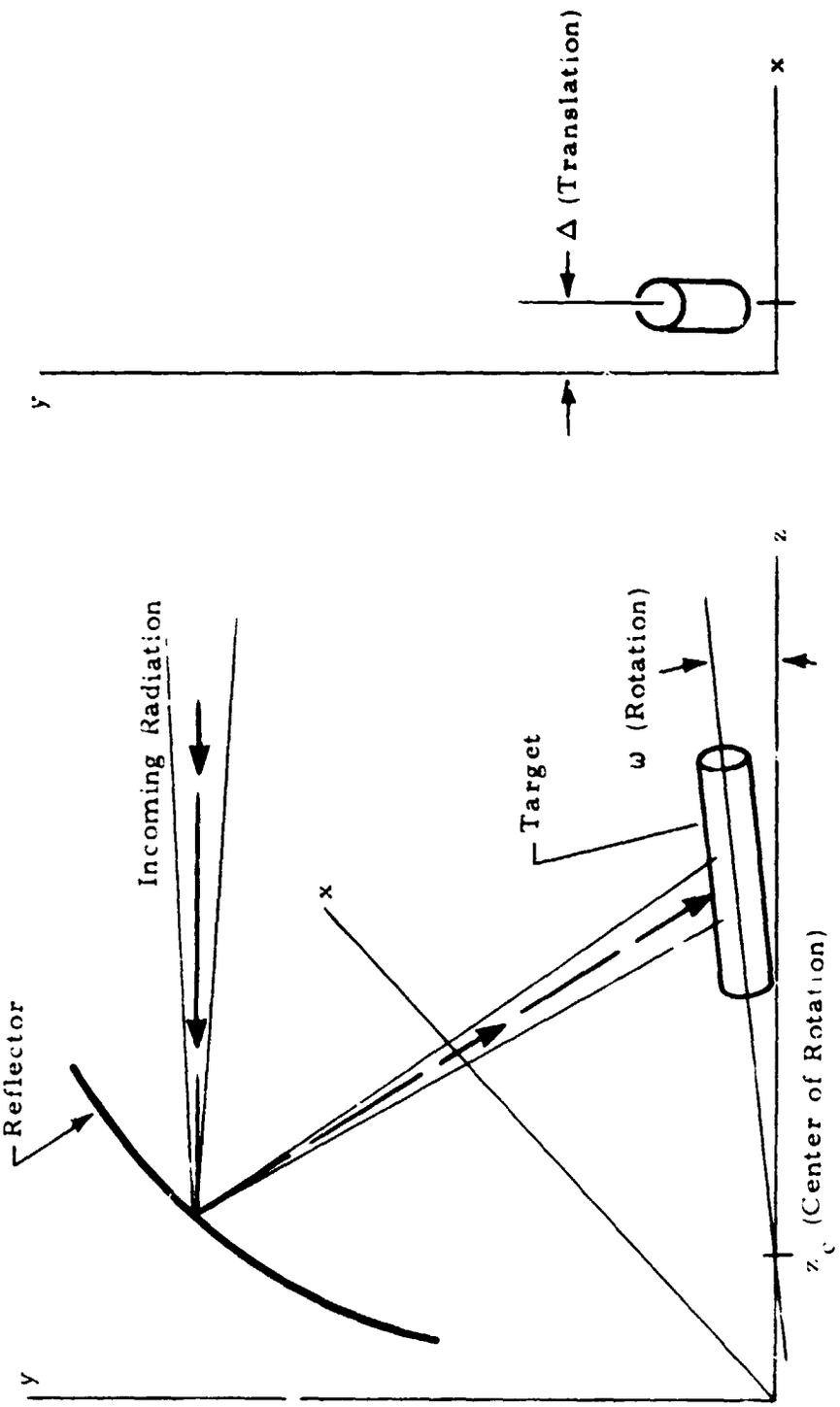

Fig. 12 - Target Placement Errors

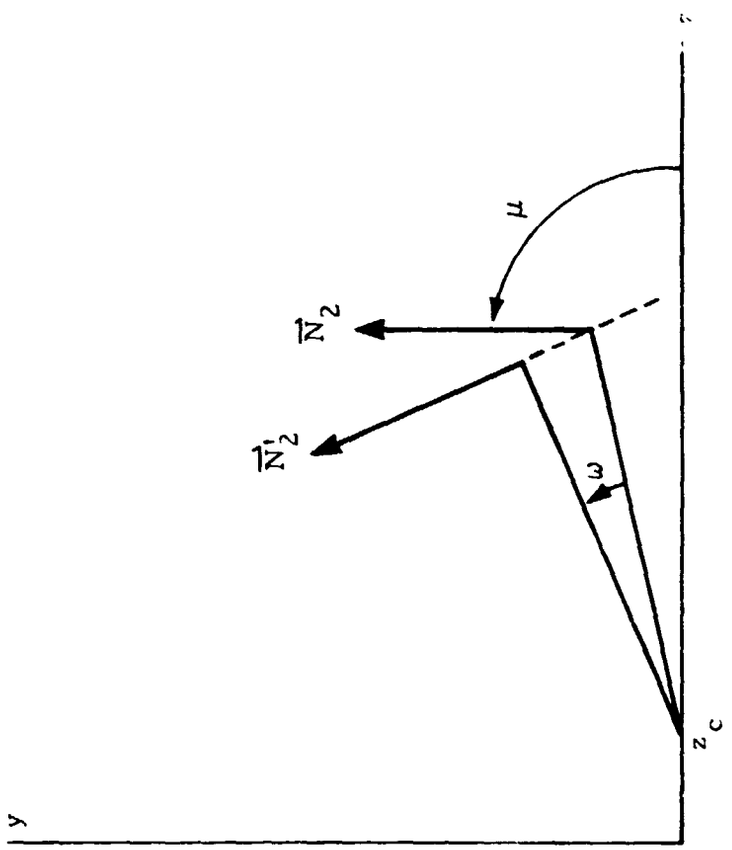

Fig. 13 - Rotation of Surface Normal Vector

$$\sin\mu = \frac{\partial S_2}{\partial y} / \left|\vec{n}\right| \tag{63}$$

and

$$\cos(\mu + \omega) = \left(\frac{\partial S_2}{\partial z}\right)' / \left|\vec{n}\right| \tag{64}$$

$$\sin(\mu + \omega) = \left(\frac{\partial S_2}{\partial y}\right)' / \left|\vec{n}\right| \tag{65}$$

By making use of the identities

$$\cos(\mu + \omega) = \cos\mu \cos\omega - \sin\mu \sin\omega$$
$$\sin(\mu + \omega) = \sin\mu \cos\omega + \cos\mu \sin\omega$$

and the above we can show that

$$\left(\frac{\partial S_2}{\partial z}\right)' = \frac{\partial S_2}{\partial z} \cos\omega - \frac{\partial S_2}{\partial y} \sin\omega \tag{66}$$

$$\left(\frac{\partial S_2}{\partial y}\right)' = \frac{\partial S_2}{\partial y} \cos\omega + \frac{\partial S_2}{\partial z} \sin\omega \tag{67}$$

Thus the new surface normal vector is

$$N = \vec{i}\,\frac{\partial S_2}{\partial x} + \vec{j}\left(\frac{\partial S_2}{\partial v}\cos\omega + \frac{\partial S_2}{\partial z}\sin\omega\right)$$
$$+ \vec{k}\left(\frac{\partial S_2}{\partial z}\cos\omega - \frac{\partial S_2}{\partial y}\sin\omega\right) \tag{68}$$

and the new coordinates of a point on the surface can be expressed

$$
\begin{aligned}
x' &= x + \Delta \\
y' &= y \cos\omega + z \sin\omega \\
z' &= z \cos\omega - y \sin\omega
\end{aligned}
\tag{69}
$$

3.6 OPTICAL ERRORS

Any reflecting surface will have some degree of geometric imperfection or waviness that occurs because of fabrication techniques, stresses, etc. The exact nature of these imperfections are very difficult to determine a priori. These imperfections do not normally follow a normal statistical distribution and are probably very dependent on the individual reflector. It has been pointed out by Stewart [44] that the imperfections cannot be simulated by a Gaussian distribution. However, if data describing the geometric imperfections is not available the use of random surface errors as described by a Gaussian distribution can give some insight to the influence of geometric imperfections. The approach for randomly introducing surface errors is illustrated in Fig. 14. The surface slope is perturbed randomly between 0 and three standard deviations in a Gaussian manner. The angular imperfections corresponding to one standard deviation must of course be specified.

3.7 REFLECTOR DESIGN

By coupling the geometric optics and energy balance analyses to finite difference formulas, reflectors that give prescribed irradiative distributions can be designed. The idea of overlaying the thermal images produced by differential elements of reflecting surface is utilized. If an irradiative distribution is prescribed, a reflector surface is determined by 'building up' the reflector by forward differencing schemes. The irradiative distribution requirements and source characteristics guide the differencing scheme in arriving at the surface shape. This idea is illustrated in Fig. 15.

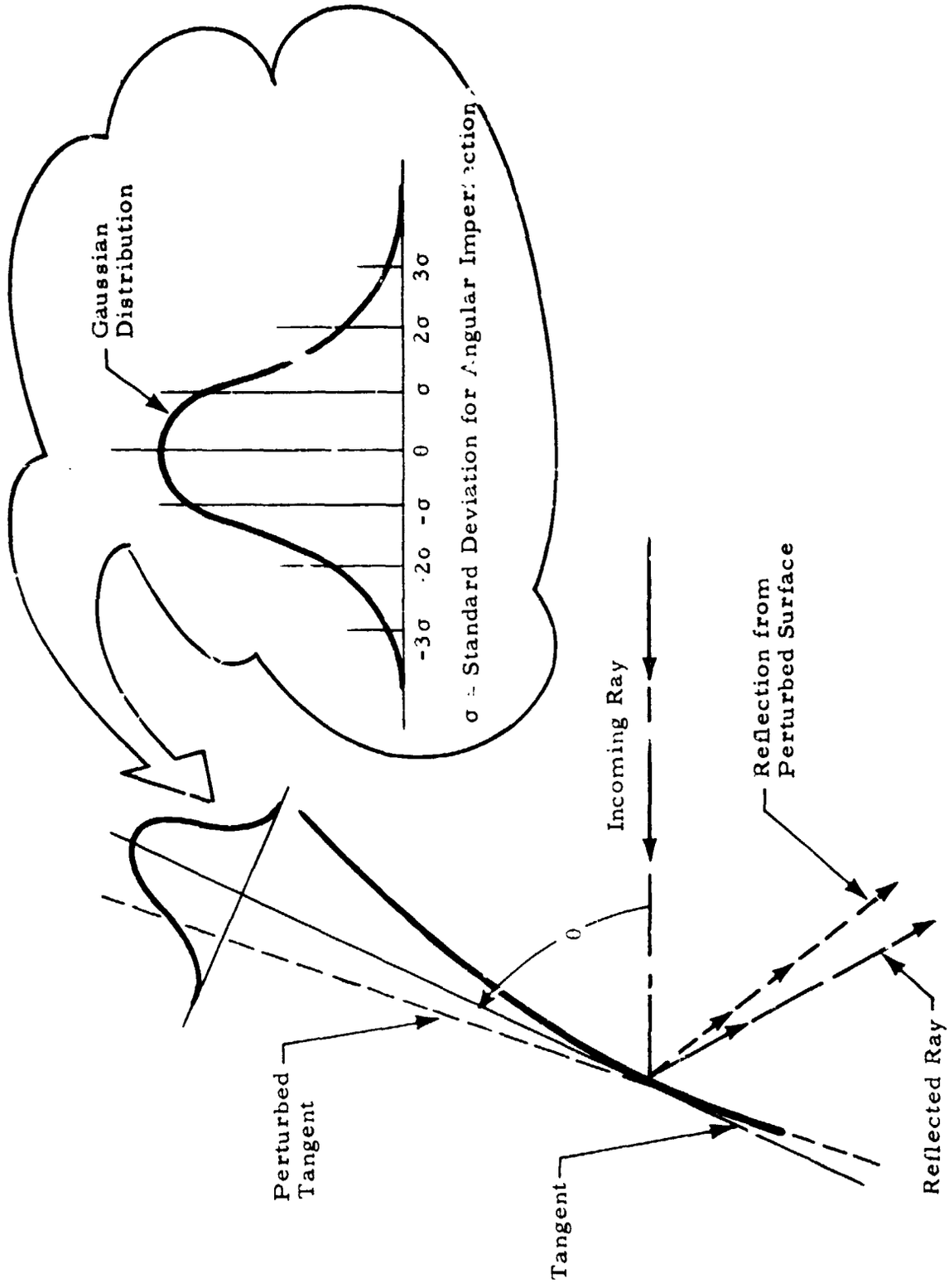

Fig. 14 - Statistical Perturbation of Reflector Surface

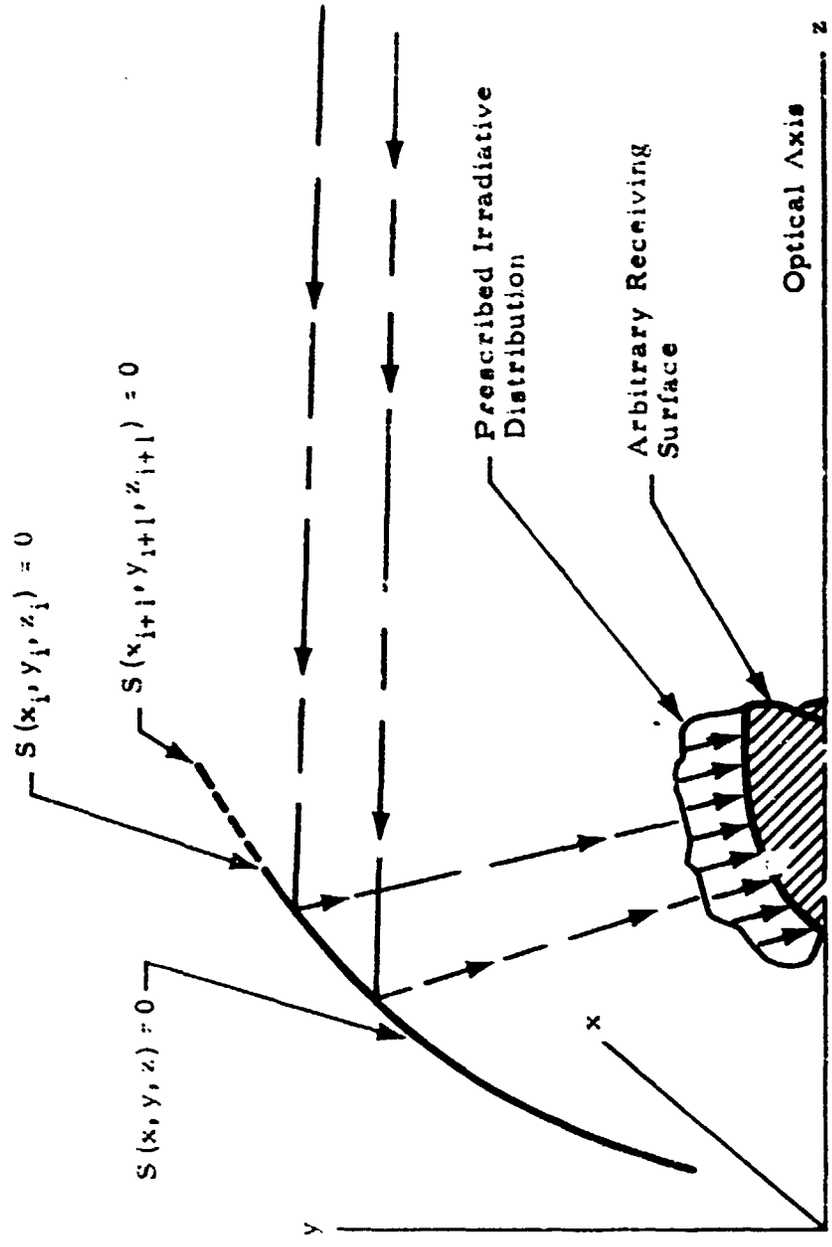

- Finite Difference Formulas
- Energy Requirements
- Geometric Optics
- Source Characteristics

Fig. 15 - Reflector Surface Design

While this technique can be applied to any source-receiver combination it should be pointed out that there are inherent limitations when an extended source is used. If a point or collimated source is used the reflector is defined by a differential equation as shown in [62-63] and the only constraining factor is the energy available. However for an extended source an integral equation defines the reflector shape. For this situation the source characteristics determine whether a particular irradiative distribution can be achieved. For example, as pointed out in Ref. [63] irradiative distributions with large gradients along the receiver surface may be very difficult or impossible to achieve.

3.8 PARAMETER DEFINITIONS AND NON-DIMENSIONALIZING THE EQUATIONS

It is rather easy to non-dimensionalize the equations developed in the analysis for solar concentrators. Only a characteristic dimension and a characteristic radiant quantity are needed. The obvious choice for the characteristic radiant quantity is the solar constant K. The characteristics dimension chosen will be a focal length f. Although this quantity is somewhat nebulous for concentrators without a true 'focal point' it is the quantity that will be used. Most of the results published in the open literature are for paraboloids. An important parameter for any optical device is the aperture ratio — which is the ratio of the aperture or opening that receives radiation to the focal length. Results are normally presented as a function of this parameter.

Hiester, et al., [47] defined the concentration ratio as the ratio of the heat flux at the sun image of a sun furnace to the actual flux received from the sun at normal incidence after reflection. This definition can be applied to any point on a receiving surface. Actually this definition will become evident upon non-dimensionalizing the irradiation given by Eq. (57) i.e.,

$$C = E_{tot}/K \tag{70}$$

Another useful parameter defined in [47] is the concentration efficiency. This is the ratio of the power reflected by the concentrator to that received by the target. That reflected can be obtained by integrating Eq. (47), i.e.,

$$\Phi_2 = \iint_{\psi\, z_1} d\Phi_2 = \iint_{\psi\, z_1} \gamma_1(\beta_1) K s s' \, d\psi \, dz_1 \tag{71}$$

The power incident on the receiver is obtained by integrating the irradiative distribution on the receiver, i.e.,

$$\Phi_r = \iint_{z\, \theta} E(z,\theta) \, dz \, d\theta \tag{72}$$

and the concentration efficiency is given by

$$\eta = \Phi_r / \Phi_2 \tag{73}$$

This of course takes into consideration radiation 'spillage' due to target geometry and orientation.

A parameter that describes the amount of radiation actually absorbed will not be defined. Such a parameter would depend on too many factors concerning the target surface properties and shape and would not be good for making comparisons in general.

A catch-all factor called the 'furnace factor' is often defined for a situations such as that being considered. It is felt that the definitions of this quantity in the literature are not consistent, therefore it will be avoided.

Section 4
PROCESS HEAT BALANCE

The solar concentrator analysis computer code simulates the concentrator-receiver configuration and predicts the heat flux distribution on the molten zone. However, the geometry of the molten zone, the optical properties of the process material surfaces, and the thermal and physical properties of the process material dictates the thermal energy requirements and thus the solar concentrator size. Therefore a heat balance on the molten zone and the connecting material has been performed.

It has been mentioned previously that crystal quality and shape depend on meniscus shape and the solid-liquid interface shape. The meniscus shape depends on geometry and surface temperature. The solid-liquid interface shape, however, is very implicit in the total thermal environment of the process. The detailed thermal analysis to predict the solid-liquid interface is rather formidable. Such an analysis must be coupled with the solar concentrator analysis to optimize solar concentrator shape, positioning of the process, etc. However, such an analysis did not fit within the time frame of the present study. Therefore the simplified one-dimensional analysis presented in Ref. [9] will be modified for estimating concentrator size versus process size.

If the isotherms in a cylindrical ingot are very nearly flat and perpendicular to the axis of symmetry, the following one-dimensional differential equation results for the heat balance (see Fig. 16)

$$\kappa \frac{d^2T_s}{dz^2} - V\rho C_p \frac{dT_s}{dz} - \frac{P}{A} q = 0 \qquad (74)$$

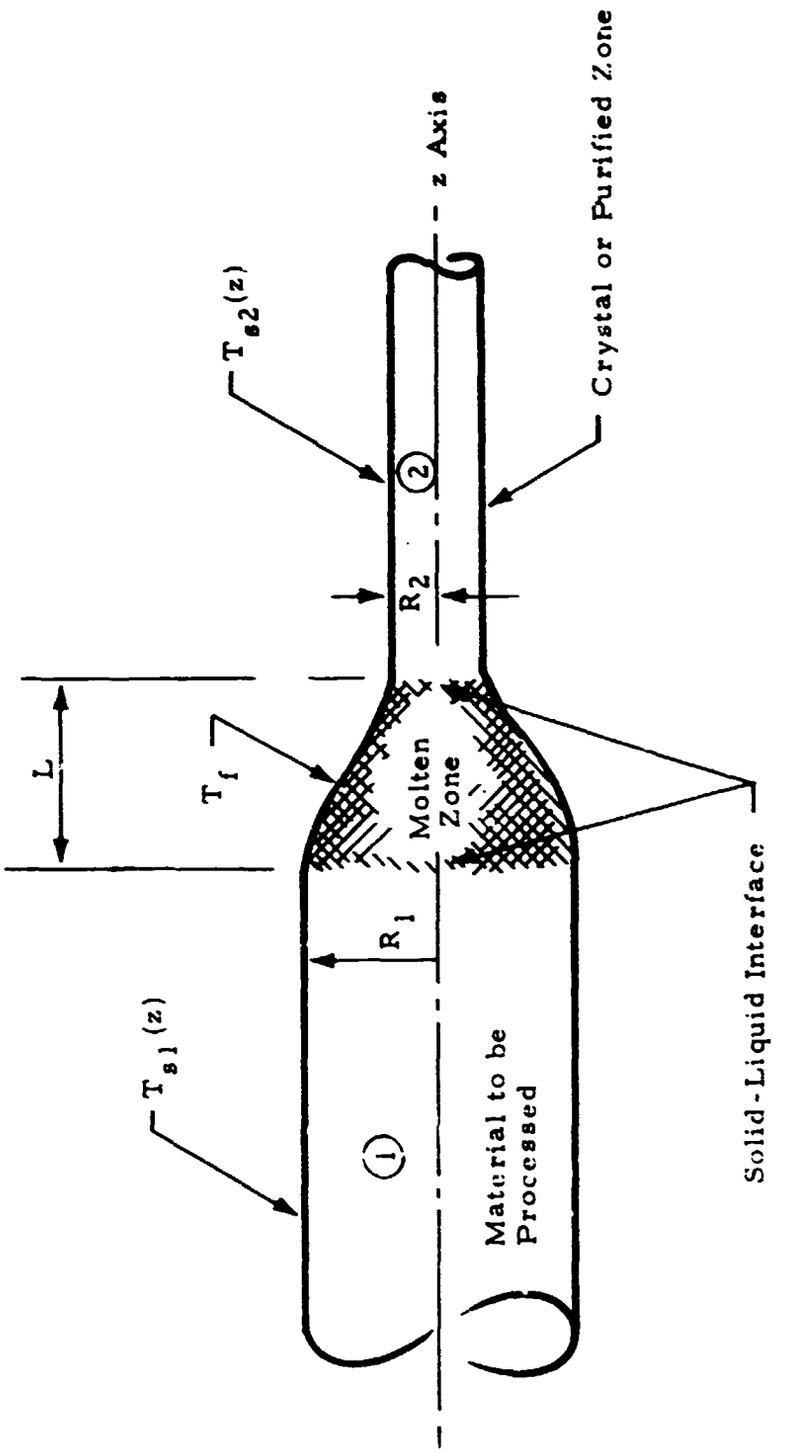

Fig. 16 - Configuration for Heat Balance

where

T_s = surface temperature
z = axial coordinate
k = conductivity
V = velocity of the solid-liquid interface
ρ = density of the material
C_p = specific heat of the material
P = perimeter of the bar
A = cross-sectional area of the bar
q = net heat flux at the surface

If the solar concentrator is directing radiation only to the molten zone and if the process is being conducted in the vacuum of space, the heat losses along the solid bar are primarily due to radiation. This can be expressed as

$$q = \sigma\epsilon F(T_s^4 - T_a^4) \tag{75}$$

where

σ = Stefan-Boltzmann constant
ϵ = emissivity of the material
F = radiation geometry factor
T_a = ambient temperature

For the situation under consideration, $T_a << T_s$, thus

$$q = \sigma\epsilon F T_s^4 \tag{76}$$

If the melt velocity is very small, with the aid of Eq. (76) and noting that $P/A = 2/R$ for a cylinder, Eq.(74) becomes

$$\frac{d^2T_s}{dz^2} - \left(\frac{2\epsilon\sigma F}{Rk}\right) T_s^4 = 0 \tag{77}$$

The solution to this differential equation is

$$T_s = T_f \left[1 + \left(\frac{9\epsilon \sigma F T_f^{\,3}}{5Rk} \right)^{1/2} z \right]^{-2/3} \tag{78}$$

where

T_f = freezing temperature of the material
R = radius of the cylinder

Thus the heat loss along a cylinder of length L can be expressed

$$Q_s = 2\pi R \epsilon \sigma F \int_0^L T_s(z)dz \tag{79}$$

and by using Eq. (78) and integrating

$$Q_s = \frac{6}{5}\pi R \epsilon \sigma F T_f^4 W \left[1 - \frac{1}{(1 + L/W)^{5/3}} \right] \tag{80}$$

where

$$W = \left(\frac{5Rk}{9\epsilon \sigma F T_f^3} \right)^{1/2} \tag{81}$$

If appreciable stirring occurs in the molten zone (this will probably be the case since Marangoni convection will be present) then the surface of the molten zone can be assumed to be at the freezing temperature T_f. The radiation from the molten zone surface will be

$$Q_m = \epsilon \sigma F T_f^4 \int_0^L P(z)dz \tag{82}$$

where

L = molten zone length

$P(z)$ = perimeter of the molten zone as a function of z

The integral is the surface area of the molten zone, thus let us define

$$A_m = \int_0^L P(z)\,dz \tag{83}$$

Thus with the aid of Eqs. (81), (82) and (83), the total heat loss by the process will be

$$Q_t = Q_m + Q_{s1} + Q_{s2} = \sigma\epsilon_m F_m T_f^4 A_m$$

$$+ \frac{6}{5}\pi\ R_1\epsilon_1\sigma F_1 T_f^4 W_1 \left[1 - \frac{1}{(1 + L/W_1)^{5/3}}\right]$$

$$+ \frac{6}{5}\pi\ R_3\epsilon_2\sigma F_2 T_f^4 W_2 \left[1 - \frac{1}{(1 + L_2/W_2)^{5/3}}\right] \tag{84}$$

where

$$W_1 = \left(\frac{5 R_1 k_1}{9\epsilon_1\sigma F_1 T_f^3}\right)^{1/2} \tag{85}$$

$$W_2 = \left(\frac{5 R_2 k_2}{9\epsilon_1\sigma F_2 T_f^3}\right)^{1/2} \tag{86}$$

With the above analysis the thermal energy requirements for a particular molten zone can be established and the solar concentrator can be sized.

This analysis offers some flexibility in that a transition in bar size can be treated and the molten zone can be of arbitrary shape.

Section 5
RESULTS

With the analytical tools developed in the previous sections several sets of computations have been made to illustrate the influence of various factors on the thermal image produced on a receiving surface by a solar concentrator. The factors considered are:

- Target Geometry
- Target Location
- Concentrator Size
- Concentrator Types, and
- Optical Errors

Before computations can be made a model of the solar source must be specified. As mentioned previously, several models have been proposed; however, for the calculations made here the model proposed by Kamada [50] will be used. This model is described in Fig. 17. The solar constant for

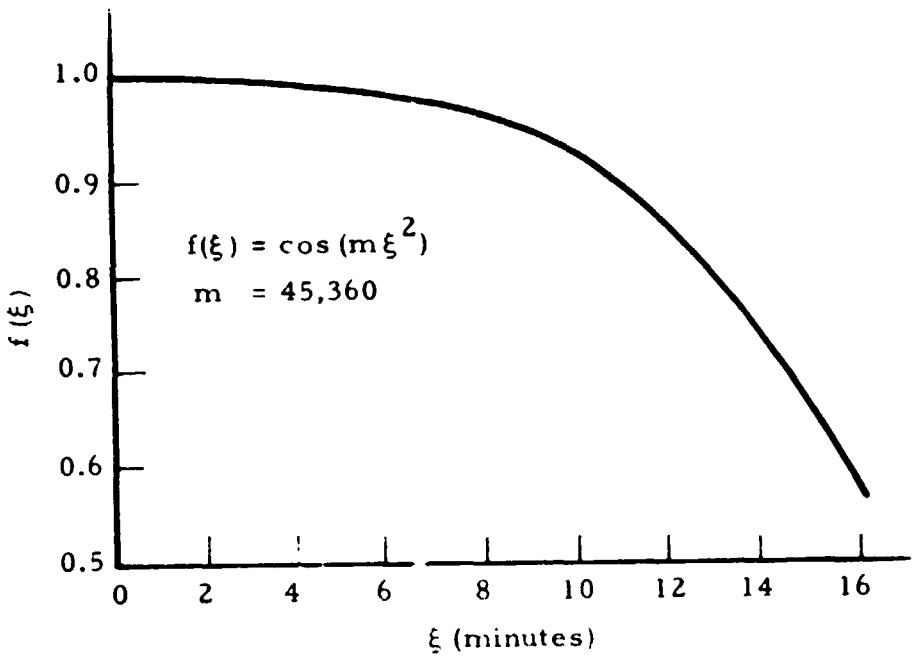

Fig. 17 - Solar Disc Model

these calculations will be 1.94 cal/cm^2-min. The results are presented in terms of concentration ratio. This allows the results to be easily applied for situations where the solar constant is not 1.94, e.g., terrestrial applications. The concentration ratio can be converted to watts per square centimeter by multiplying by 0.1353.

When radiation is used for heating, computation of temperatures that can be achieved in general is meaningless. The characteristics of materials that determine the temperatures attainable, temperature gradients that will be established, etc., are both thermal and optical [18]. For a prescribed situation, the net heat flux into a material depends on its surface properties, i.e., absorptivity and reflectivity. The internal temperature distributions depend on the specific heat and thermal conductivity. Thus the results presented will not be in terms of temperature. Irradiation distributions will be presented in terms of concentration ratio.

The simplified one-dimensional heat transfer analysis in Section 4 has been used to approximate bar sizes that can be melted for prescribed situations. Although this analysis is not exact, the results presented are good approximations. These calculations have been carried out for tungsten, silicon and germanium.

A comparison of Fresnel concentrators with continuous surface concentrators is made. Also a concentrator is designed which gives a near uniform irradiation distribution.

The results presented are in non-dimensional form. As mentioned previously, all spatial variables and parameters have been non-dimensionalized by the focal length f. Thus $z = 1.0$ corresponds to the focal point. The receiver dimensions have also been divided by f. Thus the results are for any geometrically similar system.

5.1 THERMAL IMAGE ON TARGETS NORMAL AND PARALLEL TO THE OPTICAL AXIS

To develop some insight into the radiation environment in the focal region of a solar concentrator the concentration distribution on targets normal and parallel to the optical axis has been computed. These targets are located at different distances from the optical axis and from the focal point. To make comparisons with previous work, e.g., the results of Kamada [50] it was necessary to consider a paraboloid concentrator. Thus the curves in Figs. 18 and 19 are for a paraboloid with a specular surface and an aperture ratio of 4 (i.e., a = 4).

In Fig. 18 the concentration distribution on cylinders of various radii is shown. The magnitude of the concentration decreases with increasing radius. This, of course, is due to the surface being irradiated being moved further from the focal point. If the cylinder centerline is located on the optical axis and has a radius sufficient to intercept all of the radiation, then one may view this decrease in concentration with increasing radius as a result of spreading the same amount of energy over larger and larger areas.

In Fig. 19 the concentration distribution is given for a flat target placed in the focal region of the paraboloid normal to the optical axis. For this situation the concentration distribution is symmetrical about the optical axis. The parameter u in the figure gives the location of the receiving surface relative to the focal point. In non-dimensional form

$$u = z - 1.0$$

Thus, for values of $u < 0$ the receiver is between the focal point and the concentrator. The concentration distribution of course has the greatest value for $u = 0$. The curves for $u \neq 0$ may be thought of as "out of focus" conditions. Note that the distribution magnitude is somewhat smaller for positive values of u than it is for the negative values with the same absolute value. This

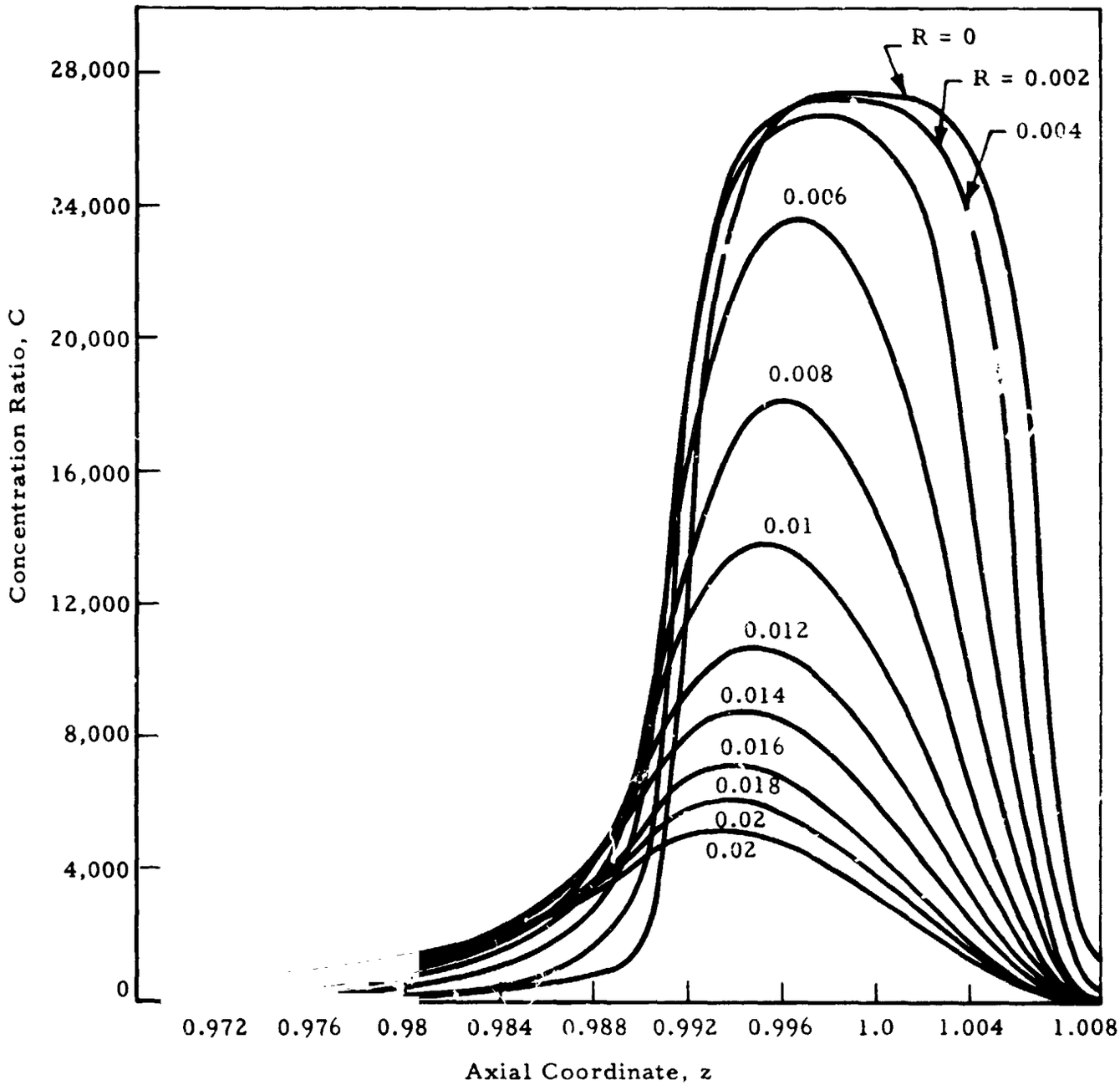

Fig. 18 - Concentration on a Right Circular Cylinder Located on the Optical Axis of a Paraboloid with an Aperture Ratio of 4

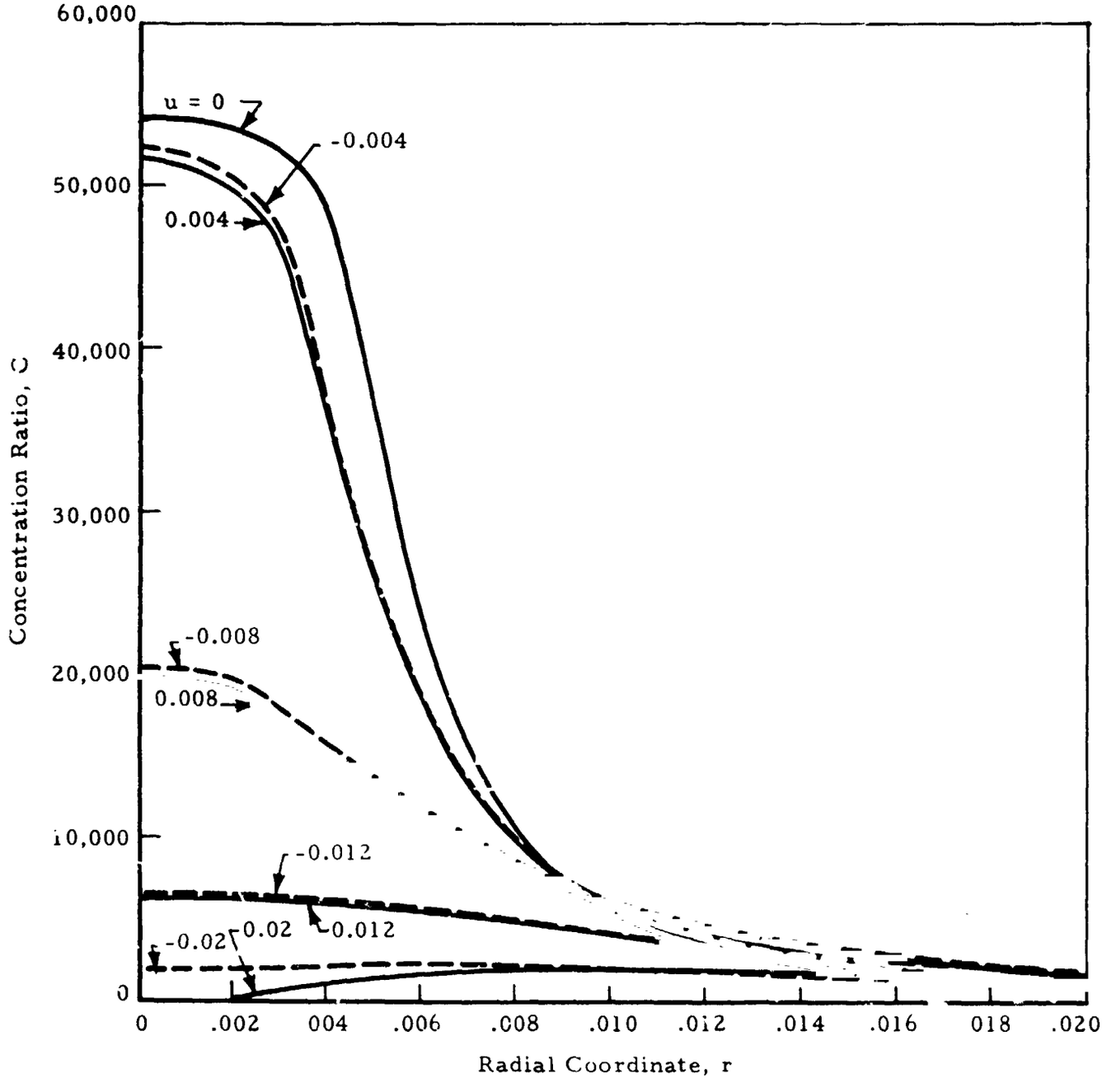

Fig. 19 - Concentration on a Flat Receiver Normal to the Optical Axis of a Faraboloid of Aperture Ratio 4

asymmetry is due to the greater distance over which the sun rays have to diverge before striking the receiver.

Although the results in Figs. 18 and 19 cannot be used to determine the concentration on any surface placed in the focal region, they do give some insight to the radiation environment in the focal region. One can see that the positioning of a surface relative to the focal point and surface orientation can drastically influence the irradiative distribution on the surface. Thus the process geometry and heating distribution are strongly coupled.

5.2 THE INFLUENCE OF PLACEMENT ERRORS ON THE THERMAL IMAGE

In the previous section the influence of target location on the thermal image was illustrated for axisymmetrical situations. The influence of asymmetrical target placement will now be considered. Again the paraboloid concentrator with an aperture ratio of four will be used. To make meaningful comparisons the target geometry must be held constant. Since a cylindrical receiver is of interest for space processing applications, a right circular cylinder with $R = 0.01$ will be used. This radius was chosen because it is near the lower limit of cylinder sizes that can intercept all the radiation (i.e., $\eta = 100\%$). (See Fig. 20).

Two types of placement errors can occur as indicated in the analysis in Section 3.6. Rotation of the target will be considered first. The center of rotation will be assumed as being at the vertex of the paraboloid, i.e., $z = 0$. Small rotations from 2 to 8 minutes have been considered. These were chosen because it was felt that they are realistic for the systems being considered. Note in Figs. 21 through 24 that the concentration distribution amplitudes begin to vary more around the receiver as ω increases. The concentration at the $\theta = 0$ position decreases. This side of the cylinder is moving away from the focal point. The $\theta = \pi$ side of the receiver is moved closer to the focal point as the cylinder is rotated. With rotation only the heating distribution for $\pi \leq \theta \leq 2\pi$ is identical to that for $0 \leq \theta \leq \pi$.

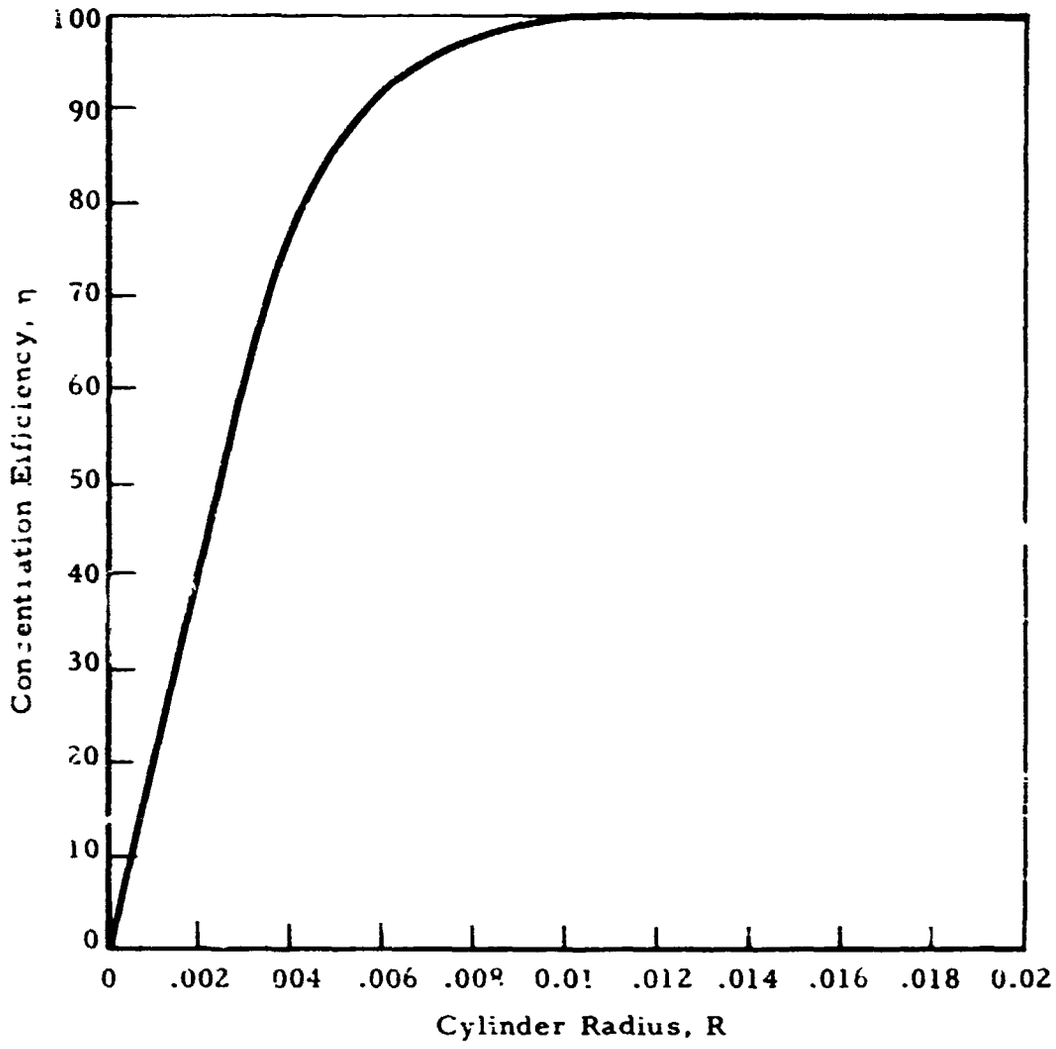

Fig. 20 - Concentration Efficiency for a Paraboloid with Aperture Ratio = 4 Irradiating a Cylinder

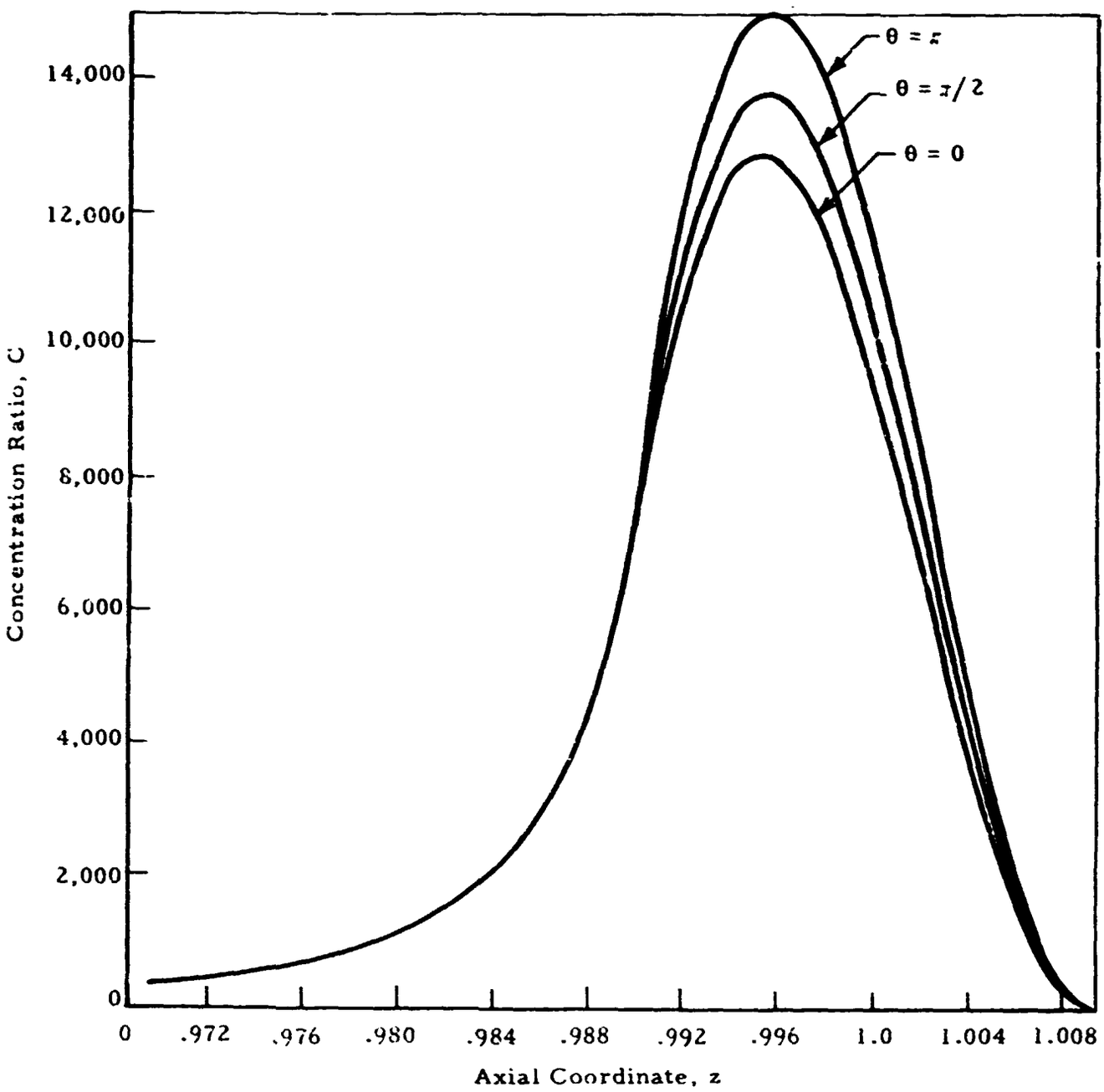

Fig. 21 - Concentration on a Cylindrical Target Rotated 2 Minutes

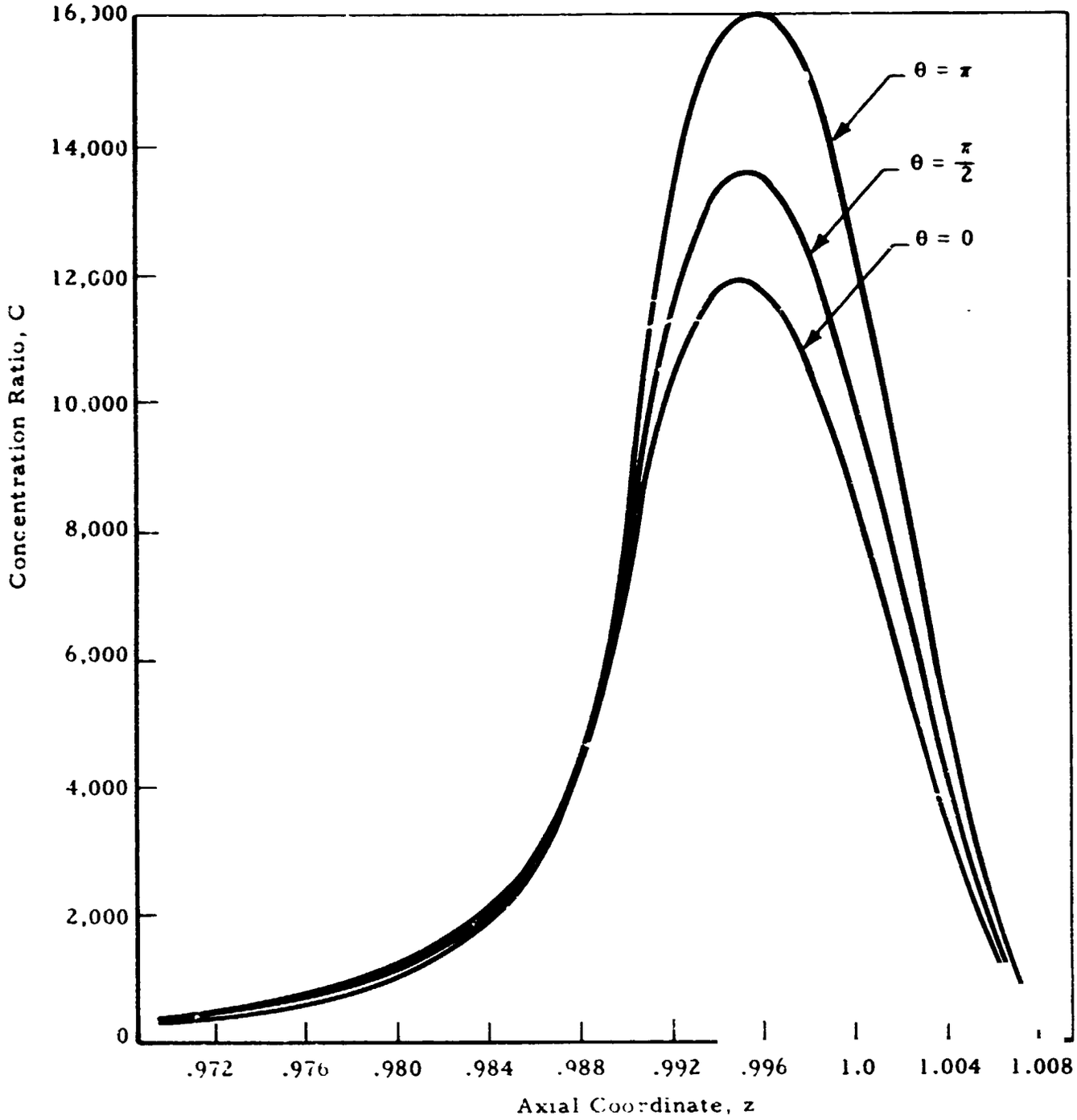

Fig. 22 - Concentration on a Cylindrical Target Rotated 4 Minutes

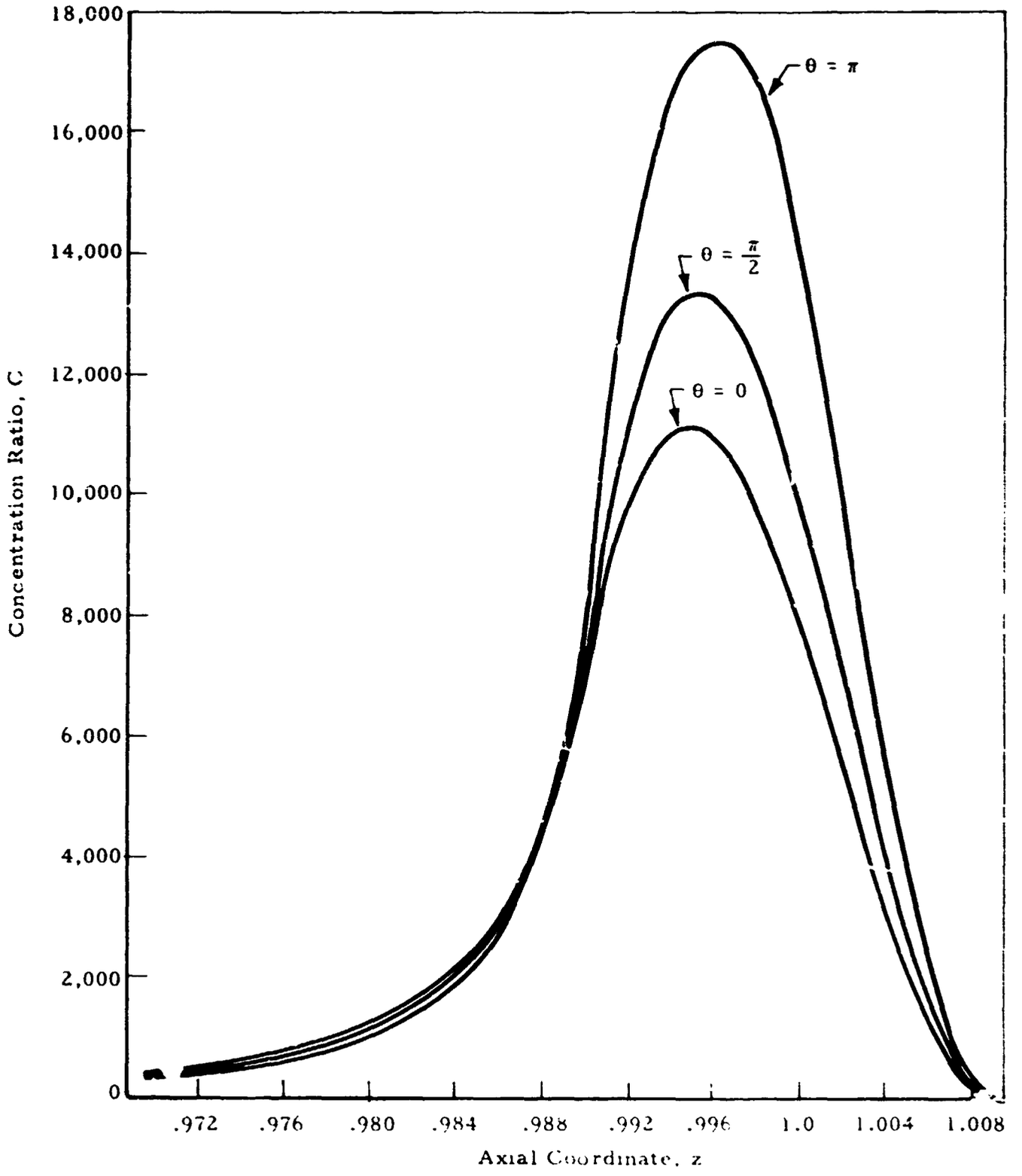

Fig. 23 - Concentration on a Cylindrical Target Rotated 0 Minutes

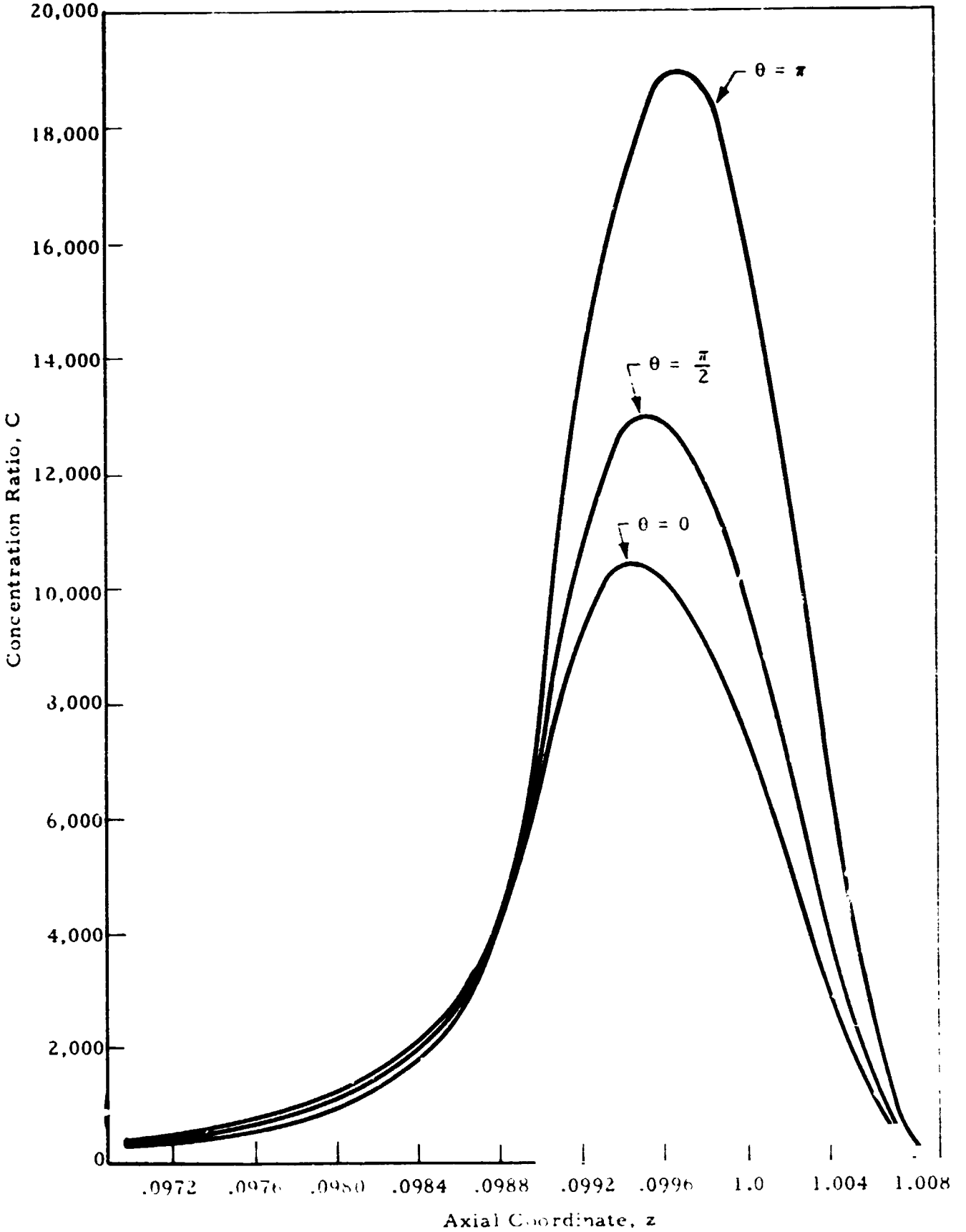

Fig. 24 - Concentration on a Cylindrical Target Rotated 8 Minutes

The concentration distributions in Figs. 25 through 28 are the result of translating the receiver from the optical axis from 0.002 to 0.008 units. The results are similar to those obtained when the receiver was rotated. The variation in the concentration amplitude is again due to the position of the various sides of the receiver relative to the focal point. The translation is along the x-axis. Thus, the heating distributions are identical for $3\pi/2 \leq \theta \leq \pi/2$ and $\pi/2 \leq \theta \leq 3\pi/2$.

Translation and rotation of the target can be treated together. For this situation there is no symmetry in the heating around the cylinder. To illustrate, results for this type situation are given in Fig. 29.

Thus the heating distribution on the process material is strongly influenced by any inaccuracies in process placement in addition to process geometry.

5.3 OPTICAL ERRORS

The influence of imperfections in the geometry of the concentrator has also been considered. As pointed out earlier, the surface errors do not normally follow a normal distribution. However, to illustrate the influence of concentrator surface errors. A normal distribution of random imperfections has been used. Figure 30 illustrates the influence of various amounts of surface error on concentration distribution; σ is one standard deviation of the surface in minutes of arc. As one would suspect these surface errors tend to "flatten" the distribution.

5.4 A COMPARISON OF FRESNEL AND PARABOLOID CONCENTRATORS

Fresnel concentrators have the disadvantages that all of their area cannot be utilized and they cannot produce concentrations as high as an equivalent paraboloid. The loss in usable area is inherent in the design as shown in Fig. 31. With the same amount of usable reflecting area a Fresnel concentrator cannot produce concentrations as high as a paraboloid. This is due to

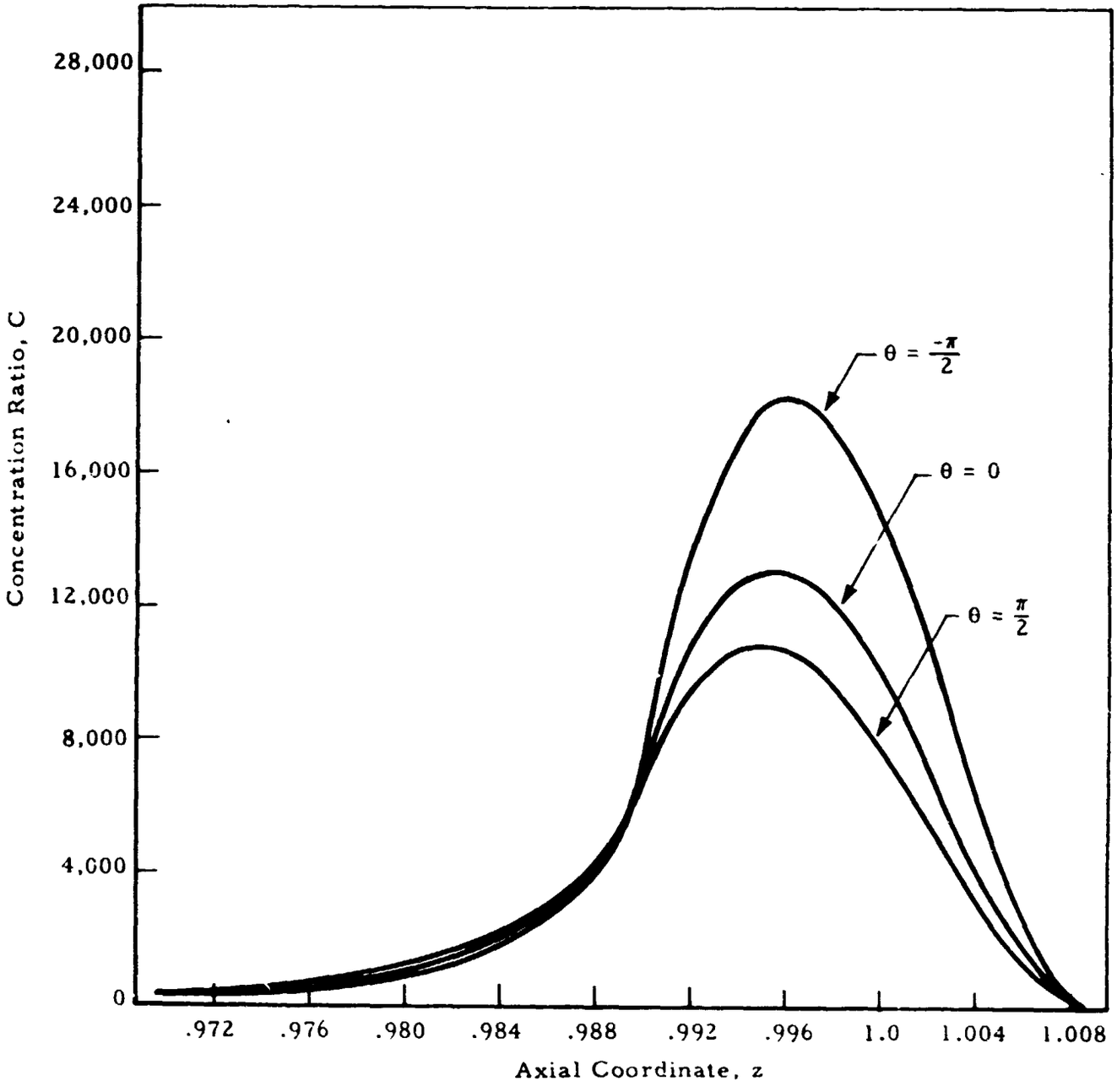

Fig. 25 - Concentration on a Cylindrical Target Translated 0.002 Units from the Optical Axis

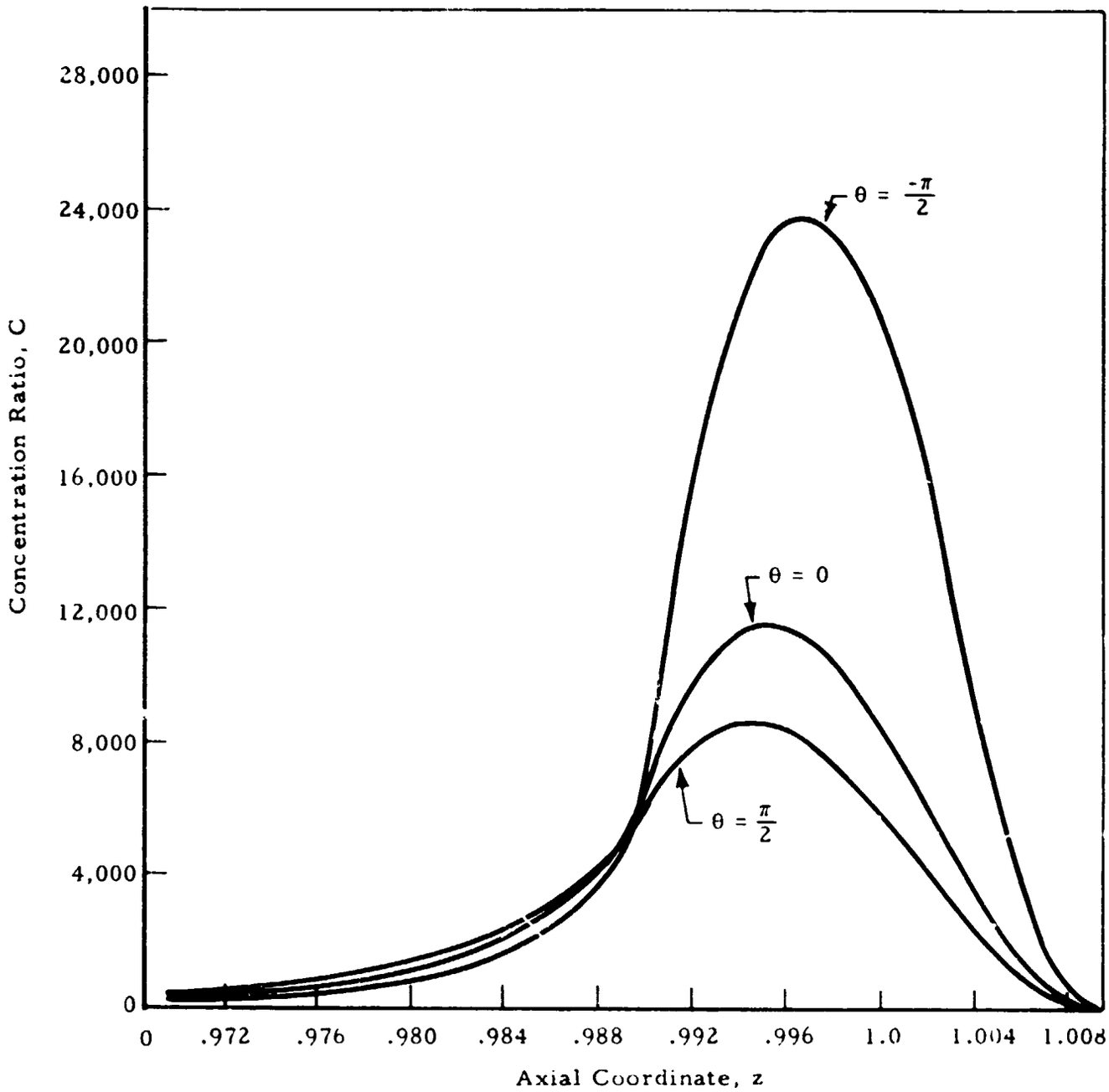

Fig. 26 - Concentration on a Cylindrical Target Translated 0.004 Units from the Optical Axis

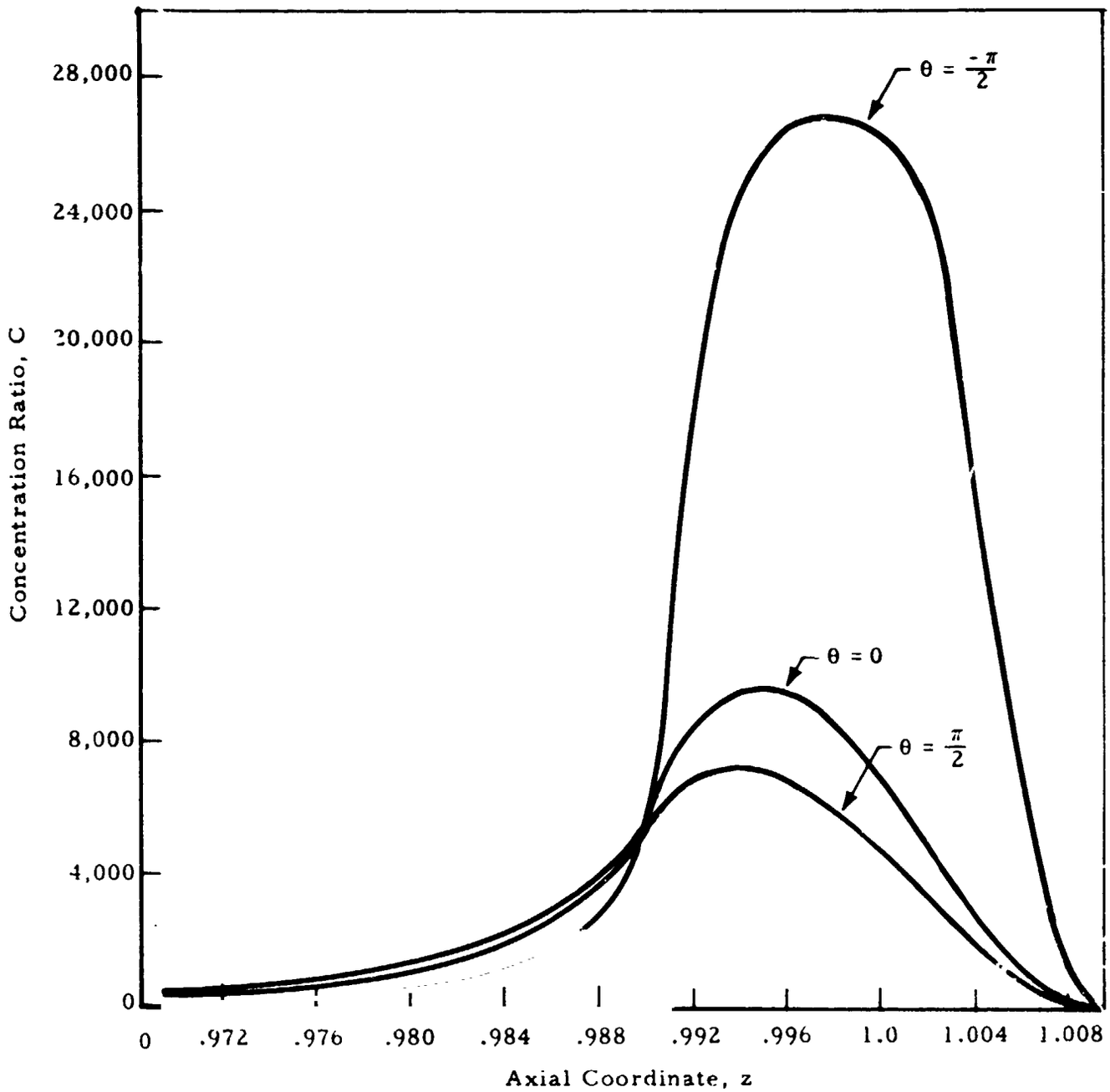

Fig. 27 - Concentration on a Cylindrical Target Translated 0.006 Units from the Optical Axis

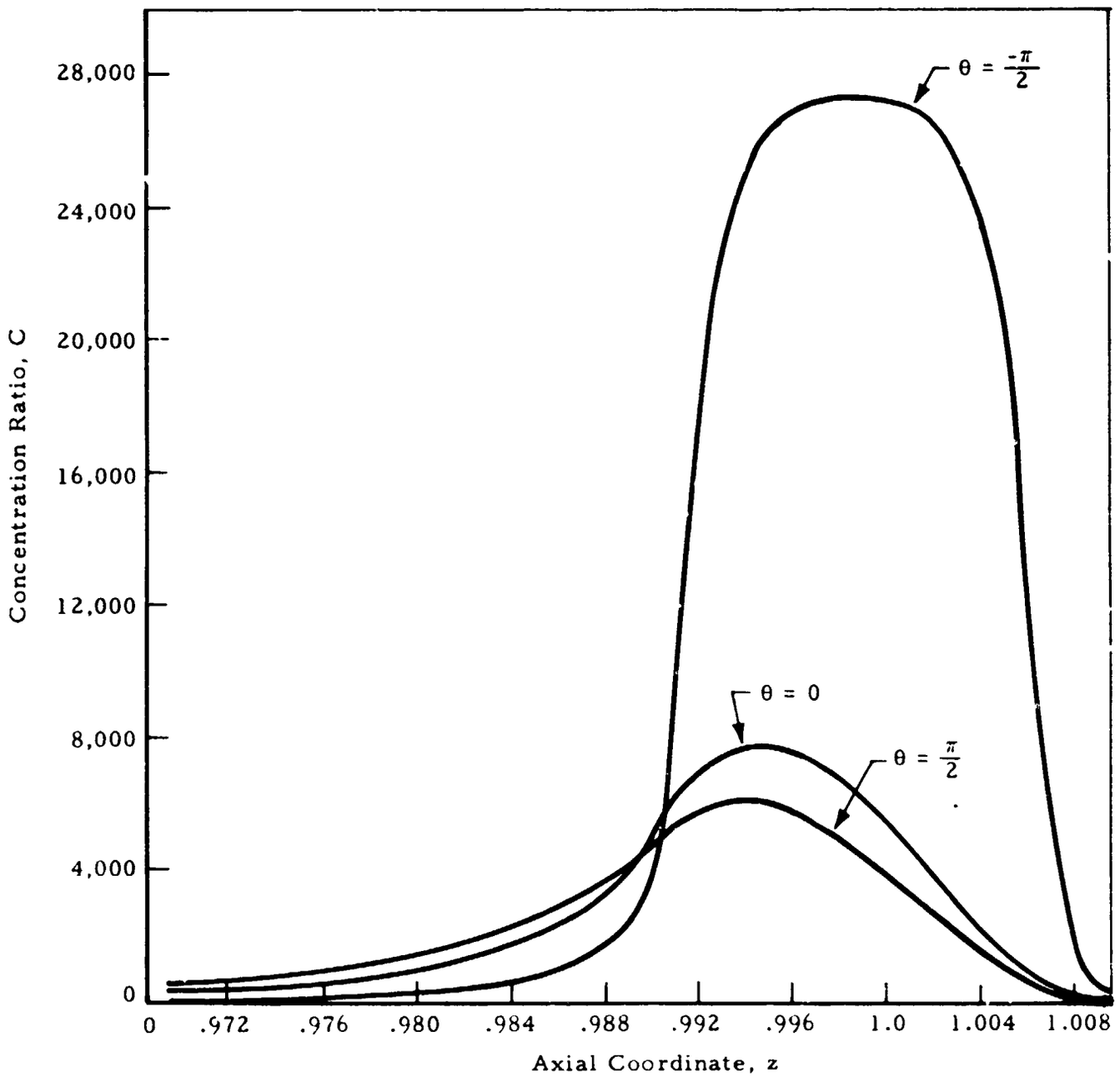

Fig. 28 - Concentration on a Cylindrical Target Translated 0.008 Units from the Optical Axis

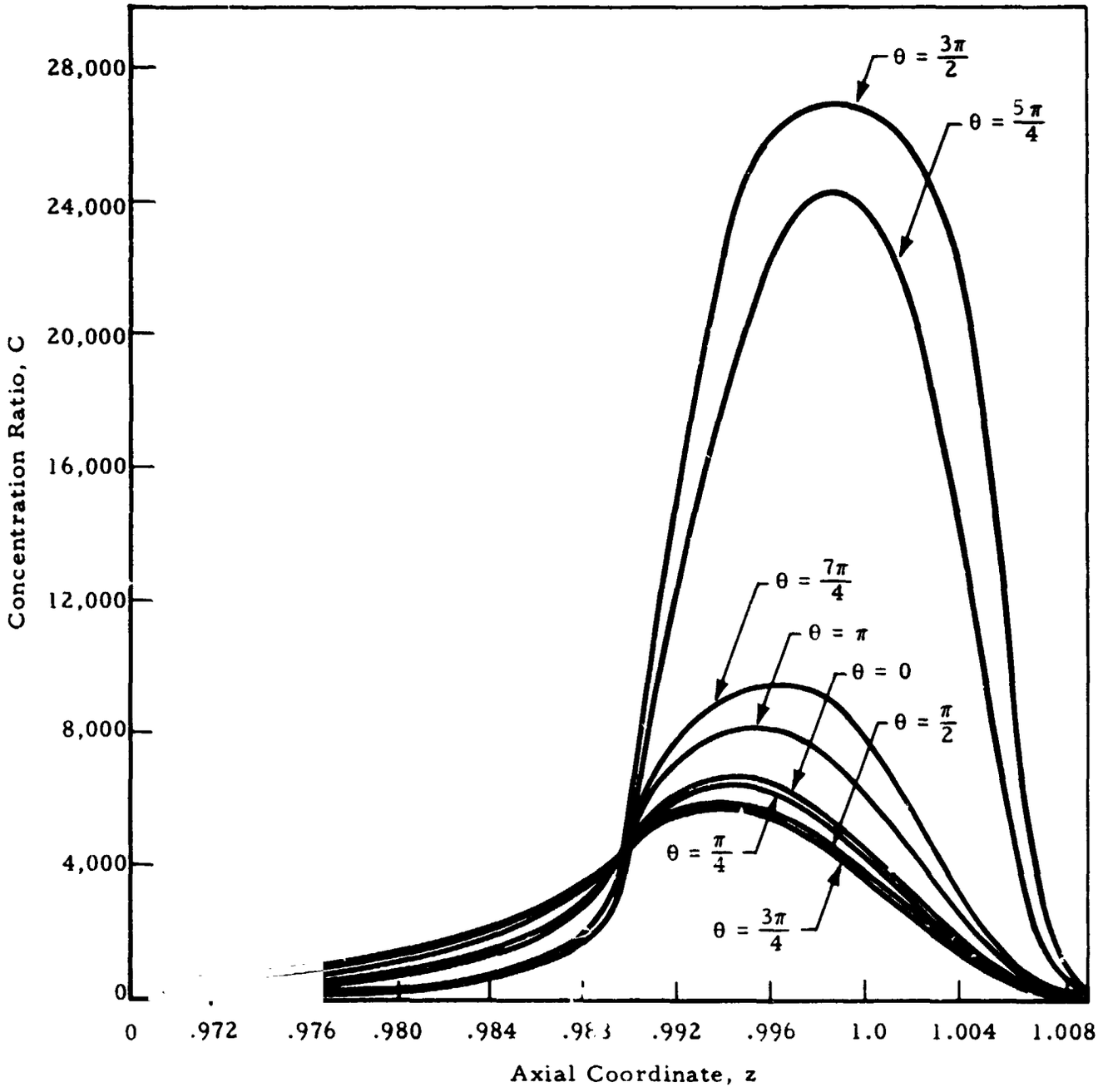

Fig. 29 - Concentration Distribution on a Cylindrical Target Translated 0.008 Units and Rotated 8 Minutes

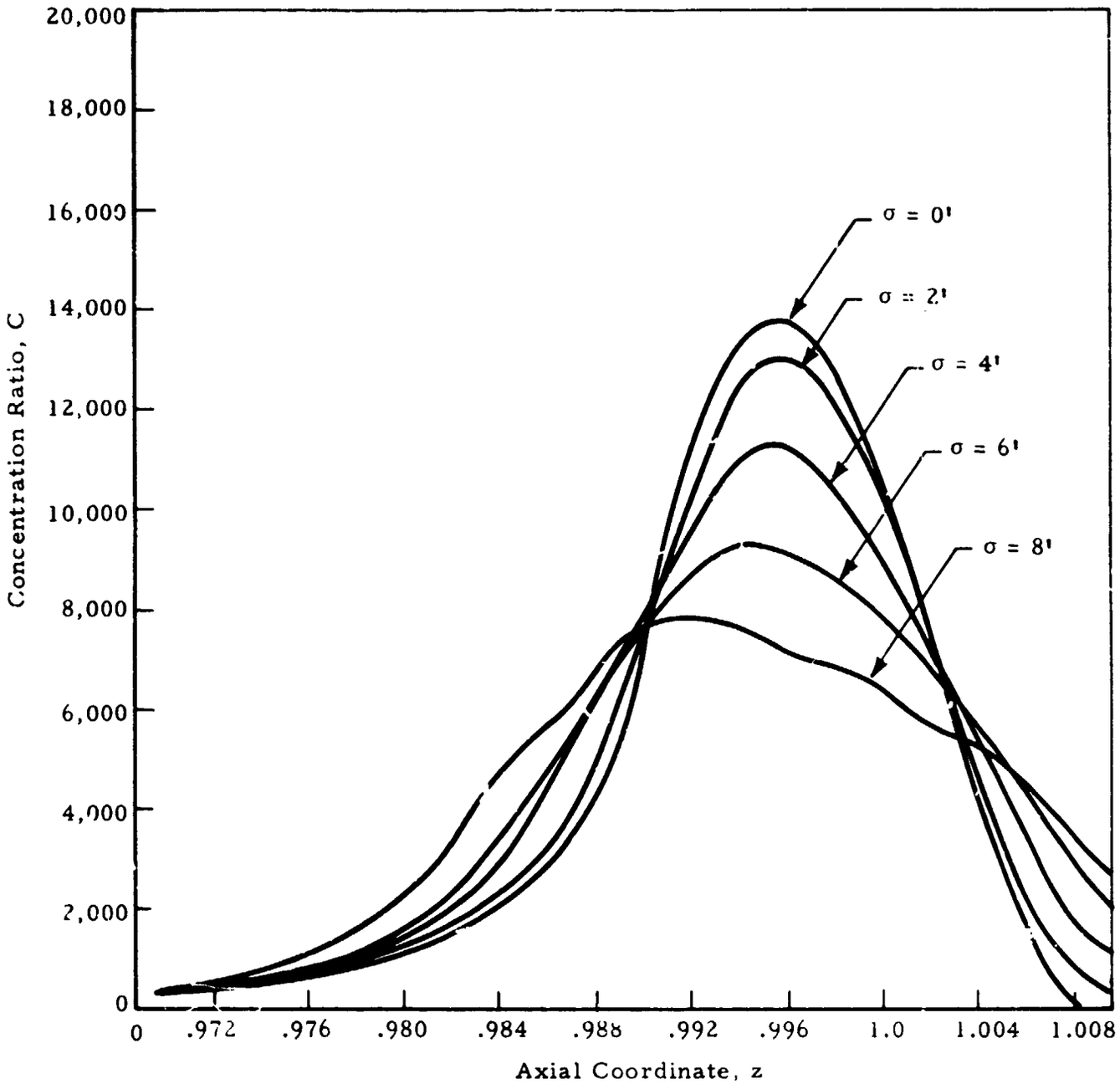

Fig. 30 - Influence of Optical Errors on Concentration Distribution

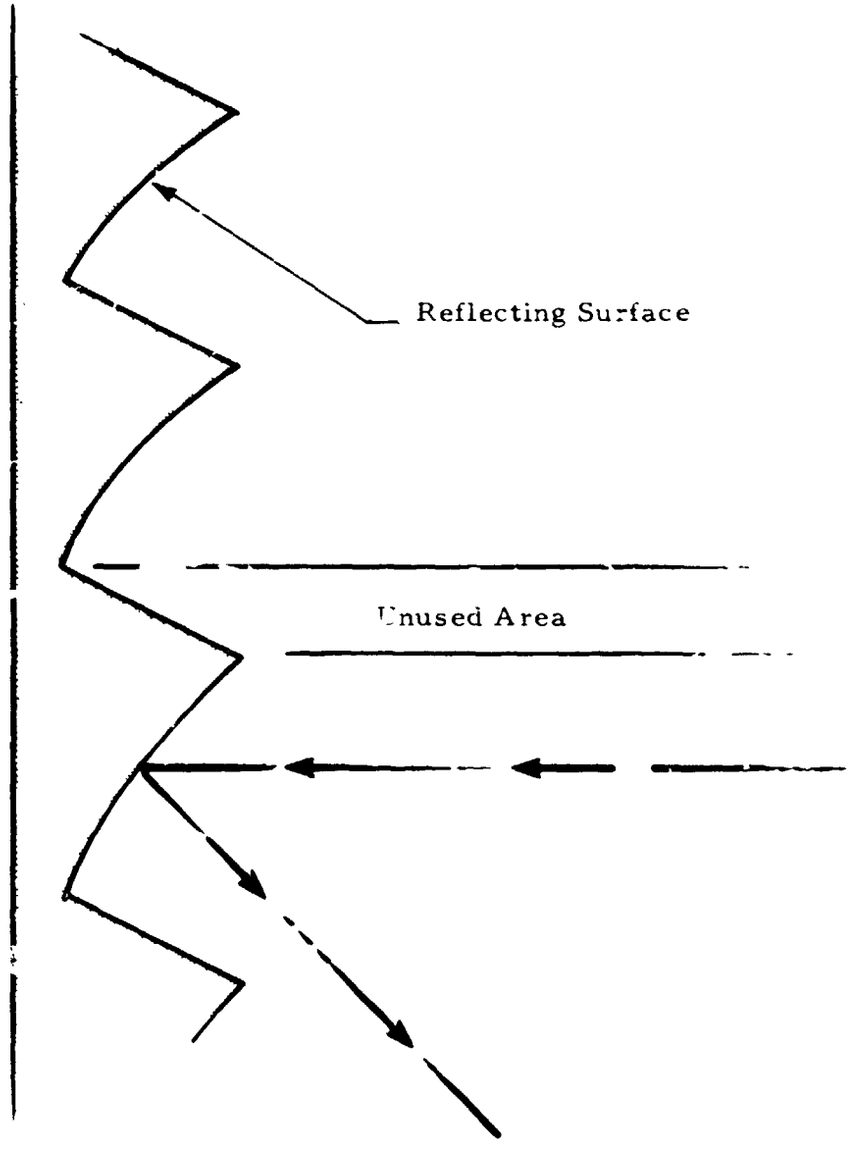

Fig. 31 - Area Utilization for Fresnel Concentrators

the reflecting elements being farther from the focal point. The sun rays have a greater distance over which to diverge. However the Fresnel geometry is desirable in some situations, e.g., a foldable concentrator. The results in Fig. 32 indicate the loss in concentration and radiant flux in going from a paraboloid concentrator to a Fresnel concentrator with the same aperture ratio. Again, the R = 0.01 cylindrical receiver is used. Figure 33 gives a description of the Fresnel concentrator.

If process heating requirements fall within the range achievable by Fresnel configurations a foldable Fresnel configuration may be attractive.

5.5 DESIGN OF A SOLAR CONCENTRATOR TO GIVE A PRESCRIBED CONCENTRATION DISTRIBUTION

As mentioned in Section 3.8 the analytical tools developed can be used to design concentrators as well as determine the irradiative distribution on targets for prescribed concentrators. To illustrate, a concentrator surface has been determined which will give a concentration of about 4000 on a section of surface of a cylinder of radius R = 0.01. Due to the problems discussed previously(in the development of the analysis)it is not always possible to develop a design that will give an exact irradiative distribution if an extended source is being used. Figure 34 gives the concentrator geometry and Fig. 35 gives the concentration distribution on the cylinder. The waviness in the distribution is due to several factors. The source characteristics and the points chosen on the receiver for the numerical calculations are probably the most important factors. By manipulating various parameters that must be chosen, such as receiver points for the design, the distribution could be made more uniform. However, the point is that concentrators to give prescribed irradiative distributions can be designed.

In Fig. 34 the concentrator profile appears to be that of a paraboloid. Actually the surface is very close to being a paraboloid. This is due to the fact that the region over which the radiation is being directed is very small

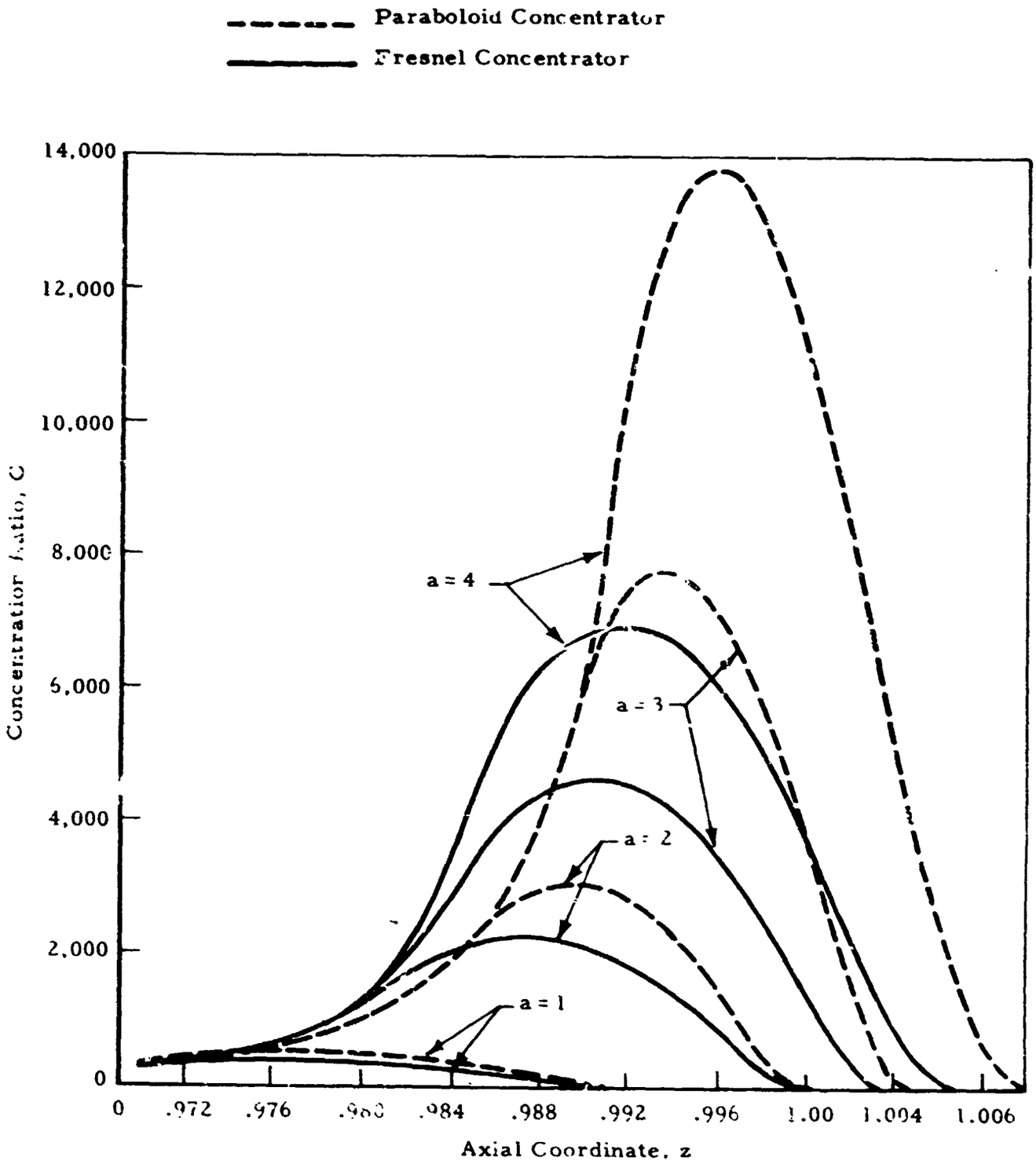

Fig. 32 - A Comparison of Concentration Distribution of Paraboloid and Fresnel Concentrators

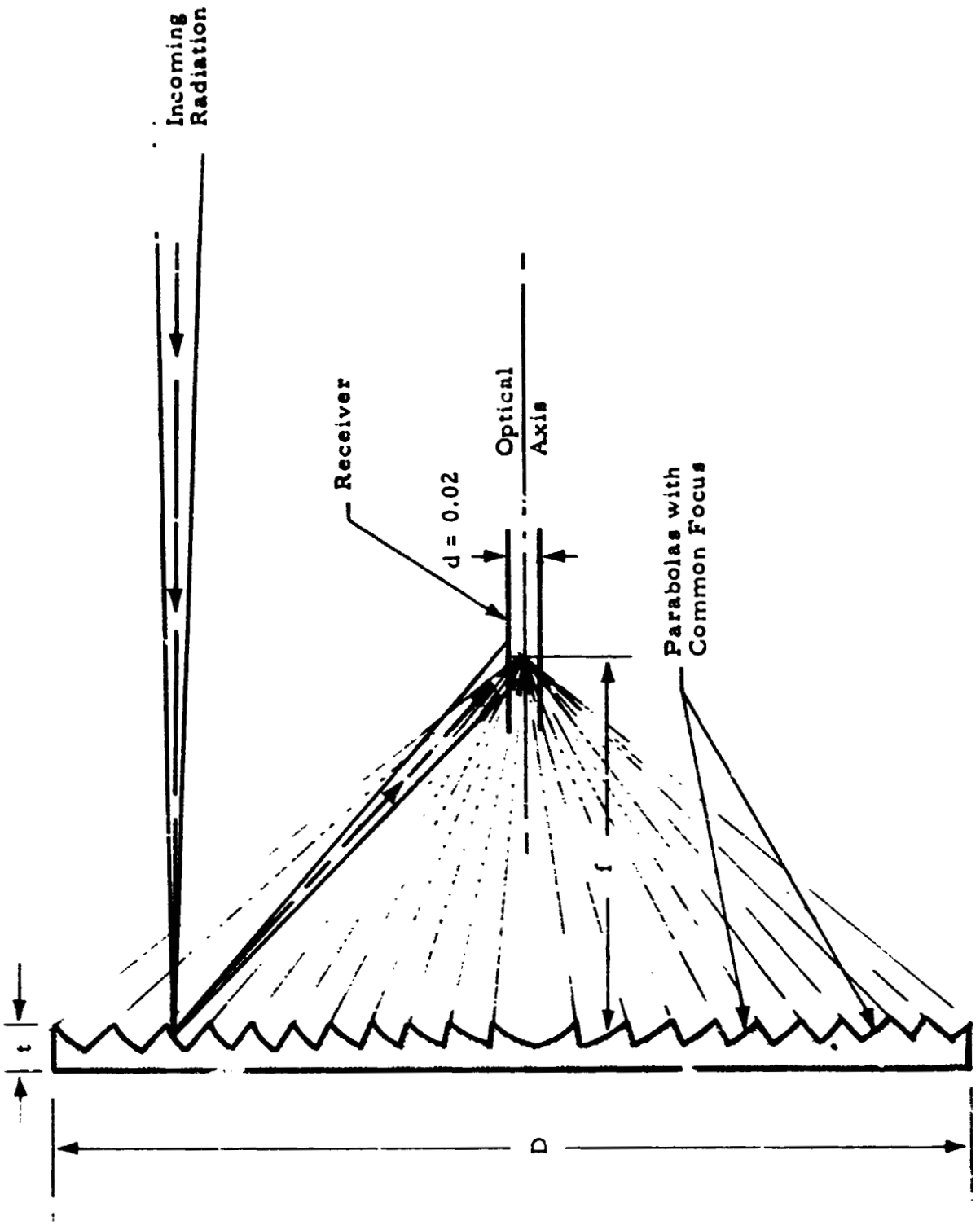

Fig. 33 - Fresnel Concentrator

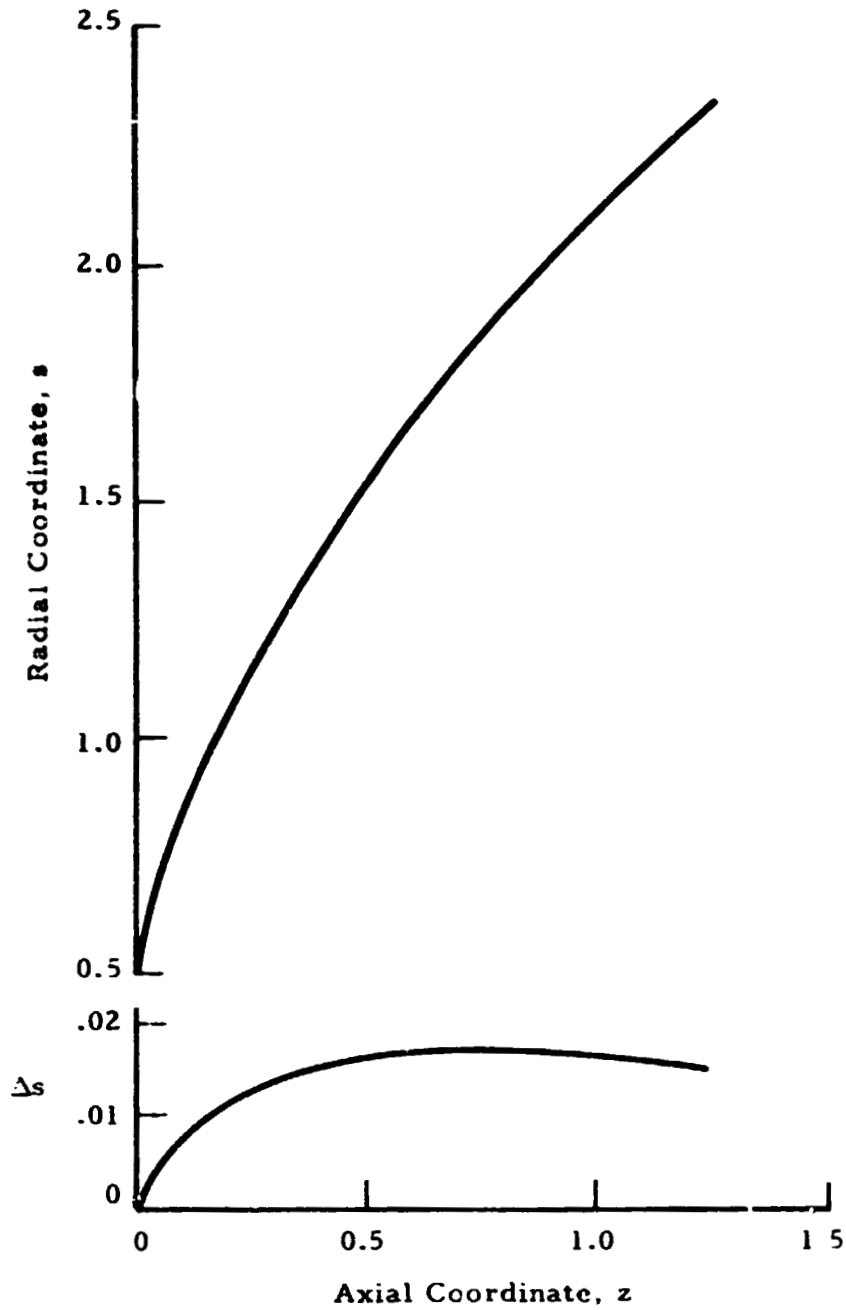

Fig. 34 - Solar Concentrator Geometry to Give Prescribed Concentration Distribution

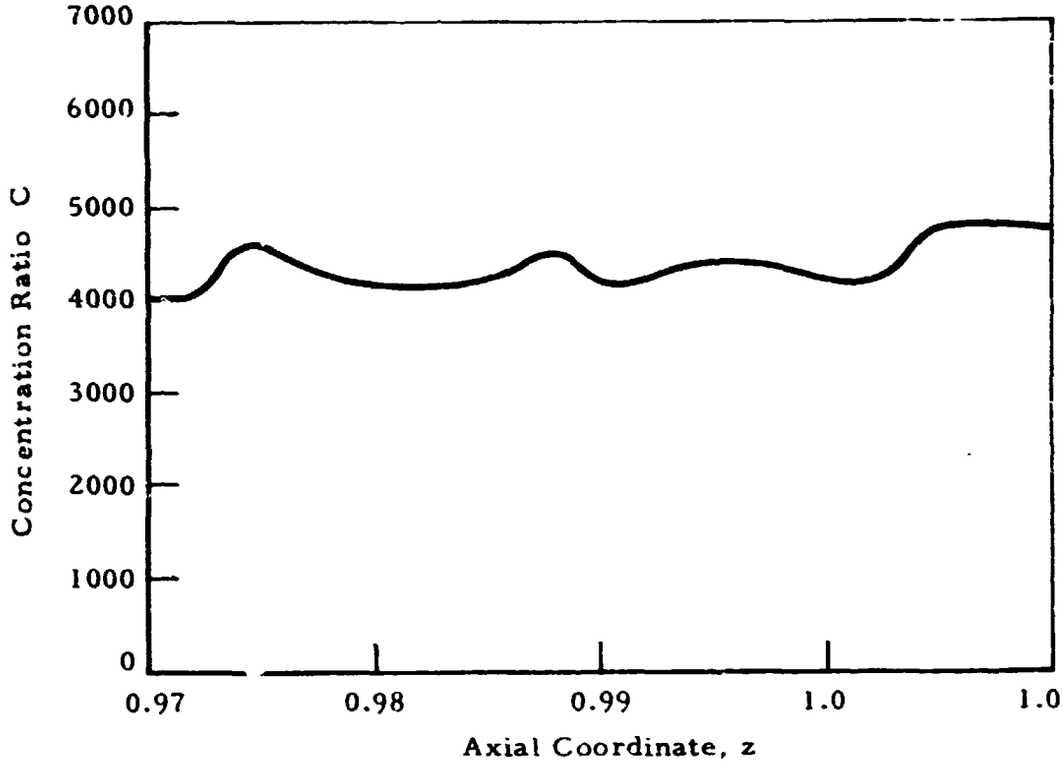

Fig. 35 - Thermal Image on a Cylinder From a Custom Concentrator

relative to the concentrator dimensions. However, the surface in Fig. 34 is not a paraboloid as shown in the lower portion of the figure. The quantity Δs is the variation of the surface from a paraboloid, i.e..

$$\Delta s = s_{paraboloid} - s$$

5.6 ESTIMATION OF CONCENTRATOR SIZES FOR OBTAINING MOLTEN ZONES

The analysis in Section 4 has been used to estimate the power required to maintain molten zones in various size bars of tungsten, silicon and germanium. With this calculation the solar concentrator that will give the required power can be determined. Before performing these calculations a number of assumptions must be made and data on the thermal and optical properties of the materials obtained. The thermal properties given in Table 3 for the three materials can be found in a number of references. However, material surface properties such as absorptivity are rather difficult to obtain and the available data is rather scattered. Upon examing the data compiled in [64] it was decided to assume that $\alpha = \epsilon = 0.5$ for all three materials.

It was assumed that the material to be processed was a cylinder and the molten zone was two cylinder diameters long. It was also assumed that one diameter of length on each end of the molten zone was not insulated. Since access to the focal region from the center of the concentrator would perhaps be desirable in a design, it was assumed that the inner diameter of the concentrator is one meter. Also, to take into consideration the reflectively of the concentrator and any obscuration that might result from process supports, etc., it was assumed that $\gamma_1 = 0.9$.

Except for the region of the molten zone being irradiated the process material will be radiating to the blackness of space either directly or through

Table 3

MATERIALS PROPERTIES

Material → / Property ↓	Si	W	Ge
$k \left(\frac{cal}{sec\ cm\ ^oK}\right)$	0.075	0.23	0.09
$\rho \left(\frac{gm}{cm^3}\right)$	2.33	17.5	5.49
$C_p \left(\frac{cal}{gm\ ^oK}\right)$	0.25	0.04	0.095
$T_f\ (^oK)$	1685	3683	1210
α	0.5	0.5	0.5
ϵ	0.5	0.5	0.5

the reflecting concentrator surface. In view of this the radiation geometry factors were assumed to be unity.

With the above assumptions the curves in Figs. 36 and 37 were generated using the analysis in Section 4. For the situation chosen the concentrator aperture is directly proportional to the bar diameter for a given material. If a bar of material 10 cm in diameter (about 4 inches) is to be melted we can see that about 8 kW would be required for silicon, about 18 kW for germanium and about 40 kW for tungsten. This corresponds to solar concentrator diameters of about 4 meters, 6.5 meters and 29 meters, respectively (for the assumptions that have been made). The power requirements and thus the concentrator diameter increases exponentially with melt temperature. This of course is due to the radiation losses.

5.7 SPECIFIC POWER COMPARISONS

For the space processing of materials on a production basis thermal energy for processing must come from the solar source or a nuclear reactor. If the solar source is used, the only competitor currently with solar concentrators is solar cells. A meaningful comparison can be made only if complete systems are designed. However, the surfaces used to collect the solar radiation are a major portion of the process system and specific power for these surfaces is a good indication of system specific power. The comparisons shown in Table 4 are made for the collecting surfaces.

In Table 4 specific power comparisons are made for a solar concentrator with efficiency of 25, 50 and 100%. Based on previous studies, materials optical properties, etc., an overall efficiency of 50% is realistic and perhaps a little conservative. This 50% efficiency is the actual thermal energy that could be used. In the case of solar cells the electrical energy would have to be converted to thermal energy and directed onto the melt zone. There would, of course, be losses in converting and applying this energy. In view of this the solar concentrator is actually more attractive than is indicated in the table.

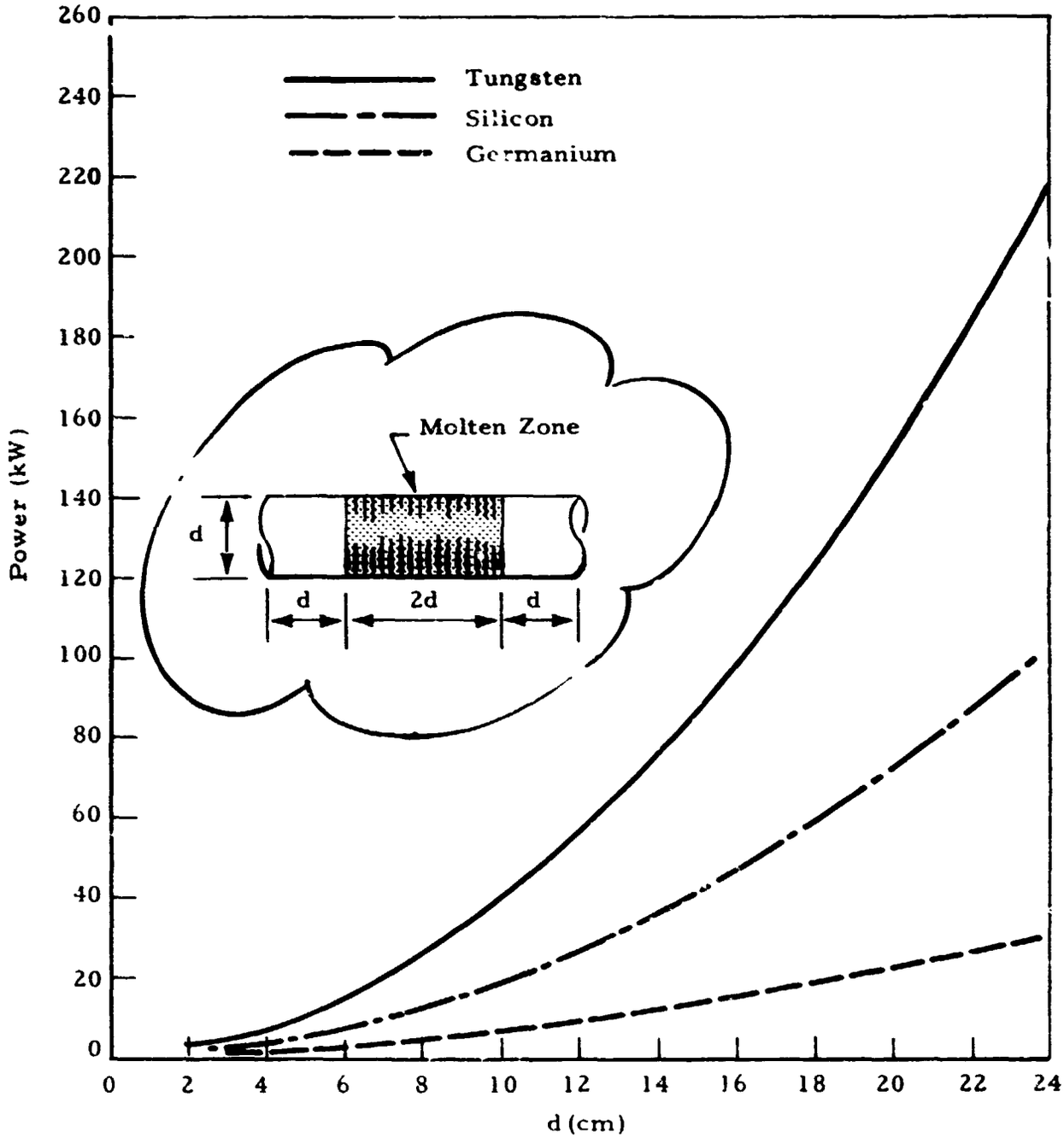

Fig. 36 - Power Requirements for Cylindrical Molten Zones

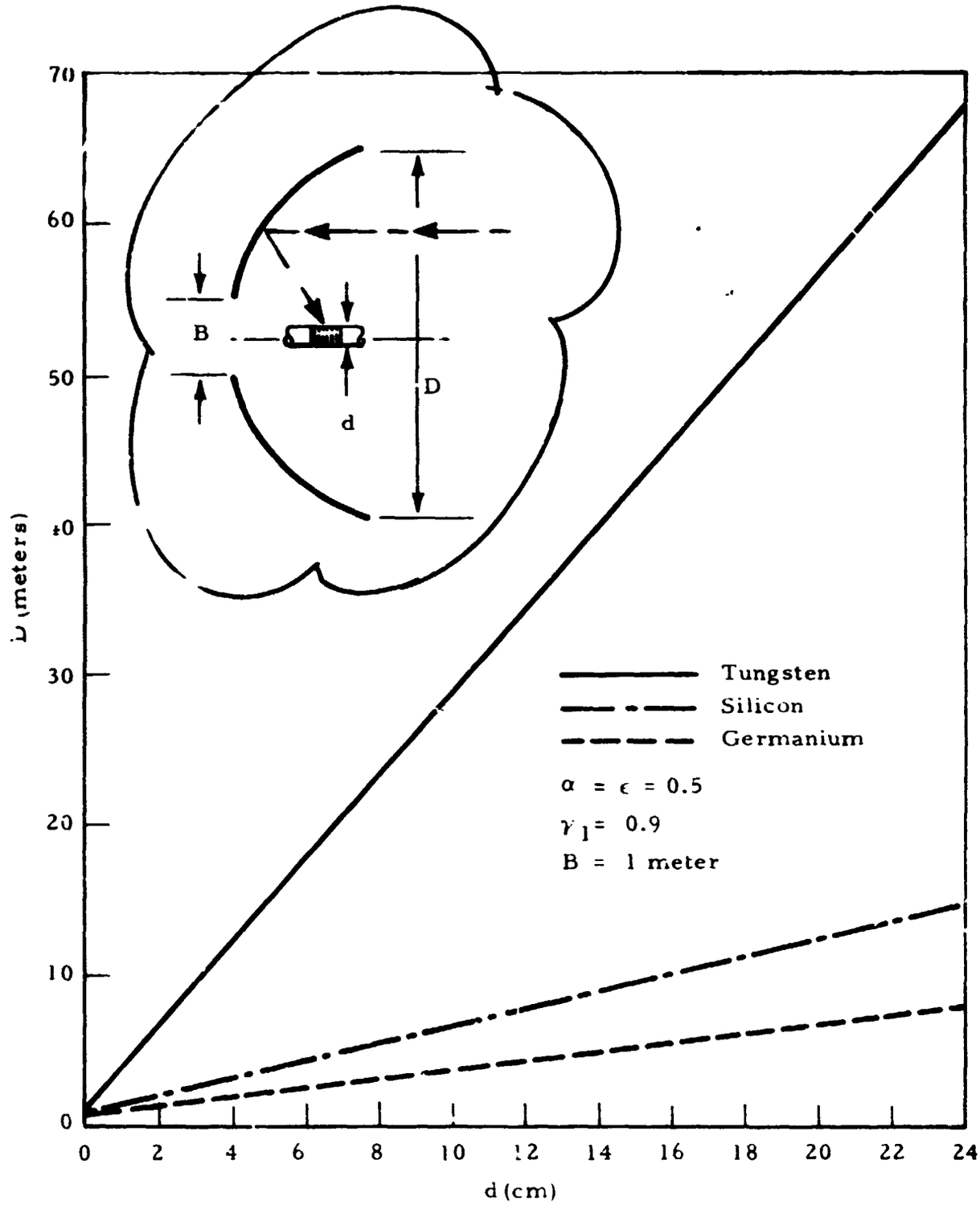

Fig. 37 - Process Bar Diameter versus Concentrator Aperture

Table 4

SPECIFIC POWER COMPARISONS

Collecting Surface	Specific Power (Watts/Pound)
Solar Concentrator* Efficiency = 100%	144.5
Solar Concentrator* Efficiency = 50%	72.2
Solar Concentrator* Efficiency = 25%	36.1
Solar Cells** 10 kW Panel for Skylab	2.63
Solar Cells** 34 W Unit for ATM Module	6.8

*Based on 0.87 lb/ft^2 of projected area in the sun direction [44].

**Data obtained from Electronics and Control Laboratory, Marshall Space Flight Center.

Section 6
CONCLUSIONS AND RECOMMENDATIONS

Previous studies that are applicable to the space processing of materials with a solar concentrator have been reviewed. Also, an analysis and associated computer code has been developed which can be used to determine the heating distribution on any surface placed in the focal region of a solar concentrator. The computer code can consider optical errors, target placement errors, limb darkening effects, etc. This computer code can also be used to design solar concentrators to give prescribed heating on a target. A simplified analysis is also developed to determine the relation between concentrator size and process size. Based on these analyses and the literature reviewed the following observations are apparent.

- The proper thermal environment is very important to process success.
- Solar concentrators can provide thermal energy for space processing.
- Solar concentrators can be designed to give specific thermal environments using the analysis in this report.
- Solar concentrators can probably give more accurate heating control than other heating techniques.
- The heating distribution on targets in the focal region of solar concentrators is sensitive to target placement.
- The technology is available for producing large orbiting solar concentrators.
- The technology for pointing solar concentrators accurately is available.
- The technology is available for controlling the solar concentrator – processing system.

Although many points that are important to solar concentrator design have been covered a detailed design of a solar concentrator system is beyond the scope of this study. Also, before a detailed design is undertaken firm

decisions must be made concerning the material(s) to be processed, size of the process, etc.

The most important conclusions one can draw from this study are that solar concentrators are very attractive for space processing, and they currently appear more attractive than alternate systems. The first conclusion is the result of showing that solar concentrators can provide sufficient thermal energy and showing that a great deal of flexibility is available for tailoring the process thermal environment. The second conclusion is based on the specific power comparison that was made with solar cells.

From the insight gained from previous studies and the analysis developed, the following observations have been made concerning the design of solar concentrators for processes that require specific thermal environments.

- A solar concentrator can be designed to provide the thermal environment for a specific process geometry.
- Multiple-purpose solar concentrators can probably be achieved through the use of a changeable secondary element (such as the "flux trap" mentioned earlier) or by using a segmented concentrator whose elements can translate along the optical axis.

If the space processing of materials with a solar concentrator is to be a reality, it is recommended that the following efforts be initiated.

- Terrestrial experimental studies of crystal growth and zone refining with a solar concentrator.
- Develop a detailed analytical model of the process heat transfer considering convection, conduction, and radiation.
- An economic and weight comparison of a complete solar concentrator-space processing system with alternative space processing systems.
- Initiate a program to provide a space processing system and facility for the shuttle program.

REFERENCES

1. Ulrich, D.R., A.M. Chung, C S. Yan and L.R. McCreight "Economic Analysis of Crystal Growth in Space," DCN-1-1-50-1366 (1[illegible]), General Electric Co Philadelphia, Pa., July 1972.

2. General Electric Co. "Beneficial Uses of Space, Final Report, Phase II, Vol. 1, SD No. 73SD4281, Philadelphia, Pa., November 1973.

3. Steg, L., and L.R. McCreight, "Space Processing — Status Prospects and Problems — 1974," International Astronautical Federation, XXVth Congress, Amsterdam, 30 September - 5 October 1974.

4. Laudise, R.A., The Growth of Single Crystals, Prentice-Hall, Englewood Cliffs, N.J., 1970.

5. Chu, T.L., "Physical Phenomena Related to Crystal Growth in the Space Environment," NASA CR-2281, July 1973.

6. De La Rue, R.E. and F.A. Halden, "Arc Image Furnace for Growth of Single Crystals," Rev. Sci. Instr., Vol. 31, 1960, p. 35.

7. Field, W.G., and R.W. Wagner, "Thermal Imaging for Single Crystal Growth and Its Application to Ruby," J. Crystal Growth, Vol. 3, 1968 p. 799.

8. Poplawsky, R P. and J.E. Thomas, Jr., "Floating Zone Crystals Using an Arc Image Furnace," Rev. Sci. Inst., Vol. 31 1960, p. 1303.

9. Zief, M., and W.R. Wilcox (editors), Fractional Solidification, (Marcel Dekker, Inc., New York, 1967), Vol. 1.

10. Carruthers, J.R., and M. Grasso, "The Stabilities of Floating Liquid Zones in Simulated Zero Gravity," Crystal Growth, Vols. 13/14, 1972, pp. 611-614.

11. Carruthers, J.R. and M. Grasso, "Studies of Floating Liquid Zones in Simulated Zero Gravity," Vol. 43, J. Appl. Phys., 1972, pp. 436-435.

12. Green, R.E., Jr., "Governing Equations for the Shapes of Molten Zones," J. Appl. Phys., Vol. 35, No. 4, 1964, pp. 1297-1301.

13. James, D.E., "The Meniscus Shape on the Outside of a Small Circular Cylinder," J. Fluid Mech., Vol. 63, Part 4 1974, pp. 657-664.

14. Keck, P.H., M. Green and M. L. Polk, "Shapes of Floating Liquid Zones Between Solid Rod," J. Appl. Phys., Vol. 24, No. 12, 1953, pp. 1479-1481.

15. Shults, E.C., R. Frankowsky and H. V. Bohm, "Image Furnace Radiant Power Control," Rev. Sci. Inst., Vol. 34, No. 2, 1963, p. 168.

16. Conn, W.M. and J. Braught, "Separation of Incident and Emitted Radiations in a Solar Furnace by Means of Rotating Sectors," J. Opt. Soc. Am., Vol. 44, No. 15, 1954, p. 15.

17. Glaser, Peter E., "Flux Redistribution," Solar Energy, Vol. 7., No. 1, 1963, p. 12.

18. Trombe, F., M. Foex and Ch. Henry la Blanghetais, "Conditions de Traitement et Mesures Physiques Dans les Fours Solaires," U.N. Conference on New Sources of Energy, IIIF, S/35, Rome, 1961, p. 415.

19. Laszlo, T.S. et al., "Emittance Measurement of Solids above 2000°C," Solar Energy, Vol. 8, 1961, p. 105.

20. Giutronich, J.E., "Techniques for Measuring Spectral Emittance of Solids at High Temperatures Using a Solar Furnace," Solar Energy, Vol. 10, 1966, p. 81.

21. Kamada, O., "Method of Measuring Target Temperature in Solar Furnace," Applied Optics, Vol. 3, 1964, p. 1397.

22. Laszlo, T.S., "Measurement and Application of High Heat Fluxes in a Solar Furnace," Solar Energy, Vol. 6, No. 2, 1962, p. 69.

23. West, Jr., W.E. and Maccalous, J.W., "Measurement of Surface Temperature in an Arc Imaging Furnace," Temperature – Its Measurement and Control in Science and Industry, Vol. 3, Part 2, 1961, Rheinhold, New York, p. 1031.

24. Gillette, R., H.E. Snyder and T. Timar, "Lightweight Solar Concentrator Developments," Solar Energy, No. 1, 1961, p. 24.

25. Wight, Ralph H., "Materials and Surfaces for Solar Furnaces," Solar Energy, Vol. 1, Nos. 2, 3, p. 84.

26. Clarke, D.R., R.B. Gillette and T.R. Beck, "Development of a Barrier-Layer Anodic Coating for Reflective Aluminum in Space," Progress in Astronautics and Aeronautics, Vol. 20, Academic Press, New York, 1967, p. 315.

27. Gillette, R.B., R.R. Brown, R.F. Seiler, and W.R. Sheldon, Progress in Astronautics and Aeronautics, Vol. 18, ed. by G. Heller, Academic Press, N.Y., 1966, pp. 413-440.

C-2

28. Gillette, R. B., "Proton and Ultraviolet Radiation Effects on Solar Mirror Reflective Surfaces," J. Spacecraft Roc., Vol. 5, No. 5, April 1968, p. 454.

29. Fong, M. C., "Spacecraft Contaminant Flowfield Predictions," Lockheed Missiles & Space Company, Report EM TSS-145, Sunnyvale, Calif., 21 December 1973.

30. Beverly, W. D., R. B. Gillette and G. A. Cruz, "Removal of Hydrocarbon Contaminant Film from Spacecraft Optical Surfaces Using a Radio Frequency-Excited Oxygen Plasma," Progress in Astronautics and Aeronautics, Vol. 31, MIT Press, 1973, p. 159.

31. Reynolds, T. W., "Adsorption-Desorption Behavior of Homogeneous and Heterogeneous Metal Surfaces," NASA TN D-4789, September 1968.

32. Hoez, M. and M. Foex, "Remarks Concerning Solar Furnaces in Space," International Solar Energy Society, Conference, Melbourne, Australia, March 1970.

33. Schweiger, R. N. and T. S. Laszlo, "A Simple Guidance System for Solar Furnaces," Solar Energy, Vol. 11, No. 2, 1967, p. 85.

34. Laszlo, Tibor S., William F. de Dufour and Joseph Erdell, "A Guiding System for Solar Furnaces," Solar Energy, Vol. II, No. 1, p. 18.

35. Moore, James G., and Pierre St. Amand, "A Guidance System for a Solar Furnace," Solar Energy, Vol. I, No. 4. p. 27.

36. Schrenk, G. L., and R. O. Whitaker, "A Biaxial Control System for Orientation of Appendages to a Space Vehicle," Solar Energy, Vol. 7, No. 1, 1963, pp. 22-26.

37. Griswold, N. R., "Collection of Solar Thermal Energy for Space Power System Application," Boeing Document D2-5523, Seattle, Wash., January 1960.

38. "60-Inch Stretch-Formed Aluminum Solar Concentrator," NASA CR-47, Thompson Ramo Wooldridge, Inc., Cleveland, Ohio, June 1964.

39. Jouriles, N., and C. E. Welling, "Rigidized Inflatable Solar Energy Concentrators," NASA CR-53991, Goodyear Aerospace Corp., Akron, Ohio, April 1964.

40. Houck, O. K., and A. R. Heath, Jr., "Characteristics of Solar Concentrators as Applied to Space Power Systems," 867C SAE-ASME National Aeronautic Meeting, New York, 27-30 April, 1964.

41. Heath, A. R., Jr., and E. L. Hofmfan, "NASA Solar Concentrator Development," Progress in Astronautics and Aeronautics, Academic Press, 1966, Vol. 16, p. 397.

42. Macauley, B.T., "The Development of a 15 kW Solar Mechanical Engine for Space Application and Its Relationship to the Fabrication of Similar Engines for Terrestrial Usage," Proceedings of the U.N. Conference on New Sources of Energy, Rome, 21-31 August 1961, Vol. 4, Solar Energy: I. p. 38.

43. "Experimental Reflector Orbital Shot (EROS)," Tech. Documentary Rept. Aeronautical Systems Div. TDR-63-266, Vol. I, Part I, April 1963.

44. Stewart, D.E., "Brayton Cycle Solar Collector Design Study," NASA CR 195, Electro-Optical Systems, Inc.. Pasadena, California, April 1965.

45. Gardon, R., "A Segmented-Mirror Solar Furnace for High-Intensity Thermal Radiation Studies," Rev. Sci. Instr., Vol. 25, No. 5, May 1954, p. 459.

46. Cobble, M.H., "Theoretical Concentrations for Solar Furnaces," Solar Energy, Vol. 5, No. 2, 1961, p. 61.

47. Hiester, N.K., T.E. Tietz, E. Lohn and P. Duwez, "Theoretical Considerations on Performance Characteristics of Solar Furnaces," Jet Propulsion, Vol. 27, No. 5, May 1957, pp. 507-513.

48. Baum, W.A. and J.D. Strong, "Basic Optical Considerations in the Choice of a Design for a Solar Furnace," Solar Energy, Vol. II, Nos. 3-4, p. 37.

49. Mazur, P., "Determination of Focusing Properties of Solar Collectors by an Integral Formula, Solar Energy, No. 1, 1962, p. 23.

50. Kamada, O., "Theoretical Concentration and Attainable Temperature in Solar Furnaces," Solar Energy, Vol. 9, No. 1, 1965, pp. 39-47.

51. De La Rue, Robert E., Jr., Eugene Loh, Joel L. Brenner and Nevin K. Hiester, "Flux Distribution Near the Focal Plane," Solar Energy, Vol. I, Nos. 2-3, p. 94.

52. Hukuo, Nobuhei, and Hisao Mii, "Design Problems of a Solar Furnace," Solar Energy, Vol. I, Nos. 2-3, p. 108.

53. Simon, Alfred W., "Calculation of the Concentration of Energy at Points Outside the Focal Spot of a Parabolic Condenser," Solar Energy, Vol. III, No. 4, p. 67.

54. Farber, J. and B.I. Davis, "Analysis of Large Aperture Parabolic Mirrors for Solar Furnaces," J. Optical Soc Am., Vol. 47, No. 3, March 1957, pp. 216-220.

55. Jose, Paul D., "The Flux Through the Focal Spot of a Solar Furnace," Solar Energy, Vol. I, No. 4, p. 19.

56. Bliss, Raymond W., Jr., "Designing Solar Furnaces for Specific Performance," Solar Energy, Vol. I, Nos. 2-3, p. 55.

57. Bliss, Raymond W., Jr., "Notes on Performance Design of Parabolic Solar Furnaces," Solar Energy, Vol. I, No. 1, p. 22.

58. Angstrom, A.K., and K.H. Angstrom, "The Distribution of Radiation over the Sun's Disk," Solar Energy, Vol. 13, pp. 243-250.

59. Wysocki, J.J., "Photon Spectrum Outside the Earth's Atmosphere," Solar Energy, Vol. 6, No. 3, 1962, p. 104.

60. Thekaekara, M.P., "The Solar Constant and Spectral Distribution of Solar Radiant Flux," Solar Energy, Vol. 9, No. 1, 1965, pp. 7-20.

61. Loewe, F., and B. Van Meurs, "The Effective Radiative Distance of the Sun," Solar Energy, Vol. 15, 1973, pp. 191-192.

62. McDermit, J.H., and T.E. Horton, "Reflective Optics for Obtaining Prescribed Irradiative Distributions from Collimated Sources," Applied Optics, Vol. 13, No. 6, June 1974, p. 1444.

63. McDermit, J.H., "Curved Reflective Surfaces for Obtaining Prescribed Irradiation Distributions," Ph.D. Dissertation, University of Mississippi, August 1972.

64. Touloukian, Y.S. (editor), Thermophysical Properties of High Temperature Solid Materials, Vol. 1: Elements, MacMillan Co., New York.

Appendix A

SOLAR CONCENTRATOR ANALYSIS PROGRAM

Appendix A

A computer code has been developed based on the analyses in this report. The program has a great deal of flexibility in that it can determine solar concentrator geometries that give a desired heating distribution as well as determine the heating on any target placed in the focal region of a concentrator. The highlights of this program are summarized below:

- Computation of heat flux distribution on any receiver from specified reflectors
- Design of continuous or faceted reflectors to give prescribed heat flux
- Computation of heat flux distribution on receiver perturbed from desired position
- Statistical perturbation of ideal reflectors to simulate real reflector imperfections, and
- Limb darkening effects.

A simplified flow chart, showing the interaction of the main components of the program, is presented in Chart A-1.

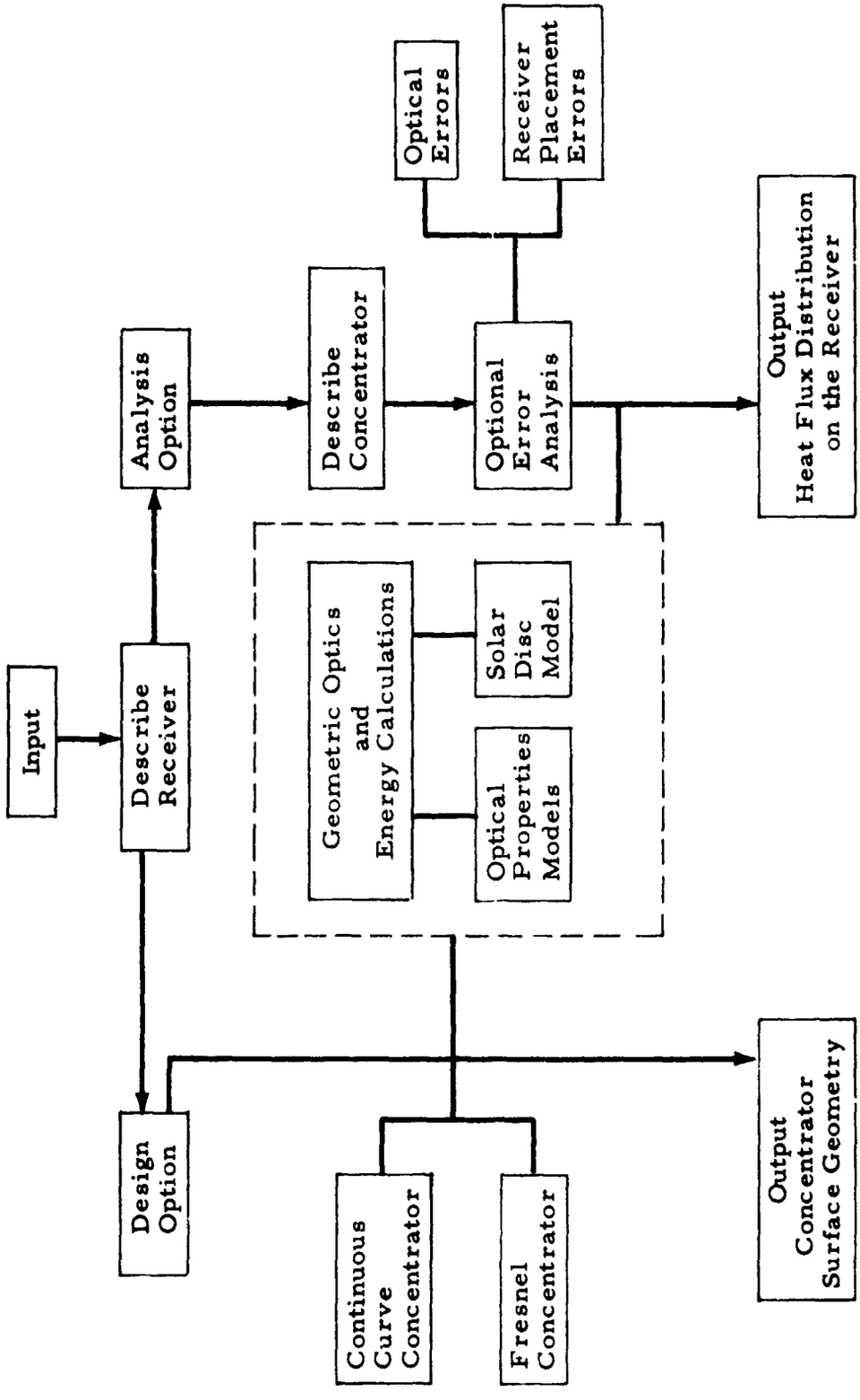

Chart A-1 - Simplified Flow Chart for SCAP